

Technische Universität Wien

Diplomarbeit

Color Sensitive Photodetectors and Measurement Setup

Ausgeführt zum Zwecke der Erlangung des akademischen Grades eines
Diplom-Ingenieurs unter Leitung von

Univ. Prof. Dr. Ing. Horst Zimmermann

und

DI Wolfgang Gaberl

E354

Institut für elektrische Meß- und Schaltungstechnik

eingereicht an der Technischen Universität Wien
Fakultät für Elektrotechnik und Informationstechnik

von

Andreas Polzer

9325896

Jenschikweg 4, 1170 Wien

Wien, im Juni 2008

Andreas Polzer

ACKNOWLEDGMENT

I want to thank Univ.Prof. Mag.rer.nat. Dr.techn. Horst Zimmermann, who offered me a lot of freedom and room for my own attempts to the problem.

I want to express my deepest gratitude to Dipl.-Ing. Wolfgang Gaberl for his creative and scientific suggestions, they were an essential basis for the successful completion of this work.

Further I want to thank Michael Hofbauer, Belinda Pilz, Jürgen Gruber and Rainer Jungwirth for their support and assistance.

And I want to thank my parents for their love and their care. They made so much possible.

Holzhacken ist deswegen so beliebt, weil man bei dieser Tätigkeit den Erfolg sofort sieht.
Albert Einstein

INTRODUCTION AND PROBLEM DEFINITION

The aim of this work is the simulation, design and realization of integrated color sensitive photodetectors. In contrary to existing techniques, using surface mounted filters e.g. CCD or CMOS sensors, this work focuses on ideas to realize the color sensitivity using standard BiCMOS technology without any additional layers or production steps. The main advantage of such novel detectors is the possibility to integrate color sensitive photodetectors with analog or digital readout circuitry. For the detectors a standard BiCMOS process (X-FAB 0.6 μ m BiCMOS) without any process modifications should be used. The optical bandwidth should cover the full visible spectrum range (\approx 400-700nm) and should extend to the near infrared range (\approx 700-900nm).

The final outcome should be an integrated color sensitive photodetector realized without any additional costs compared to the standard available photodiodes.

To verify the color sensitivity of the realized diodes a complete measurement setup has to be developed. The measurement process has to be fully automated to verify a relevant large number of diodes.

ABSTRACT

The aim of this work is the realization of color sensitive silicon photodetectors without the use of external filters or additional production steps to keep the costs as low as possible. The production process that should be used is the X-FAB 0.6 μ m BiCMOS process without any additional masks or modifications. The first task is to decide which effects can be used to make a standard photodiode into a color sensitive photodiode. Two elementary physical effects can be taken into account:

- Different available layers in the X-FAB 0.6 μ m BiCMOS can be placed over a standard PIN photodiode to function as an optical color filter.
- The different penetration depth of light with different wavelength into silicon might be used to detect the color.

The first effect is evaluated using detectors based on the standard X-FAB PIN photodiode. Additional to this standard PIN photodiode layout different available layers of the X-FAB 0.6 μ m BiCMOS process are applied on the surface as color filters.

The detectors using the second effect are based on the different penetration depth. They consist of two vertically stacked active diode regions – a shallow one near the surface and a deep one in the depth of the semiconductor. Due to the effect that short wavelengths light only penetrates shallow into silicon, the shallow diode generates a photocurrent when the incident light is in the blue-green regime, while the deep diode generates a photocurrent when the radiation is in the red or NIR regime (wavelength with deep penetration depth).

To compare the different diode types a computer controlled measurement setup (LabVIEW application) was developed. The responsivity curve of the different diodes was measured in the wavelength range from 400 to 900nm and was compared with the standard PIN photodiode used as reference.

It turned out that in principle both approaches are capable for color detection. Due to the better performance of photodetectors based on the different penetration depth they seem to be more suitable for integrated color detection.

KURZFASSUNG

Das Ziel der folgenden Arbeit ist die Realisierung von farbsensitiven Photodetektoren, die ohne zusätzliche Filter oder Produktionsschritte hergestellt werden können, um die Produktionskosten so gering als möglich zu halten. Die Photodetektoren sollen mit dem X-FAB 0,6 μ m BiCMOS Prozeß ohne Verwendung von zusätzlichen Masken und ohne Prozeßmodifikationen hergestellt werden. Die erste Aufgabe ist es nach Möglichkeiten und physikalischen Effekten zu suchen, um aus einer normalen Photodiode eine farbsensitive Photodiode zu machen. Dabei dienen als Grundlage zwei verschiedene Ansätze:

- Verschiedene, standardmäßig im X-FAB 0,6 μ m BiCMOS Herstellungsprozeß vorhandene, Halbleiterschichten werden auf die Oberfläche einer normalen PIN Photodiode als Farbfilter aufgebracht.
- Die unterschiedlichen Eindringtiefen des Lichts unterschiedlicher Wellenlängen in Silizium werden benutzt, um die Lichtfarben unterscheiden zu können.

Die Photodetektoren, die mit zusätzlichen Strukturen als Farbfilter arbeiten, basieren auf einer normalen PIN Photodiode, auf deren Oberfläche verschiedene Strukturen, welche im X-FAB 0.6 μ m BiCMOS Prozeß standardmäßig vorhanden sind, aufgebracht werden. Dazu eignen sich im speziellen die transparenten Polysiliziumschichten des BiCMOS Prozesses.

Die Farbdetektoren, die auf der unterschiedlichen Eindringtiefe von Licht unterschiedlicher Wellenlänge basieren, bestehen aus zwei vertikal untereinander liegenden Photodioden – eine knapp unter der Oberfläche und eine in der Tiefe des Halbleiters. Da Licht kurzer Wellenlänge weniger tief in Silizium eindringt als Licht langer Wellenlänge, erzeugt die obere Diode einen Photostrom wenn Licht mit blau-grünem Spektrum eingestrahlt wird während die tief liegende Diode bei Einstrahlung von Licht mit rotem oder nahen infrarotem Spektrum Strom erzeugt.

Um die unterschiedlichen Diodentypen vergleichen zu können, wurde ein Meßsystem entwickelt, welches mit Hilfe eines Computers (LabVIEW Programms) angesteuert wird. Die Responsivitätskurve der einzelnen Dioden wird im Wellenlängenbereich von 400 bis 900nm vermessen und mit der normalen PIN Photodiode, die als Referenzdiode verwendet wird, verglichen.

Es hat sich herausgestellt, daß im Prinzip beide Ansätze geeignet sind, um farbsensitive Dioden zu realisieren. Allerdings zeigen die Dioden, die auf der unterschiedlichen Eindringtiefe basieren, eine stärkere Farbabhängigkeit und eine größere Responsivität. Daher dürften diese Dioden besser für die Entwicklung von farbsensitiven Photodetektoren geeignet sein.

1. CONTENTS

1.	CONTENTS	1
2.	LIST OF SYMBOLS	3
3.	LIST OF ABBREVIATIONS	5
4.	BASICS AND THEORY	6
4.1.	BASICS OF OPTICAL ABSORPTION	6
4.2.	SEMICONDUCTOR MATERIALS	7
4.3.	SEMICONDUCTOR EQUATIONS	8
4.3.1.	<i>Carrier Drift</i>	9
4.3.2.	<i>Carrier Diffusion</i>	11
4.3.3.	<i>Quantum Efficiency and Responsivity</i>	13
4.4.	PIN PHOTODIODE	15
4.5.	COLOR DETECTION	17
4.5.1.	<i>Color Detection with Filter Pattern</i>	17
4.5.2.	<i>Color Detection by Penetration Depth Effects</i>	20
5.	PHOTODIODE DESIGN.....	24
5.1.	X-FAB 0.6 μ m BICMOS OPTICAL PIN DIODE	24
5.1.1.	<i>Doping Profiles</i>	26
5.2.	FILTERING EFFECTS	26
5.2.1.	<i>Oxide layers and Silicon Nitride as Color Filter</i>	27
5.2.2.	<i>Polysilicon Layer 1 as Color Filter</i>	29
5.2.3.	<i>Polysilicon Layer 2 as Color Filter</i>	30
5.2.4.	<i>Polysilicon 1 and Polysilicon Layer 2 as Filter</i>	30
5.2.5.	<i>Mixed Structures</i>	31
5.3.	PENETRATION DEPTH EFFECTS	33
6.	MEASUREMENT SETUP.....	35
6.1.	ASB-XE-175 XENON LIGHT SOURCE	35
6.2.	DIGIKRÖM CM110 MONOCHROMATOR	37
6.2.1.	<i>Grating Fundamentals</i>	38
6.2.2.	<i>Grating Characteristics</i>	40
6.2.3.	<i>Monochromator Characteristics</i>	41
6.2.4.	<i>Color Filter</i>	44
6.2.5.	<i>f-number Fiber Optic Adapter</i>	46
6.2.6.	<i>Monochromator Software</i>	46
6.3.	FIBER OPTIC BEAM SPLITTER	47
6.4.	OPHIR NOVA OPTICAL POWER METER	49
6.4.1.	<i>Photodiode Head PD-300</i>	49
6.4.2.	<i>Software</i>	51
6.5.	KEITHLEY 6517A ELECTROMETER	52
6.6.	WAFER PROBER	53
6.7.	COMPLETE SETUP	54
7.	LABVIEW APPLICATION	56
7.1.	LABVIEW OVERVIEW	56
7.2.	PROGRAM FUNCTIONS	57
7.2.1.	<i>Straight-Trough Operation (Full Spectrum)</i>	57
7.2.2.	<i>Single Wavelength Measurement (Single Step)</i>	57
7.2.3.	<i>Responsivity Curve Measurement</i>	58
7.3.	PROGRAM MANUAL	58
7.3.1.	<i>Device Settings</i>	59
7.3.2.	<i>Full Spectrum</i>	60

1. Contents

7.3.3.	<i>Single Step</i>	60
7.3.4.	<i>Responsivity Curve</i>	60
7.3.5.	<i>Status</i>	61
7.3.6.	<i>Exit</i>	61
7.4.	BLOCK DIAGRAM.....	61
8.	MEASUREMENT RESULTS	63
8.1.	PIN PHOTODIODE.....	64
8.2.	PIN PHOTODIODE WITHOUT OPTICAL WINDOW.....	65
8.3.	PHOTODIODE WITH POLYSILICON LAYER 1.....	67
8.4.	PHOTODIODE WITH POLYSILICON LAYER 2.....	69
8.5.	PHOTODIODE WITH POLY 1 AND POLY 2 LAYER.....	70
8.6.	MIXED PHOTODIODE.....	72
8.7.	PENETRATION DEPTH EFFECT DIODE.....	73
9.	CONCLUSION AND OUTLOOK	75
10.	FIGURE INDEX	77
11.	TABLE INDEX	79
12.	REFERENCES	80
13.	APPENDIX A: DATASHEET LIGHT SOURCE	82
14.	APPENDIX B: DATASHEET MONOCHROMATOR CM110	84
15.	APPENDIX C: DATASHEET ORDER SORTING FILTERS	86
16.	APPENDIX D: DATASHEET F-NUMBER FIBER OPTIC ADAPTER	88
17.	APPENDIX E: DATASHEET OPHIR NOVA POWER/ENERGY METER	90
18.	APPENDIX F: DATASHEET PHOTO-DIODE HEAD PD-300	92
19.	APPENDIX G: DATASHEET KEITHLEY 6517A ELECTROMETER	93

2. LIST OF SYMBOLS

Symbol	Description	Unit
c	Speed of light in a medium	cm/s
c_0	Speed of light in vacuum	cm/s
d	Groove spacing	nm
d_{ARC}	Thickness of antireflection coating	μm
E	Photon energy	eV
\mathbf{E}	Electric field	V/cm
\bar{E}	Etendue	
E_g	Energy bandgap	eV
F	Instrumental focal length	mm
G	Photo generation (e-h-p)	cm^{-3}/s
\bar{G}	Groove density	gr/mm
h	Planck constant	Js
I	Current	A
I_0	Intensity factor	ehp/cm ³
I_{ph}	Photocurrent	A
m	Diffraction order	
N	Impurity concentration	cm^{-3}
\bar{n}	Refractive index	
\bar{N}	Number of grooves	
\bar{n}_{ARC}	Refractive index of antireflection coating	
\bar{n}_S	Refractive index of surroundings	
\bar{n}_{SC}	Refractive index of semiconductor	
\bar{P}	Optical power in a semiconductor	W
P_{blue}	Optical power blue fiber	W
P_m	Measured optical power	W
P_{opt}	Incident optical power	W
P_{white}	Optical power white fiber	W
R	Resolving power	
\bar{R}	Reflectivity	
R_g	Grating diffraction efficiency	
R_m	Mirror reflectance	
S_h	Slit height	cm
S_w	Slit width	cm
T	Absolute temperature	K
\bar{T}	Transmission efficiency	
t_d	Drift time	s
t_f	Fall time	s
t_r	Rise time	s
W	Width of space charge region	μm
W_g	Grating width	mm
y	y direction	μm
α	Absorption coefficient	μm^{-1}

2. List of Symbols

Symbol	Description	Unit
η_i	Internal quantum efficiency	%
η_o	Optical quantum efficiency	%
θ	Grating rotation angle	°
$\bar{\kappa}$	Extinction coefficient	
λ	Wavelength in a medium	nm
λ_0	Wavelength in vacuum	nm
λ_c	Wavelength corresponding to E_g	nm
$\Delta\lambda$	Resolution	nm
μ	Mobility	cm ² /Vs
μ_n	Electron mobility	cm ² /Vs
μ_p	Hole mobility	cm ² /Vs
ν	Frequency of light	Hz
τ_n	Electron lifetime	s
τ_p	Hole lifetime	s
v	Carrier velocity	cm/s
v_{sat}	Saturation velocity	cm/s
ϕ	Ebert angle	°

3. LIST OF ABBREVIATIONS

ARC	Anti Reflection Coating
BiCMOS	Bipolar Complementary Metal Oxide Semiconductor
CCD	Charge Coupled Device
CD	Compact Disc
CMOS	Complementary Metal Oxide Semiconductor
CYGM	Cyan Yellow Green Magenta
DVD	Digital Versatile Disc
EDA	Electronic Design Automation
GPIO	General Purpose Interface Bus
IEEE	Institute of Electrical and Electronic Engineers
IR	Infrared
JPEG	Joint Photographic Experts Group
LabVIEW	Laboratory Virtual Instrumentation Engineering Workbench
NIR	Near Infrared
PC	Personal Computer
PIN	Positive Intrinsic Negative
PN	Positive Negative
RGB	Red Green Blue
RGBW	Red Green Blue White
ROM	Read Only Memory
SCPI	Standard Commands for Programmable Instrumentation
SCR	Space Charge Region
TIFF	Tagged Image File Format
UV	Ultra Violet

4. BASICS AND THEORY

4.1. BASICS OF OPTICAL ABSORPTION

Optical absorption is a process which converts optical energy into electrical energy. Due to the work of Albert Einstein and Max Planck it is possible to describe light not only by wave formalism but also by quantum-mechanical particle formalism. The smallest known unit of light is called photon. Photons are used to characterize electromagnetic radiation from the far infrared to the extreme ultraviolet spectrum. The velocity of photons c in a medium with an optical index of refraction \bar{n} is given by

$$c = \frac{c_0}{\bar{n}} \quad (4.1)$$

where c_0 is the speed of light in vacuum ($\bar{n} = 1$). Photons are defined to be massless. They can be characterized by their frequency ν and their wavelength λ :

$$\lambda = \frac{c}{\nu} \quad (4.2)$$

The frequency of the photon is the same in vacuum and in a medium with a refraction $\bar{n} > 1$. Therefore the wavelength of a photon in a medium with $\bar{n} > 1$ is shorter than the vacuum wavelength λ_0 .

Another way to characterize photons is to describe them by their energy E where h represents Planck's constant ($h = 6.626 \cdot 10^{-34}$ J·s):

$$E = h\nu = \frac{hc}{\lambda} = h \frac{c_0}{\lambda_0} \quad (4.3)$$

This formula can be used to calculate the boundary wavelength of a semiconductor in dependence of its bandgap. The bandgap of silicon $E_g = 1.1\text{eV}$ leads to its boundary wavelength:

$$\lambda_c = \frac{hc_0}{E_g} = 1110\text{nm} \quad (4.4)$$

Therefore silicon photodiodes can only detect light with wavelengths shorter than 1110nm. For light with wavelengths longer than 1110nm silicon is transparent and no light is absorbed.

A second limit for photon absorption in silicon exists due to the fact that the penetration depth decreases for short wavelengths. At around 350nm the penetration depth is nearly zero and the electron-hole pairs are not generated in a usable depth.

These two borders describe the useable range for integrated silicon photodetectors (350-1100nm).

4.2. SEMICONDUCTOR MATERIALS

In semiconductor materials the energy of a photon can be absorbed by an electron in the valence band. If the energy of the photon is larger than the bandgap energy E_g of the semiconductor, the electron is moved from the valence band to the conduction band, the photon is absorbed and an electron-hole pair is generated [1]. Photons with energy smaller than E_g cannot be absorbed and the semiconductor is transparent for light with wavelengths longer than $\lambda_c = hc_0 / E_g$. The number of generated electron-hole pairs depends on the absorption coefficient α of the semiconductor. The absorption coefficient α determines the penetration depth $1/\alpha$ of the light in the semi-conductor according to Lambert-Beer's law:

$$I(y) = I_0 e^{-\alpha y} \quad (4.5)$$

In essence this law states the logarithmic dependence between the transmission of light through a semiconductor and the local intensity.

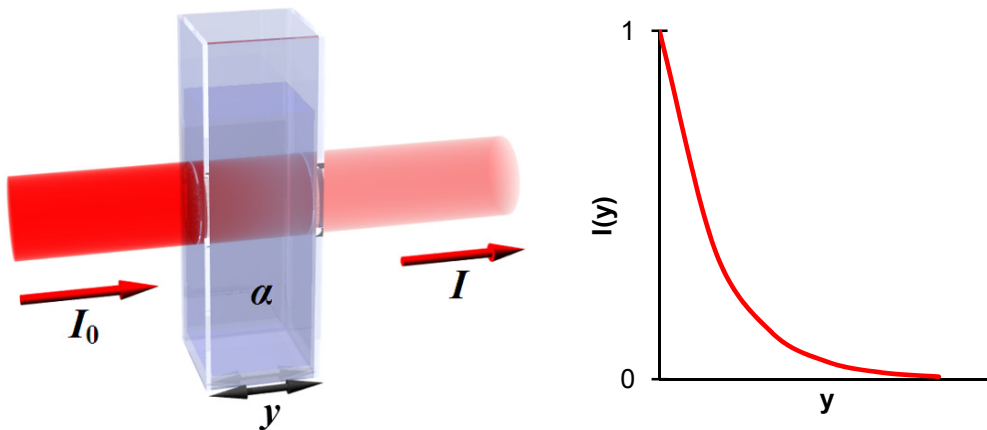


Figure 4.1 Lambert-Beer's law [2]

The absorption coefficient α depends strongly on the semiconductor material and on the wavelength of light. For wavelengths longer than λ_c the energy of light is smaller than the bandgap energy E_g and the semiconductor material is transparent. Therefore the absorption coefficient α is zero for wavelengths longer than λ_c , for wavelengths shorter than λ_c the absorption coefficient α increases to the *fundamental absorption*. Figure 4.2 shows the absorption coefficients for the most important semiconductors.

The widest wavelength range is offered by Ge including the wavelengths $1.3\mu\text{m}$ and $1.5\mu\text{m}$ which are used for long distance optical data transmission via glass fibers. The direct semiconductors GaAs and InP have high absorption coefficients in the visible and near infrared spectrum while the absorption coefficient of the indirect semiconductor Si is one or two orders of magnitude lower in this spectral range. This results in a much thicker absorption zone in silicon detectors which makes silicon photodiodes rather slow (limited carrier mobility). On the other hand silicon is the economically most important semiconductor and so it is worthwhile to research silicon optoelectronic devices and integrated circuits even with its suboptimal optical properties.

Silicon photodetectors and receivers are a good choice in case high volumes are needed and the price has to be low as e.g. in consumer electronics such as audio CD, CD-ROM and DVD systems.

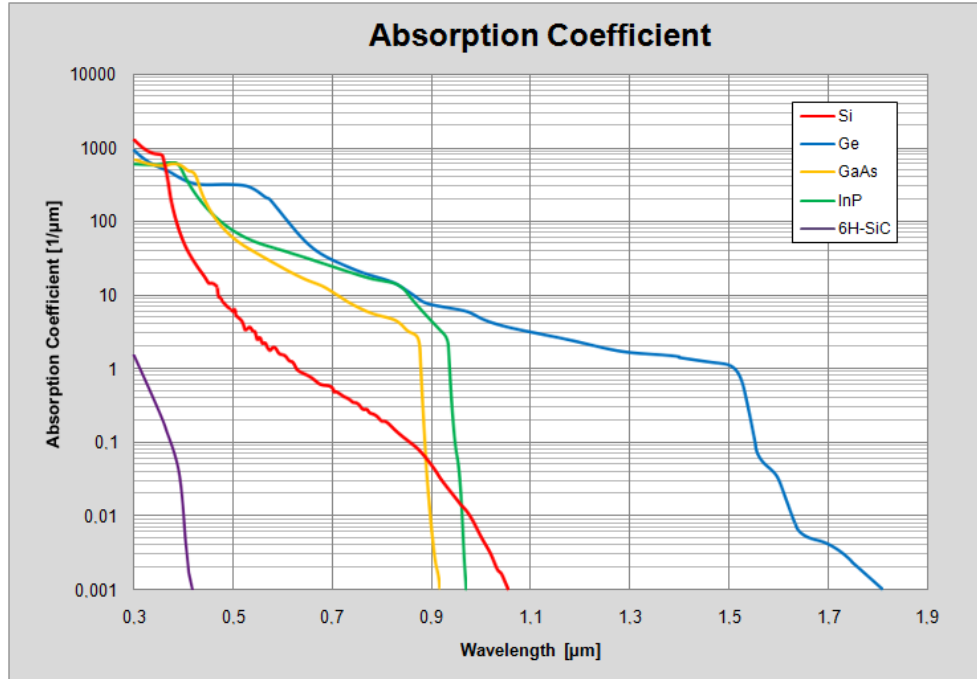


Figure 4.2 Absorption coefficients of important semiconductor materials [3]

Table 4.1 lists the absorption coefficients and the intensity factors (ehp/cm³ means electron-hole pairs/cm³) of silicon for several wavelength of technical interest.

Wavelength [nm]	α [μm^{-1}]	I_0 [ehp/cm ³]
430	5.70	9.00×10^{22}
635	0.38	6.00×10^{22}
680	0.24	3.79×10^{21}
780	0.12	1.89×10^{21}
850	0.06	95.0×10^{20}

Table 4.1 Absorption coefficients α and intensity factors I_0 of silicon [4] [5]

4.3. SEMICONDUCTOR EQUATIONS

One of the main properties of photodetectors, their speed, depends on carrier drift and minority carrier diffusion. In conventional semiconductor materials the carrier drift is a much faster process than the carrier diffusion.

For a real application also the pn junction capacitance and the serial resistance reduces the speed of the photodiode.

4.3.1. CARRIER DRIFT

As mentioned before the carrier mobility is the parameter which is liable for the speed of the photodetector. The mobility of the carriers depends on the doping concentration and on the applied electric field. Table 4.2 gives an overview over the different parameters for silicon.

Parameter	Electrons	Holes
μ_{min} [cm ² /Vs]	17.8	48.0
μ_{max} [cm ² /Vs]	1350	495
N_{ref} [cm ⁻³]	1.072×10^{17}	1.606×10^{17}
$v_{n,p}$	-2.3	-2.2
$\chi_{n,p}$	-3.8	-3.7
$\alpha_{n,p}$	0.73	0.70

Table 4.2 Electron and hole mobility and further parameters of silicon [3]

The mobility of the carriers in dependence of the total impurity concentration N_{total} and the temperature T in K is given by

$$\mu_{0n} = \mu_{n,min} + \frac{\mu_{n,max}(T/300)^{v_n} - \mu_{n,min}}{1 + (T/300)^{\chi_n} (N_{total}/N_{ref,n})^{\alpha_n}} \quad (4.6)$$

$$\mu_{0p} = \mu_{p,min} + \frac{\mu_{p,max}(T/300)^{v_p} - \mu_{p,min}}{1 + (T/300)^{\chi_p} (N_{total}/N_{ref,p})^{\alpha_p}} \quad (4.7)$$

where N_{total} is the sum of the concentrations of acceptors and donors [6] [7].

Figure 4.3 shows the connection between the carrier mobility in silicon and the doping concentration for $T = 300\text{K}$.

The dependence of the carrier mobility in silicon on the electric field can be described by

$$\mu_n = \frac{\mu_{0n}}{1 + (\mu_{0n}E/v_n^{sat})^2} \quad (4.8)$$

$$\mu_p = \frac{\mu_{0p}}{1 + (\mu_{0p}E/v_p^{sat})^1} \quad (4.9)$$

where v_n^{sat} and v_p^{sat} are the saturation velocities of the carriers in cm/s [6]. The saturation velocity can be calculated from [6]:

$$v_p^{sat} = v_n^{sat} = \frac{2.4 \times 10^7}{1 + e^{T/600}} \quad (4.10)$$

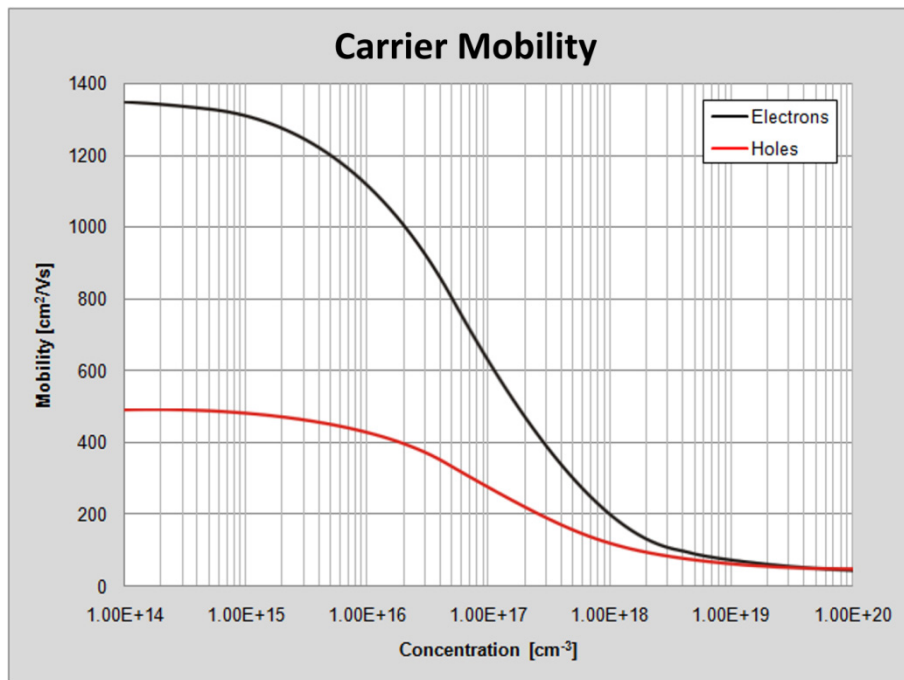


Figure 4.3 Carrier mobility in silicon versus total doping concentration

Figure 4.4 shows the dependence between the carrier mobility and the electric field calculated with (4.8) and (4.9) for a very low doping concentration as used in the intrinsic zone of a PIN photodiode.

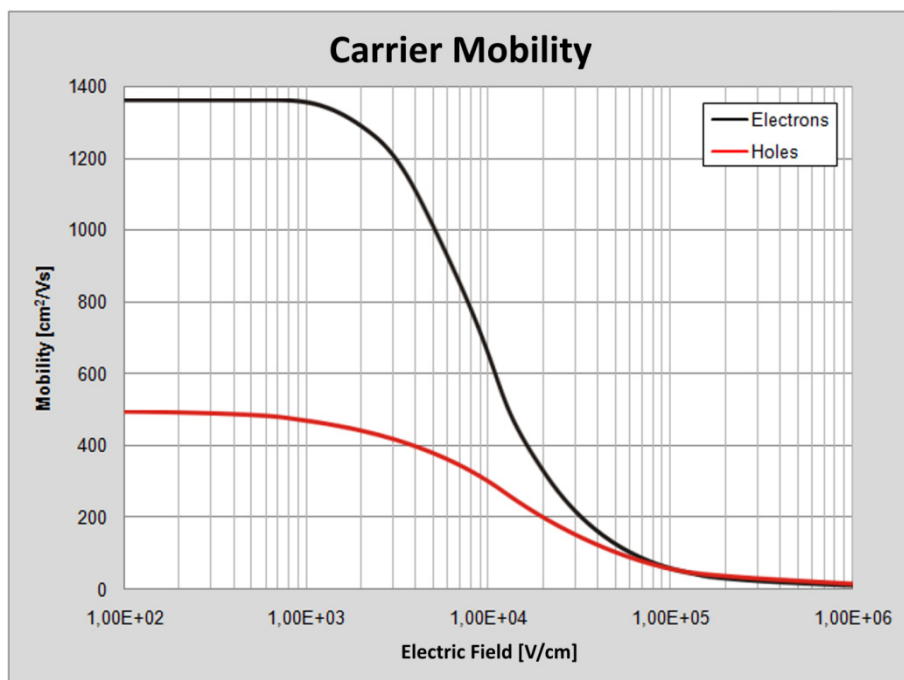


Figure 4.4 Carrier mobility versus electric field for a low doping concentration

As seen in Figure 4.4 the carrier mobility decreases for electric fields larger than approximately 2000V/cm. The drift velocities are proportional to the electric field for small values of the electric field. The electron drift velocity saturates for electrical fields larger than 10000V/cm while the electrical field has to exceed 100000V/cm to reach the hole saturation velocity.

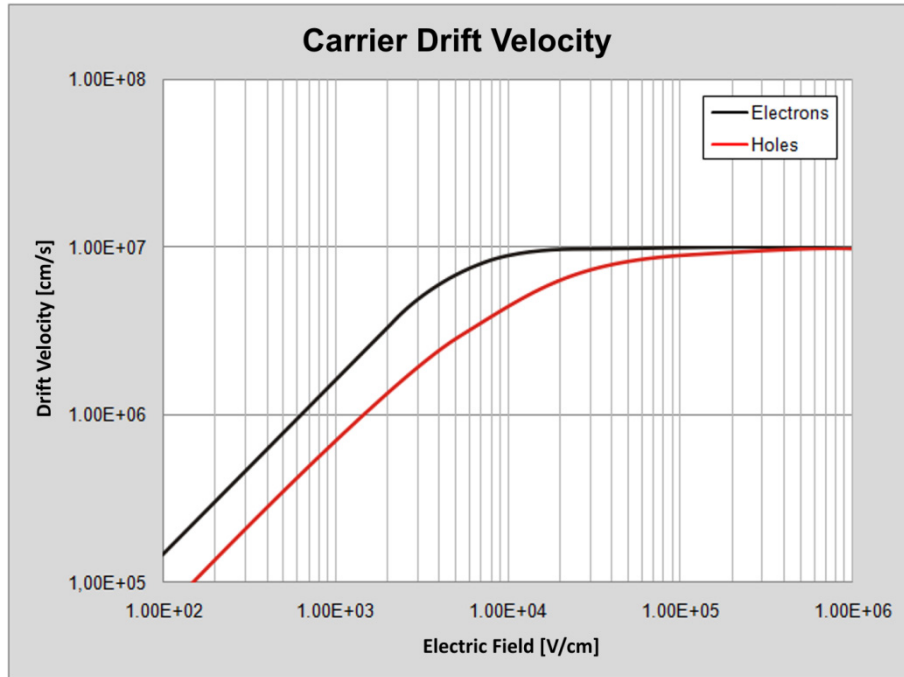


Figure 4.5 Carrier drift velocity versus electrical field for a low doping concentration

Another important quantity is the carrier drift time t_d . This is the time needed by carriers to drift through a space charge region with the width W . Its value is defined by W and the drift velocity v which depends on μ and E .

The drift time is the main limitation of rise and fall time t_r and t_f of the photodiode output signal. Therefore the maximum data rate of the photodetector is limited by the carrier drift time.

4.3.2. CARRIER DIFFUSION

Charges (electron-hole pairs) created in regions of the semiconductor without an electrical field is present, move at random due to the thermal energy. They do not immediately yield a photocurrent. In a typical photodiode there are two such regions. The first region is the heavily doped region on the surface of the diode and the other region is in the depth of the semiconductor. The surface region is in most cases not very thick so that the light can reach the pn junction with minimal losses. Hence the area without an electrical field on the surface of the semiconductor is very small. The more critical region is below the space charge region (SCR) because it is much thicker than the surface region. Therefore much electron-hole pairs might be generated in this region without electrical field. Figure 4.6 shows the heavily doped surface region p^+ , the space charge region (SCR), the lower doped n region and drift and diffusion zones of a

photodiode. The diagram on the left side shows the distribution of the electrical field inside the diode and the diagram on the right side shows the generation rate G of electron-hole pairs in dependence of different wavelengths of light – shorter wavelengths (blue light) cause a higher generation rate G in shallow regions while longer wavelengths (red or NIR light) cause a higher generation rate G in the deeper regions.

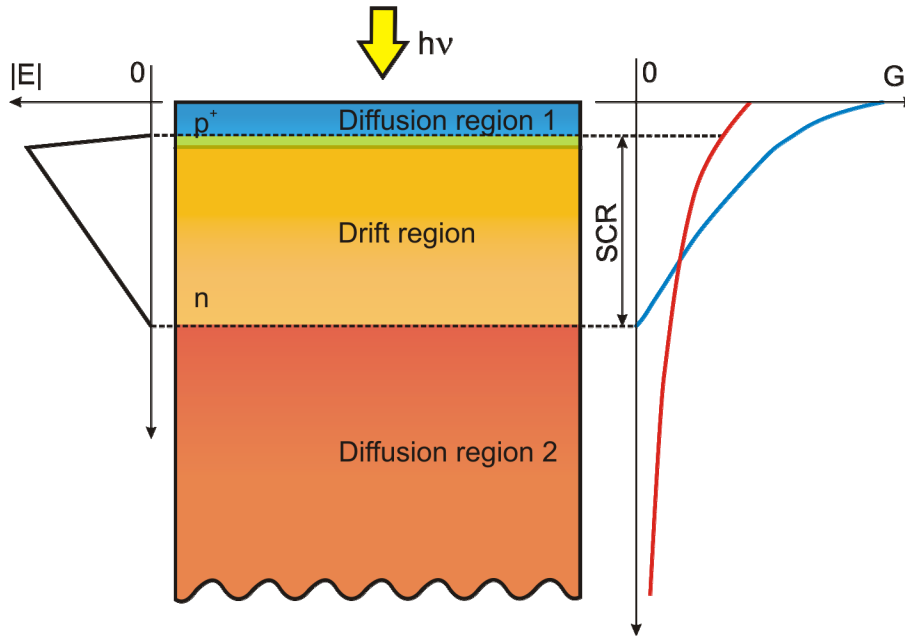


Figure 4.6 Drift and diffusion regions in a photodiode [8]

Whenever electron-hole pairs are generated in a field free area, there are two possible scenarios. Either they recombine after their lifetimes τ_n and τ_p or they can reach a drift region within τ_n and τ_p . As soon as they reach a drift region they are accelerated by the electrical field and cause a photocurrent. Hence the statistical distribution of the generated carriers (in either drift or diffusion region) causes a certain delay between the light incidence and the resulting photocurrent.

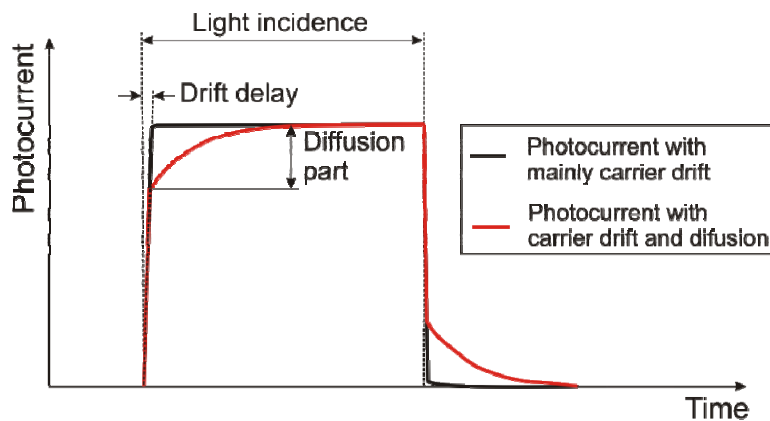


Figure 4.7 Transient behavior of the photocurrent for carrier drift and diffusion

Figure 4.7 shows the relation between the light incidence and the photocurrents caused by carrier drift and carrier diffusion. The shape of the photocurrent is characteristic for the diffusion of the carriers in the second region, because they have a longer distance to the drift zone which causes a longer delay between the light incidence and the resulting photocurrent.

In conclusion it is necessary to avoid carrier diffusion to build fast photodetectors. This can either be achieved by using short wavelengths (larger absorption coefficient) or by using a different semiconductor material. Additionally the size of the SCR can be increased by three factors: thicker intrinsic zone, larger reverse voltage or reduced intrinsic zone doping [3]. In a BiCMOS process the intrinsic zone doping and thickness can be adjusted by selecting the appropriate waver starting material. The reverse voltage is usually limited by the process specification.

4.3.3. QUANTUM EFFICIENCY AND RESPONSIVITY

The external quantum efficiency η_e is defined as the number of photo generated electron-hole pairs, which contribute to the photocurrent, divided by the number of the incident photons. It can be calculated from the measured photocurrent for a known incident optical power.

Due the different refraction indexes of the surrounding air \bar{n}_S ($\bar{n}_S = 1.00$) and the semiconductor \bar{n}_{SC} (e.g. Si, $\bar{n}_{SC} \approx 3.5$) a part of the incident optical power is reflected [4]. The reflectivity \bar{R} can be calculated by

$$\bar{R} = \frac{(1 - \bar{n}_{sc})^2 + \bar{\kappa}^2}{(1 + \bar{n}_{sc})^2 + \bar{\kappa}^2} \quad (4.11)$$

where $\bar{\kappa}$ is the extinction coefficient of an absorbing medium. The extinction coefficient is sufficient for the absorption of a medium. The absorption coefficient α is defined by:

$$\alpha = \frac{4\pi\bar{\kappa}}{\lambda_0} \quad (4.12)$$

The optical quantum efficiency η_o is calculated by:

$$\eta_o = 1 - \bar{R} \quad (4.13)$$

To reduce the reflected part of the incident optical power a antireflection coating (ARC) with the thickness d_{ARC}

$$d_{ARC} = \frac{\lambda_0}{4\bar{n}_{ARC}} \quad (4.14)$$

and the index of refraction \bar{n}_{ARC}

$$\bar{n}_{ARC} = \sqrt{\bar{n}_S \bar{n}_{SC}} \quad (4.15)$$

can be applied on the surface of the semiconductor (Figure 4.8). For silicon photodetectors, SiO_2 ($\bar{n}_{ARC} = 1.45$) or Si_3N_4 ($\bar{n}_{ARC} = 2.0$) are commonly used [3].

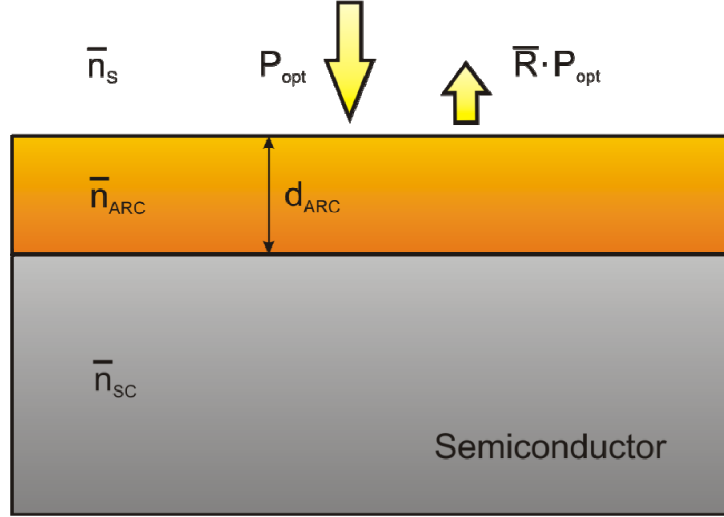


Figure 4.8 Semiconductor with antireflection coating

Due to the partial reflection of the light on the surface it is useful to define the internal quantum efficiency as the number of generated electron-hole pairs, which contribute to the photocurrent, divided by the number of photons which penetrate into the semiconductor. Therefore the external quantum efficiency is the product of the optical quantum efficiency η_o and the internal quantum efficiency η_i :

$$\eta_e = \eta_o \eta_i \quad (4.16)$$

Another important figure for the performance and usability of photodetectors is the wavelength dependent responsivity R . It is a measure of the sensitivity to light, and it is defined as the ratio of the photocurrent I_{ph} and the incident optical power P_{opt} at a given wavelength:

$$R = \frac{I_{ph}}{P_{opt}} = \frac{q \lambda_0}{hc} \eta_e = \frac{\lambda_0 \eta_e}{1.243 \text{ W}} \quad (4.17)$$

where λ_0 is given in μm . In other words, it is a measure of the effectiveness of the conversion of optical power into electrical current.

Figure 4.9 shows the responsivity of real photodetectors in dependence on the wavelength. The dashed line represents an ideal photodetector with a quantum efficiency $\eta_e = 100\%$. The responsivity of real photodetectors is always lower due to the partial reflection on the semiconductor surface and due to the partial recombination of the electron-hole pairs in the semiconductor.

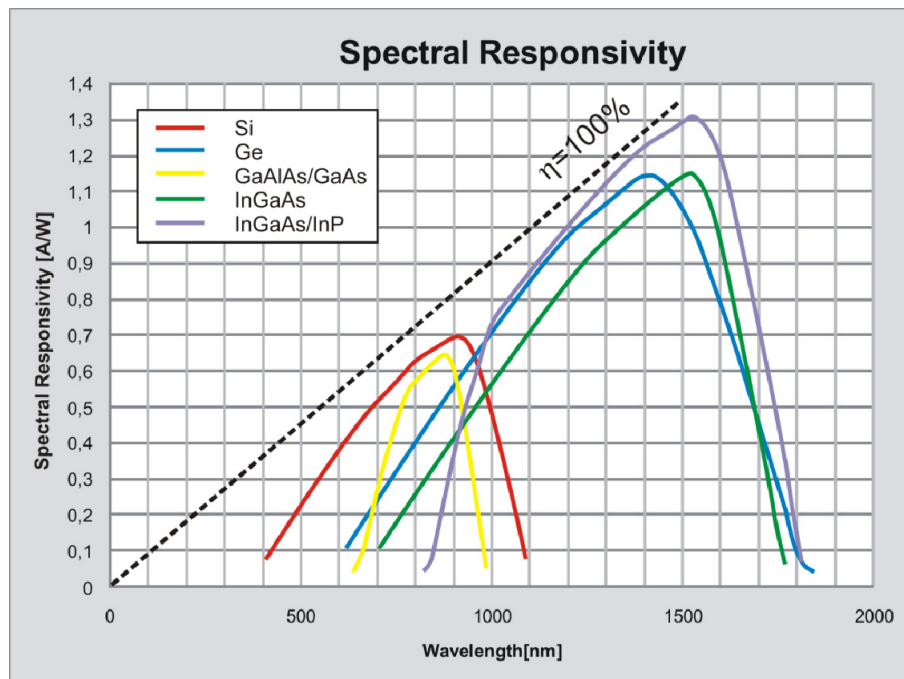


Figure 4.9 Spectral responsivity of real photodetectors and theoretical limit [9]

4.4. PIN PHOTODIODE

The PIN photodiode is structured as a sandwich with a low doped intrinsic region (down to 10^{13}cm^{-3}) [10] between the higher doped p^+ - and n^+ -zones (Figure 4.10).

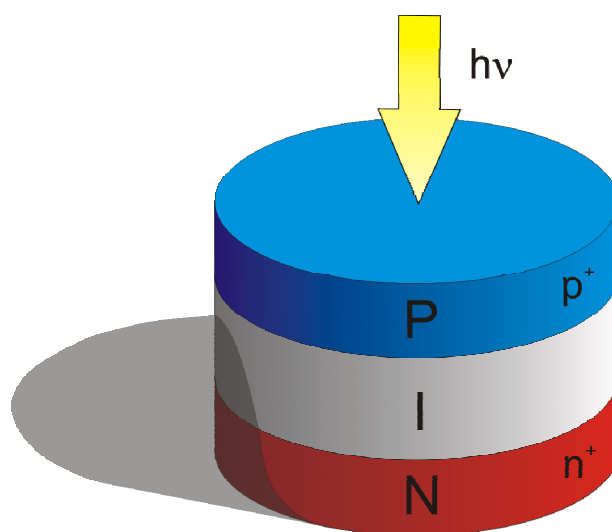


Figure 4.10 PIN photodiode

In common applications the PIN photodiode is usually reverse-biased. It acts as a current source and generates a photocurrent that is proportional to the incident light. Due to the reverse-bias the p^+ -region develops a negative charge while the n^+ -region develops a positive charge. The intrinsic region has only a small number of free carriers and is easily depleted. The intrinsic region has a very low doping concentration compared to the high doped n^+ and p^+ -region and therefore the electrical field is nearly constant in the depletion region (Figure 4.11). The drift region extends entirely over the complete intrinsic region (if the applied reverse-bias voltage is high enough). With a further increase of the reverse-bias voltage the space charge region cannot extend further into the high doped p^+ and n^+ -regions and therefore the electrical field increases inside the intrinsic zone. This accelerates the generated electrons and holes to a high velocity and increases the speed of the photodiode. This is a major improvement over the pn photodiode. Therefore PIN photodiodes are generally faster than pn photodiodes (even if the depletion region is thicker than in the pn photodiode). The thick depletion region dramatically improves the (dynamic) responsivity of the photodiode.

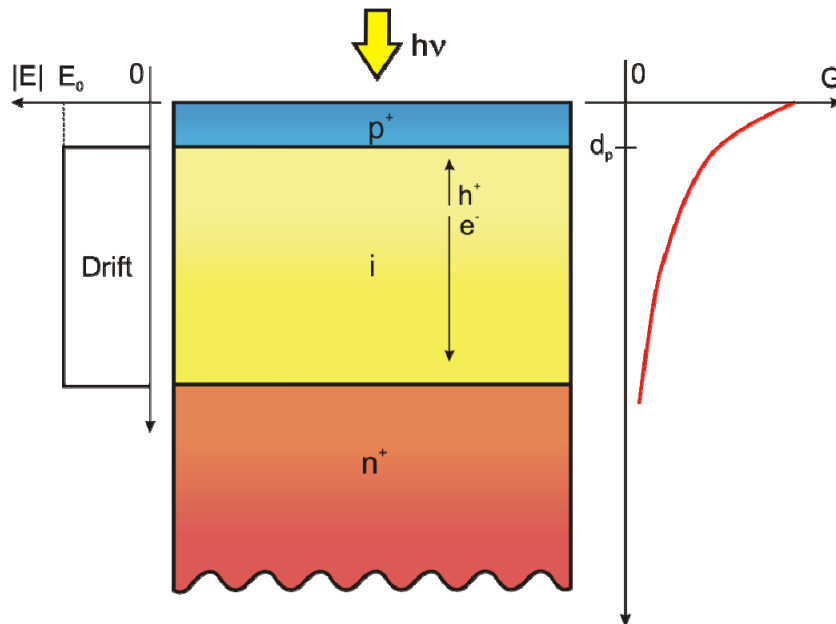


Figure 4.11 Drift region and distribution of the electric field in a PIN photodiode [8]

Since the absorption length is primarily defined by the intrinsic region, the p^+ -layer, which is penetrated by the light first, it needs only to be thick enough to provide a suitable ohmic contact to the external circuit. This reduces the carrier diffusion effects in the surface layer so that nearly all the photons that generate electron-hole pairs are absorbed in the intrinsic region, where the carriers are swept out at a high speed by the applied electric field [11].

To minimize carrier diffusion in the n^+ -layer in the depth of the semiconductor it is necessary to avoid the photo generation in regions below the edge of the space charge region SCR. Therefore it is essential to increase the thickness of the intrinsic zone (drift region) to at least in the range of the penetration depth of light. Due to the low optical absorption coefficient of silicon e.g. for a wavelength around 700nm a thickness of at

least $10\mu\text{m}$ is needed. For a PIN photodiode this can be done easily by increasing the intrinsic zone. In a semiconductor process this is done by selecting the appropriate semiconductor wafer starting material (epi wafer).

4.5. COLOR DETECTION

Typical photodiodes can only detect light intensity, but have little or no wavelength sensitivity. Thus it is not possible to separate color information without additional techniques. In that work two approaches for color detection based on PIN photodiodes will be discussed:

- Color detection using optical filter layers
- Color detection due to the different penetration depths of light with different wavelengths in semiconductor materials

4.5.1. COLOR DETECTION WITH FILTER PATTERN

A classic approach is to use an array of photodiodes with a mosaic of tiny color filters placed over the photodiodes to capture color information. Each photodiode is covered with a certain filter and records one distinct color (Figure 4.12).

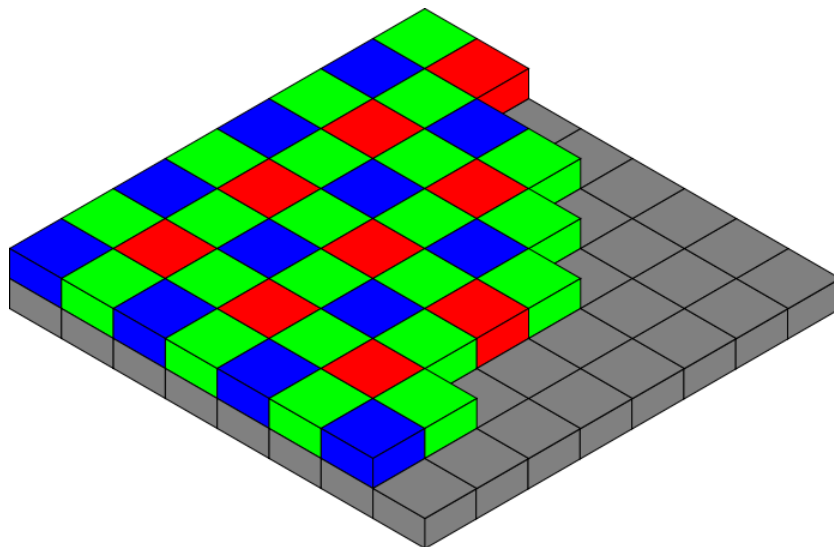


Figure 4.12 Bayer filter pattern [12]

The color filter is only transparent for a certain wavelength range. By combining different pixels with different color filters the information about the real color of light can be measured. The raw image data captured by the image sensor is converted to a full-color image by a demosaicing algorithm which is tailored for each type of color filter.

The typical Bayer color filter array shown in Figure 4.12 uses two green-filtered pixels for every red and blue one. The green photosensors are called *luminance-sensitive*

elements and the red and blue ones *chrominance-sensitive elements*. There are twice as many green elements as red or blue ones to mimic the human eye's greater resolving power with green light. The raw output of a Bayer filter camera is referred to as a *Bayer pattern* image. Since each pixel is filtered to record only one of the three colors, two-thirds of the color data is missing from each. To obtain a full-color image it is necessary to interpolate a set of complete red, green and blue values for each point (Figure 4.13).

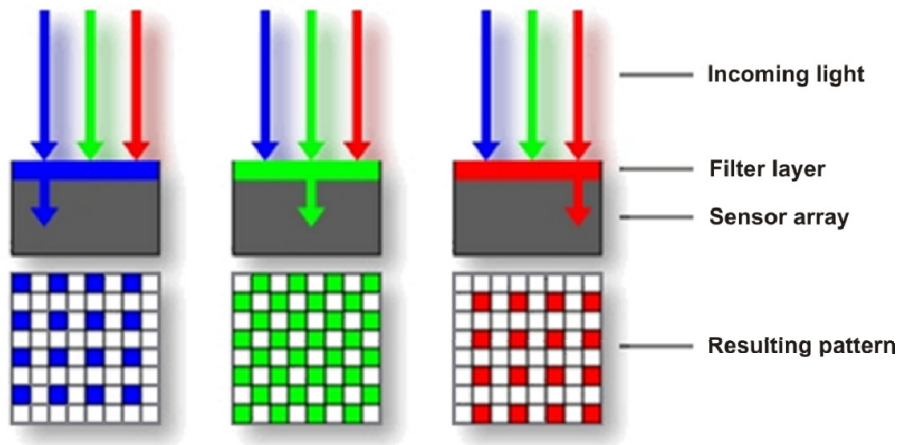


Figure 4.13 Profile/cross section of a Bayer mosaic sensor [12]

Different algorithms requiring various amounts of computing power result in varying-quality final images. This can be done in-camera, producing a JPEG or TIFF image, or outside the camera using the raw data directly from the sensor.

Although the Bayer filter type is almost universal on consumer products there are some alternatives like the RGBW filter (red, green, blue, white), the CYGM filter (cyan, yellow, green, magenta) and the RGBE filter (red, green, blue, emerald).

The basic idea of the RGBW filter is to increase the sensitivity to light of the image sensor by using some panchromatic cells sensitive to all wavelengths of visible light. In contrast to the original Bayer design, where the green pixels are used to recover most of the luminance information, in the RGBW design the panchromatic pixels are used to recover the luminance information. These panchromatic pixels are more sensitive than the green pixels, because none of the photons are filtered out. Figure 4.14 shows different patterns that can be used for a RGBW pixel sensor.

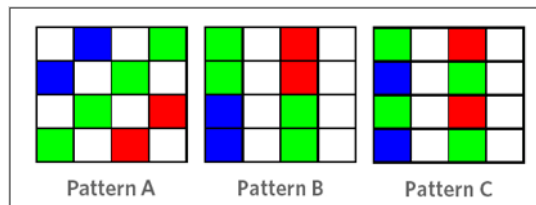


Figure 4.14 Different patterns that can be used [13]

Although color filter arrays are widely used (digital camera) they have some significant disadvantages. When considering the image quality vectors of sharpness and artifact control, the color filter array represents an inefficient use of silicon area because it is necessary to interpolate the color information from four pixels to obtain one full color pixel. Due to the sparse nature of sampling following is necessary:

- Interpolation of the missing color data to create three complete color image planes (RGB)
- Sharpening of the image to account for the inherent reduction in the sharpness of the luminance and chrominance
- Suppression of color aliasing artifacts resulting from incomplete sampling in the image plane and the phase offsets of the color channels.

To combat the third effect noted above, an optical blur filter, also known as an anti-aliasing filter, or an optical low-pass filter, is usually employed in consumer and professional digital cameras. Blur filters reduce the color aliasing artifacts caused by spatial phase differences among the color channels (i.e. the red, green, and blue filters are placed next to each other). Two blur filters are typically placed in the optical path: one to blur in the horizontal direction, the other in the vertical. The blur filters reduce color aliasing at the expense of image sharpness.

Fabricating these filters for large image sensors found in high end cameras is expensive. In the very low-end markets the costs of these blur filters are prohibitive and the current quality requirements are not such that these filters are used.

4.5.2. COLOR DETECTION BY PENETRATION DEPTH EFFECTS

The indirect bandgap of silicon makes the material semi-transparent. As light enters the sensor, it is absorbed to produce electron-hole pairs in proportion to the absorption coefficient α . High energy photons, those at the blue end of the spectrum, are absorbed near the surface whereas lower energy photons might penetrate deeper into the silicon substrate before they are absorbed. The optical power \bar{P}

$$\bar{P}(\bar{y}) = P_0 e^{-\alpha \bar{y}} \quad (4.18)$$

decreases exponentially as the light penetrates the silicon. Additionally the absorption coefficient decreases for increasing wavelength leaving only red and IR light to penetrate beyond a few μm . The penetration depth δ is defined by:

$$\delta = \frac{1}{\alpha} \quad (4.19)$$

Silicon has an absorption curve that varies by nearly two orders of magnitude over the visible range (Figure 4.17). This variation provides sufficient room to stack multiple diode junctions at different depths. These are capable of separating photons of different wavelengths. Additionally such a diode is amenable to fabrication using standard (Bi)CMOS manufacturing processes.

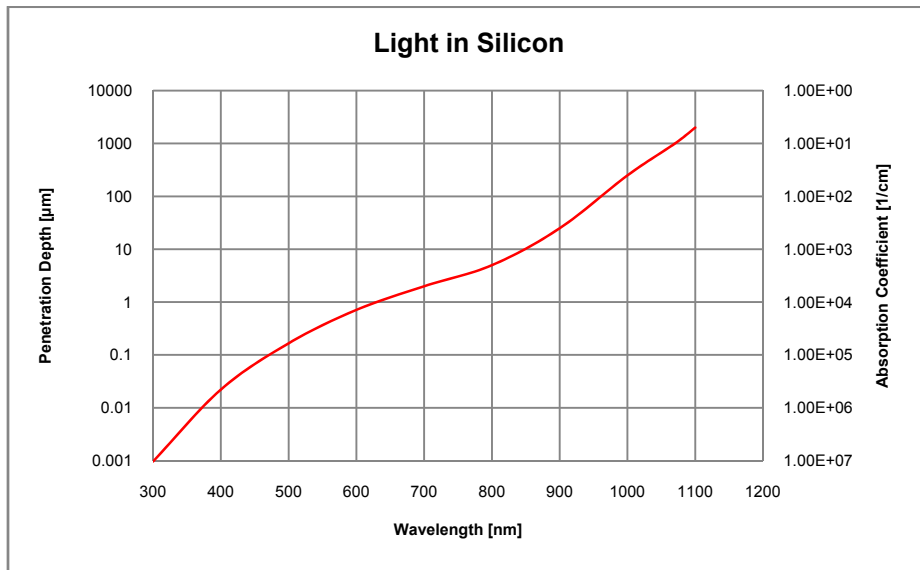


Figure 4.17 Spectral light absorption in silicon [17]

The idea is to use an array of pixels, where each pixel consists of three vertically stacked photodiodes. This array can be organized in a two-dimensional grid. Each of the three stacked photodiodes responds to different wavelengths of light due to the different penetration depths. The signals from the three photodiodes are processed. The resulting data provides the three additive primary colors red, green and blue.

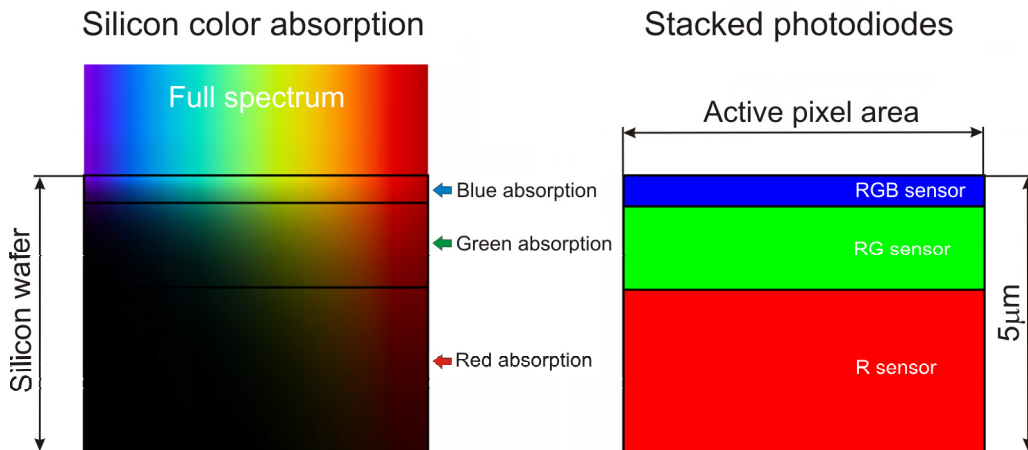


Figure 4.18 Color absorption in silicon and the vertical color sensor

Figure 4.18 shows the absorption of colors of the full spectrum according to their wavelengths as it passes through the silicon wafer. The right side shows a schematic drawing of a sensor that absorbs first the blue wavelength photons as the incident light enters the device, then the green photons, and finally the red photons at the deepest layer [18].

The benefit of this pixel sensor is the direct measurement of red, green and blue light at each location. Stacking color pixels one on top of another increases the sampling density in the image plane. This results in improved sharpness for luminance and chrominance as well as in a lack of color aliasing artifacts.

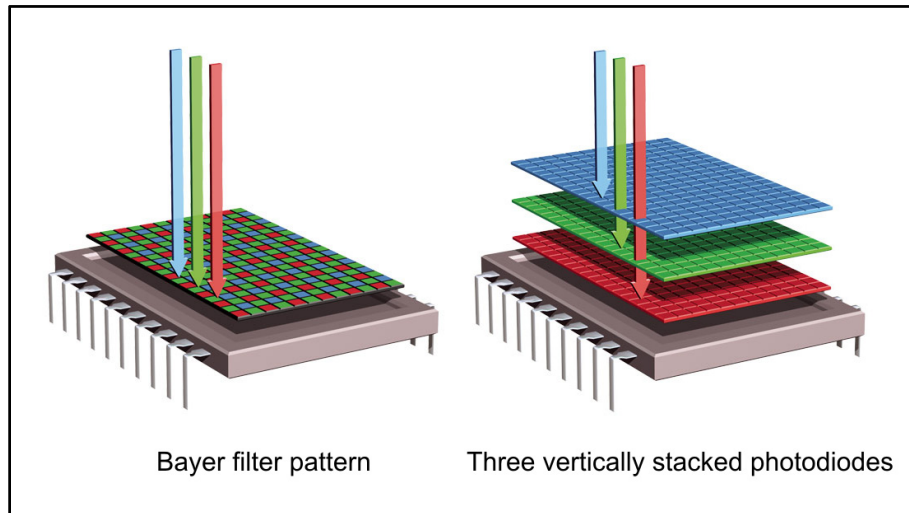


Figure 4.19 Bayer filter pattern vs. vertical image sensor [19]

Figure 4.19 shows the difference between a conventional Bayer filter pattern and a vertical image sensor. While the color information generated by the Bayer filter pattern has to be interpolated to create three complete color planes, the vertical image sensor creates the full color information for every pixel. Thus results in improved sharpness and avoids color aliasing artifacts resulting from the incomplete sampling of the image data.

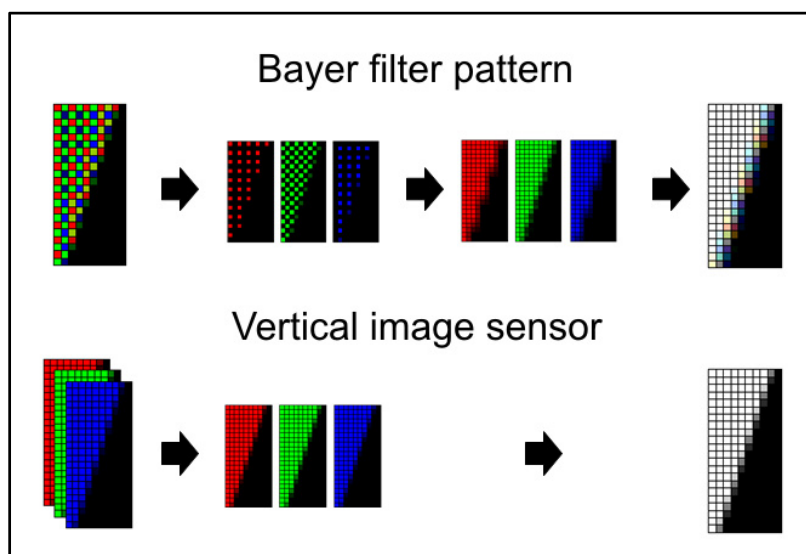


Figure 4.20 Edge detection – Bayer filter pattern vs. vertical image sensor

Figure 4.20 shows the reproduction of a sharp edge between a white and a black area. It can be seen, that there is a color aliasing resulting from incomplete color data and interpolation if using a Bayer filter pattern. The vertical image sensor captures the whole color information in every pixel and so interpolation is not necessary which results in a sharp picture without any aliasing effects.

5. PHOTODIODE DESIGN

For the design of color sensitive photodiodes two different concepts are used. One idea is to use the different semiconductor layers as color filters, which are available by default in the standard X-FAB 0.6 μm BiCMOS process. The other idea is to use the different penetration depths of light with different wavelengths in silicon. The benefit of these two concepts is that the color sensitivity can be achieved without any additional color filters or additional production steps. Therefore no additional costs are generated by the realization of color sensitive photodiodes. In this work all designed color sensitive photodiodes are based on the standard X-FAB 0.6 μm BiCMOS optical PIN diode with an active photodiode area of 100x100 μm^2 . Figure 5.1 shows the principle stack of the PIN diode. The diodes are designed with the Cadence Design System Virtuoso which is an electronic design automation (EDA) software for full-custom integrated circuit design. The Virtuoso platform includes tools for schematic entry, behavioral modeling, circuit simulation, full custom layout, physical verification, extraction and back-annotation.

5.1. X-FAB 0.6 μm BiCMOS OPTICAL PIN DIODE

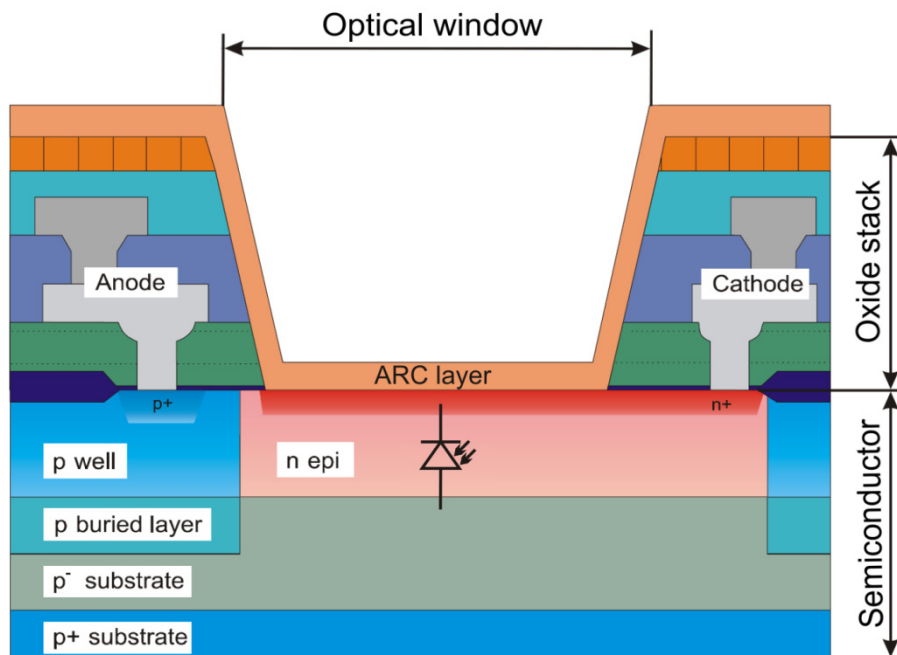


Figure 5.1 Optical PIN diode [20]

The X-FAB 0.6 μm BiCMOS process is based on a silicon wafer (epi wafer). The anode of the PIN diode is composed of the p-substrate which is contacted by the p-buried/p-well/p⁺-structure. The thin n⁺-layer near the semiconductor surface acts as the cathode. The n-epi and the p⁻-substrate acts as the intrinsic layer of the photodiode. On the top of

the semiconductor lies a stack of different oxide layers which results from the different production steps. To prevent loss of the incident light resulting from reflection and absorption at the different oxide layers, an optical window is etched through the oxide stack. To reduce the losses of the incident light by reflection on the surface of the semiconductor (due to the different refraction indexes of the semiconductor \bar{n}_{SC} and the surrounding air \bar{n}_S) an anti-reflection-coating ARC with the thickness d_{ARC} (4.14) and the refraction index \bar{n}_{ARC} (4.15) is applied on the semiconductor surface. For a cross section of a diode with an optical window etched through the oxide-layer and an ARC layer see Figure 5.2.

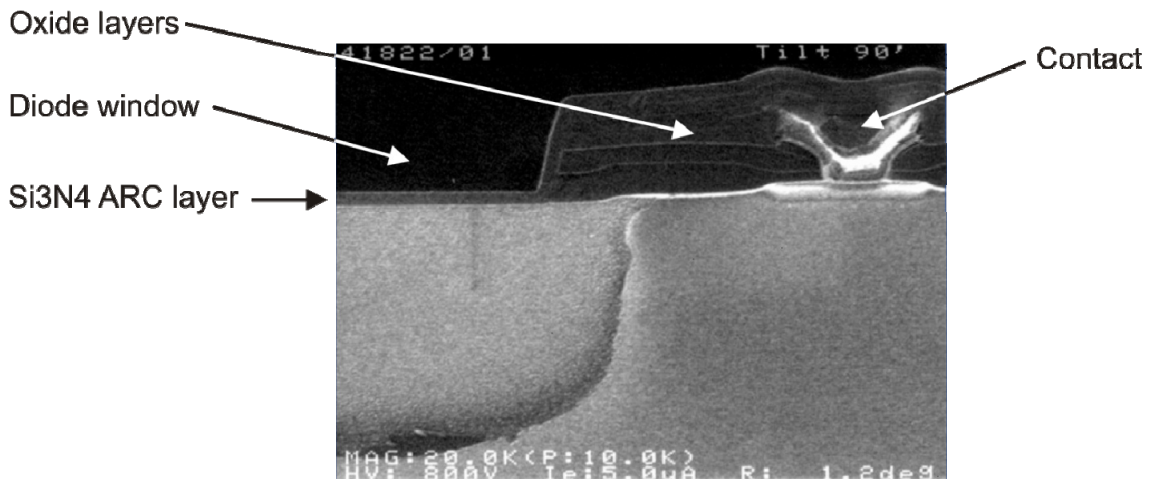


Figure 5.2 Cross section of diode window edge with ARC [17]

Figure 5.3 shows the engineering drawing of an optical PIN diode in the Virtuoso layout editor which is part of the Cadence design system.

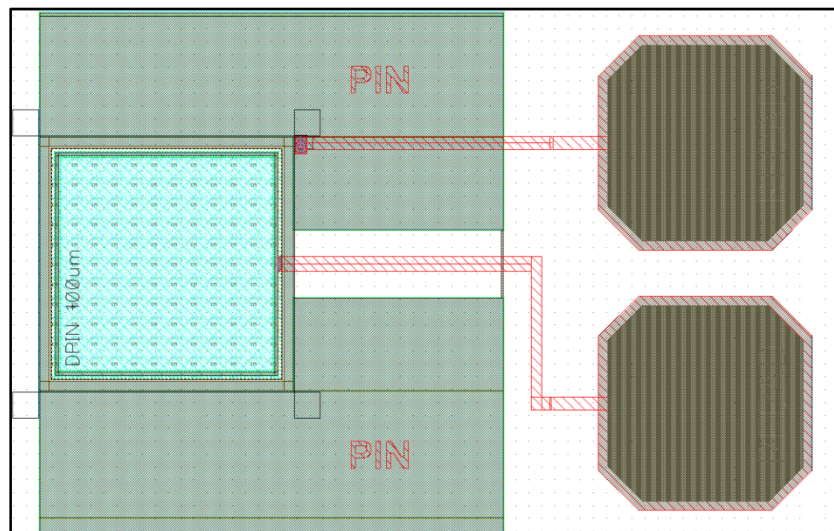


Figure 5.3 Optical PIN diode in the Virtuoso editor

On the left side is the diode with the optical window (red) and the different layers placed. The two dark brown spots on the right side are pads, needed to contact the diode for instance with a bond wire. The grey area around the diode is a metal layer to avoid light irradiance into the semiconductor beside the active diode area. This is necessary to prevent unwanted carrier diffusion.

5.1.1. DOPING PROFILES

The fastest photodiode is a construction where all carriers are generated inside the SCR, inside the electric field E . This can be realized by using a very low doped intrinsic zone (formed by n-epi and p⁻substrate layer). The anode (high doped p⁺-substrate) should be deeper than the penetration depth of light to ensure that only a small amount of charges are generated in the high doped anode (diffusion).

This can be realized in conventional BiCMOS technology using a 15μm thick epi layer waver with a doping concentration of approximately $1e^{13}cm^{-3}$ as intrinsic layer. Below the epi layer is the highly doped bulk substrate with a doping concentration of $1e^{18}cm^{-3}$ [17]. The bulk acts as anode while the n⁺ diff (BiCMOS process step) acts as cathode. The doping profiles, the depletion width and the relevant light penetration for wavelengths up to 900nm can be seen in Figure 5.4.

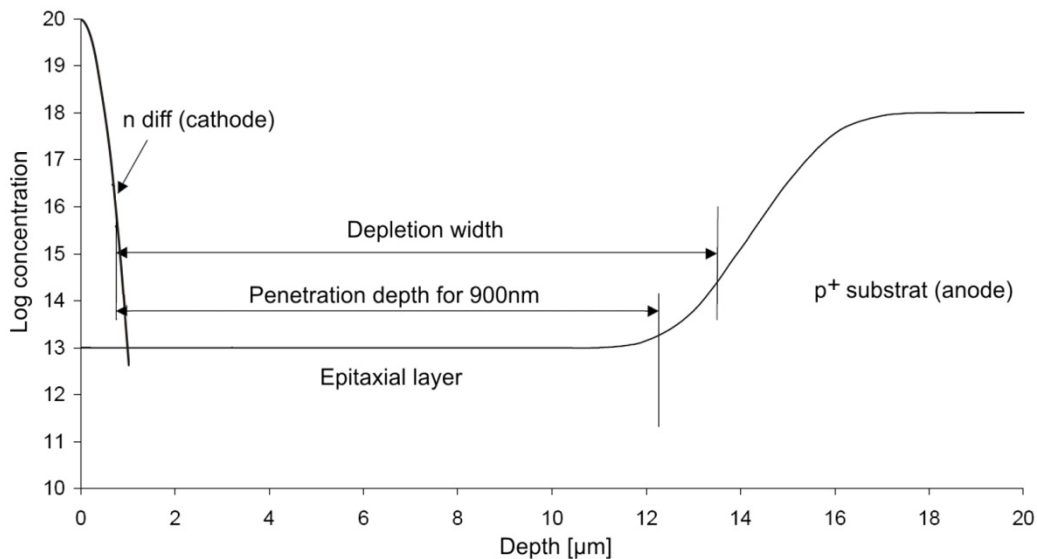


Figure 5.4 N-I-P Diode profiles, depletion width and light penetration

5.2. FILTERING EFFECTS

The basic idea is to modify the standard X-FAB PIN photodiode (Figure 5.1) with different additional layers, available by default in the X-FAB 0.6μm process. These layers are placed between the n⁺ layer on the surface of the semiconductor and the ARC layer (Figure 5.5). The color sensitivity should be achieved by the different optical

absorption properties of the added layers. Depending on the wavelength of the incident light a part of the light is absorbed in the additional layers. The remaining light passes the filter and penetrates into the semiconductor where electron-hole pairs are generated. This causes a photocurrent which is proportional to the light which is not absorbed by the extra layers. Following layers are used for this purpose:

- Oxide layers (no optical window etched)
- Polysilicon layer 1
- Polysilicon layer 2

Combinations of the different layers are possible to create additional different optical properties. Also feasible are mixed structures consisting of an array of small diodes with different filter layers. Every second diode for instance could have an additional layer as color filter while the other diodes are standard PIN type. This would result in different color sensitivities for the two different diode types (like a filter patter).

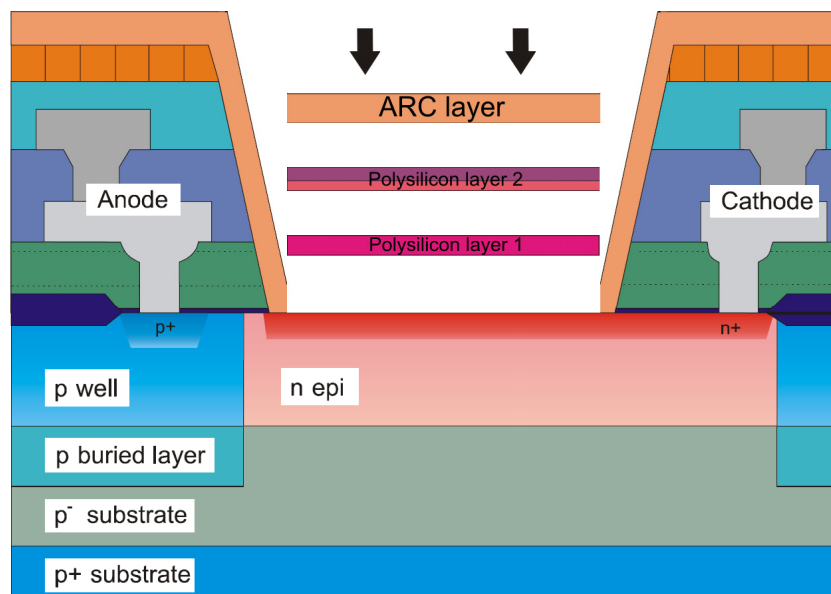


Figure 5.5 Additional layers of the BiCMOS process as color filters

5.2.1. OXIDE LAYERS AND SILICON NITRIDE AS COLOR FILTER

Before the light gets into the silicon it has to penetrate the different coating layers which are grown or deposited intentionally for insulating the different interconnection levels (metals) and for passivating the chip against environmental and mechanical influences. These layers might consist of different kinds of silicon oxide (thermally grown, deposited, spun-on), silicon nitride or mixtures of them.

These layers are basically transparent for light in the visible and near infrared (IR) range. Only silicon nitride is known for its absorption in the ultraviolet (UV) range. Figure 5.6 shows the spectral light absorption in silicon nitride.

5. Photodiode Design

Therefore it can be assumed that a photodiode with a complete oxide stack is less sensitive for light in the UV regime than for light in the visible and near IR range.

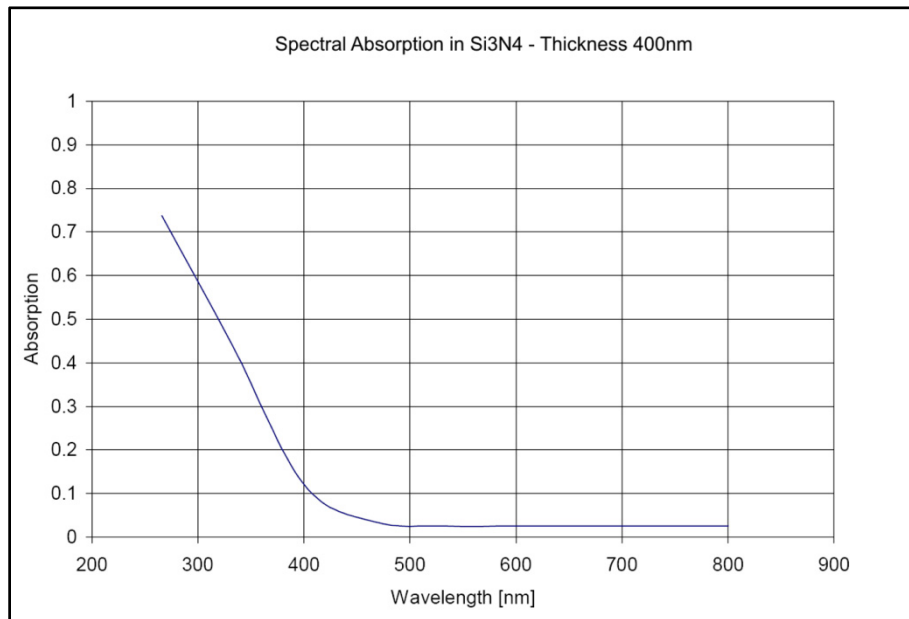


Figure 5.6 Light absorption in silicon nitride [17]

Figure 5.7 shows a schematic cross section of a PIN photodiode without an optical window etched through the different oxide layers.

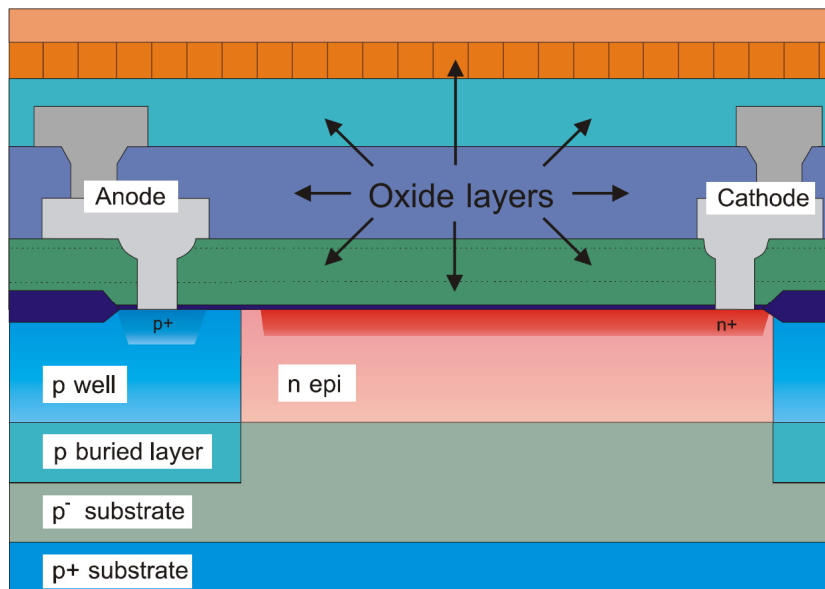


Figure 5.7 PIN photodiode without optical window

5.2.2. POLYSILICON LAYER 1 AS COLOR FILTER

Another attempt is to use the polysilicon layer 1 as color filter. The polysilicon layer 1 is green colored which can be seen under the microscope. Therefore it can be expected that light in the blue-green regime is absorbed/reflected more than in the red regime. Figure 5.8 shows a cross section of the diode.

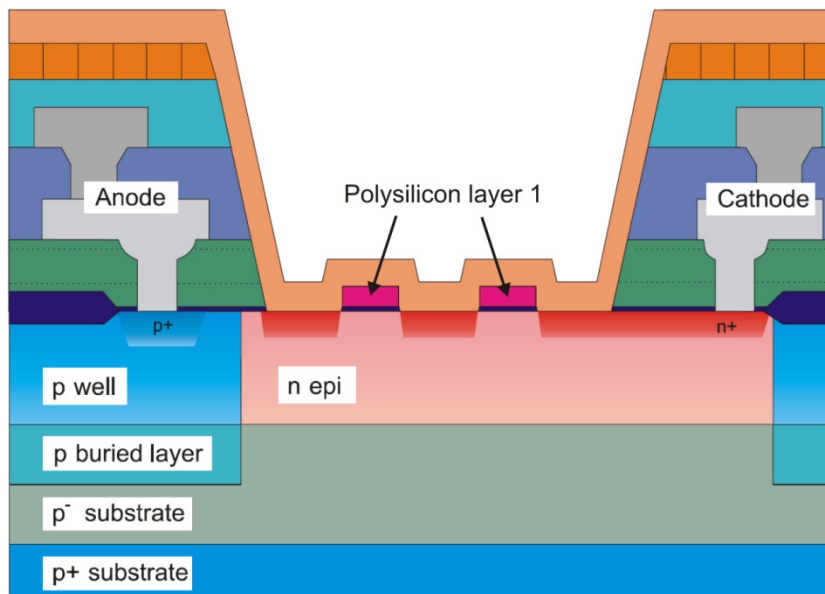


Figure 5.8 Photodiode with polysilicon layer 1

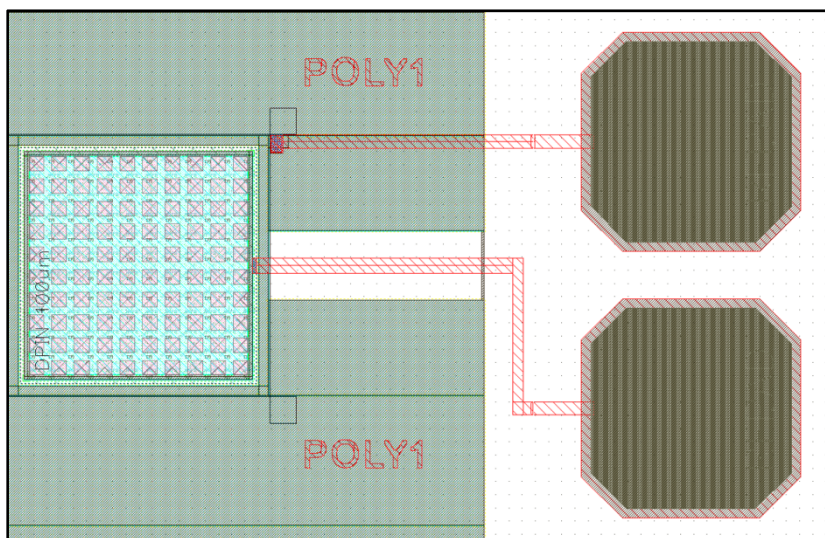


Figure 5.9 Polysilicon layer 1 grid structure

The polysilicon layer 1 is applied on the semiconductor surface some production steps previous to the n^+ layer. This is due to the fact that the polysilicon layer 1 is used as gate for MOS transistors. By processing the gate earlier than the n^+ (source and drain areas)

the so called self adjusting MOS transistor process is realized. Thus it is necessary to apply the polysilicon layer 1 in a dot structure to make an n^+ implant grid possible. This grid structure can be seen in the cross section (Figure 5.8) and in the technical drawing of the diode (Figure 5.9).

5.2.3. POLYSILICON LAYER 2 AS COLOR FILTER

For this photodiode the polysilicon layer 2 is used to achieve wavelength-dependent color sensitivity. The polysilicon layer 2 is applied in a later production step than the n^+ layer implant and therefore it is not necessary to use a dot structure as for the polysilicon layer 1 (Figure 5.10).

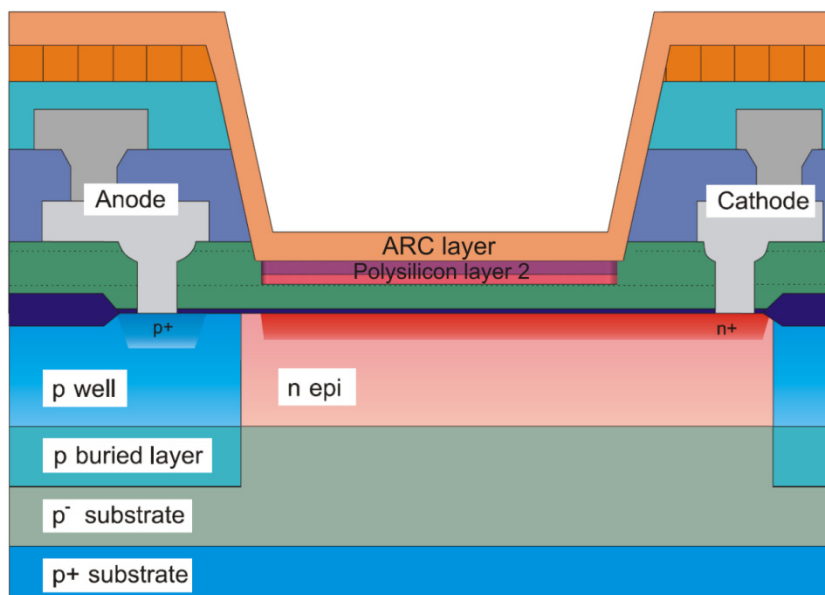


Figure 5.10 Photodiode with polysilicon layer 2

In Figure 5.10 it can be seen that there is an oxide layer between the n^+ implant and the polysilicon layer 2. This is due to the different production steps of the photodiode and cannot be avoided. It's a matter of fact, that there is an additional absorption of light in this oxide layer which cannot be prevented.

5.2.4. POLYSILICON 1 AND POLYSILICON LAYER 2 AS FILTER

In this construction both polysilicon layers are used. The polysilicon layer 1 is again carried out in a dot structure to make the implant of the n^+ layer possible. The polysilicon layer 2 on the other hand is applied over the whole photodiode area. This is possible because the polysilicon layer 2 is brought up after the n^+ layer is implanted. Again it is not possible to avoid a thin oxide layer between the polysilicon 1 and the polysilicon layer 2 which is caused by the different production steps.

It is expected that the addition of the two polysilicon layers causes a stronger absorption in the blue-green regime than one polysilicon layer alone.

Another interesting point is the higher absorption of the incident light as a consequence of the multiply layers. A cross section of this photodiode is shown in Figure 5.11.

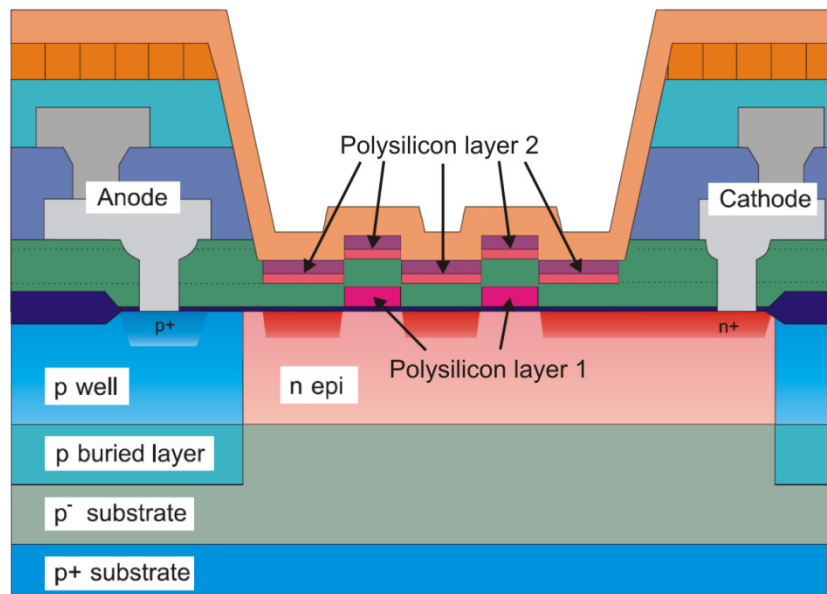


Figure 5.11 Photodiode with polysilicon 1 and polysilicon layer 2

5.2.5. MIXED STRUCTURES

For an integrated color sensitive detector it will be necessary to include more than one type of diodes into one sensor. This is due to the fact that the absolute value of the incident light has to be compared with the signal of a filtered photodetector. From the absolute value of the photodiode currents the total incident power can be calculated. From the difference of the filtered and unfiltered photodiode currents it is possible to estimate the spectral distribution. This only works if both (or more) different photodetector types are illuminated with the same power. To get an easy useable color-sensitive detector it will be necessary to design a dense array of different photodetectors so that with one spot of light an equal (and large) number of different photodetectors can be illuminated.

The idea is to integrate different diode types into a single detector. Figure 5.12 shows small PIN diodes alternating with polysilicon layer 2 diodes in an array. The normal PIN type diodes are used to detect the whole spectrum of the light, while the diodes with the polysilicon layer 2 can only detect the light in the red and IR range.

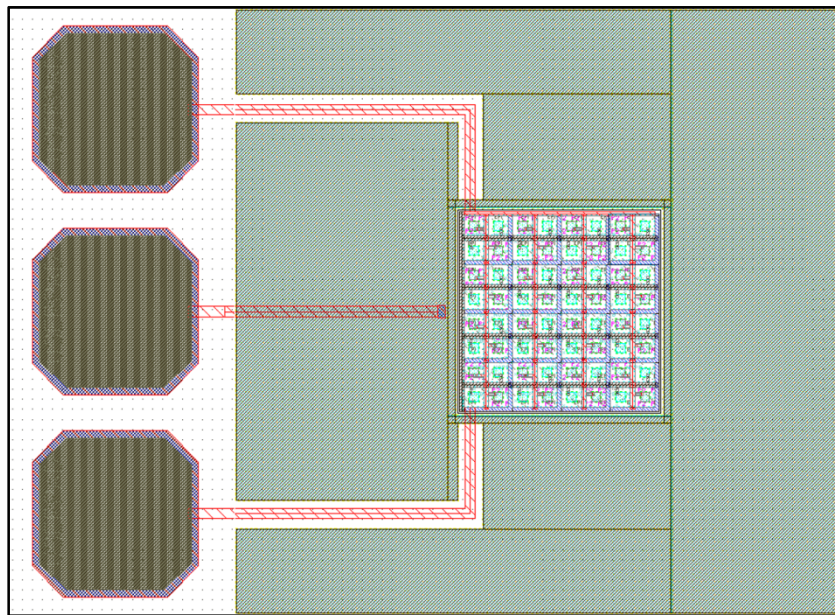


Figure 5.12 Mixed photodiode

As seen in Figure 5.12 the mixed diode has three contacts – one for the cathodes of the normal PIN diodes, one for the cathodes of the polysilicon diodes and one combined for the anodes of both diode types. Therefore it is possible to measure two photocurrents – one represents the light of the whole spectrum while the other only represents the light in the red and IR regime.

The two different diode types and their interconnections can be seen in the detailed view of the diodes array in Figure 5.13.

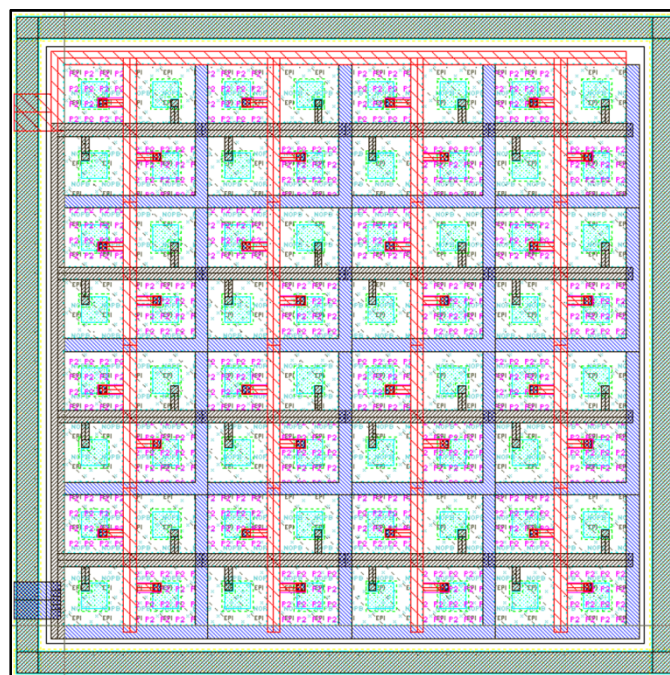


Figure 5.13 Detail of a mixed photodiode

5.3. PENETRATION DEPTH EFFECTS

The silicon bandgap of 1.12eV and the band structure cause the typical absorption/penetration behavior shown in Figure 4.17. Light with short wavelength is absorbed near the semiconductor surface while light with long wavelength can penetrate deep into the semiconductor until it is completely absorbed. Therefore light in the blue regime generates electron-hole pairs near the surface while light in the red and IR regime generates electron-hole pairs also deep in the semiconductor. This effect is used to design a color sensitive photodiode.

Figure 4.17 shows that light with 400nm wavelength only penetrates silicon about 300nm until it is absorbed. To detect light with such short wavelengths one photodiode with a very thin depletion region is placed directly under the surface of the semiconductor.

To detect light in the red and IR range another photodiode is placed in the depth of the semiconductor. As shown in Figure 4.17, light with 850nm wavelength is absorbed in a depth of around 20 μm . Therefore a thick depletion region is necessary for the second diode. A schematic drawing of this diode is shown in Figure 5.14. The thickness of the p⁻ substrate is not to scale. The depth of the n⁺ buried layer is about 1 μm and the depth of the p⁺ substrate is around 18 μm .

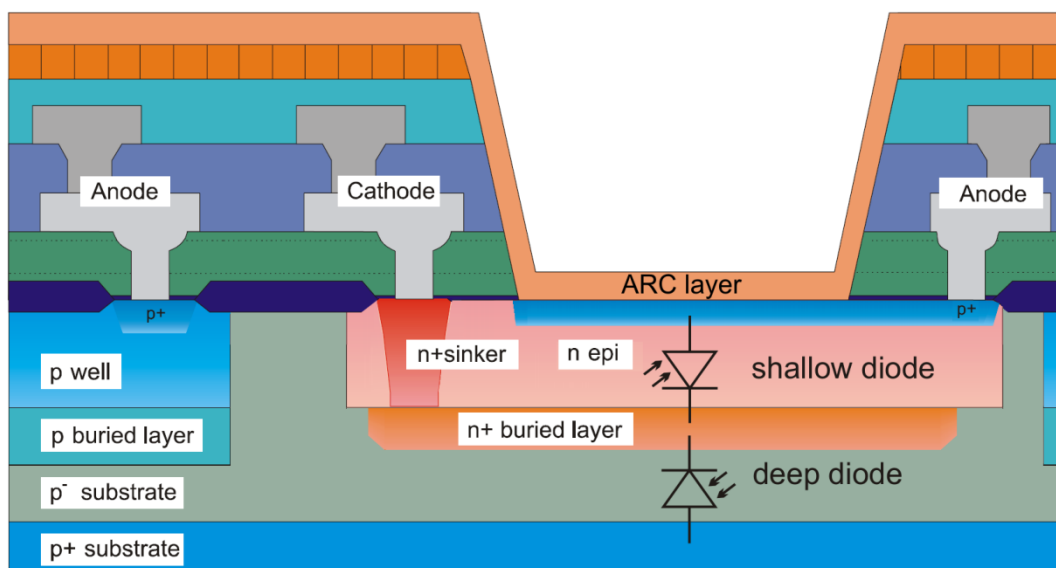


Figure 5.14 Penetration depth effect diode

The shallow diode is situated between the p⁺ implant and the n⁺ buried layer while the deep pn junction is between the n⁺ buried layer and the substrate of the semiconductor. Both diodes have their own anode while the cathode is shared.

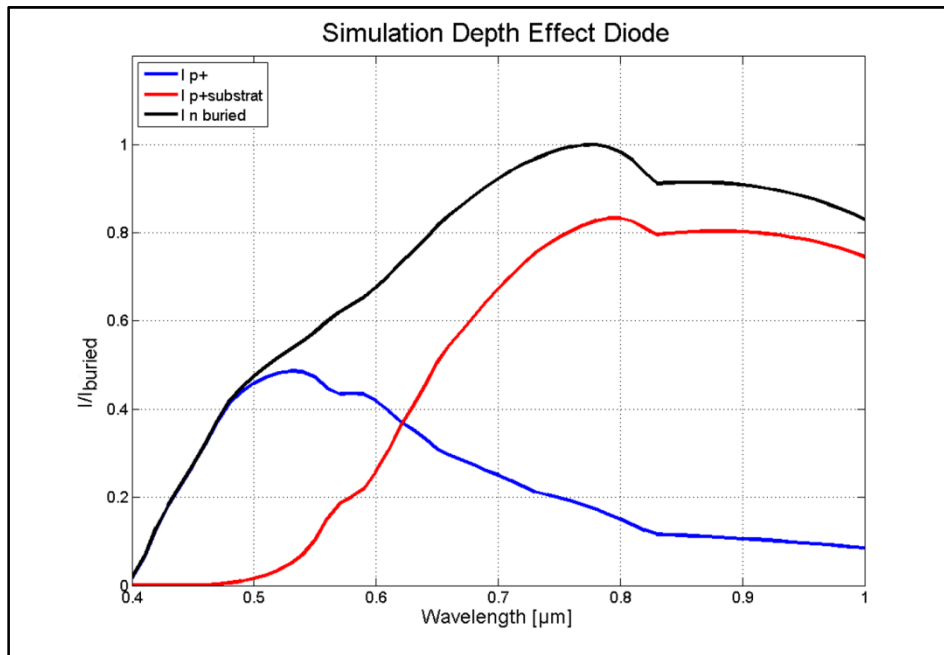


Figure 5.15 Medici simulation depth effect diode

Figure 5.15 shows a Medici simulation of the two vertical pn junctions in the depth of the semiconductor. The blue graph represents the anode current I_{p+} of the shallow diode while the red graph shows the anode current $I_{p-substrat}$ of the deep diode. The black graph displays the current I_n buried of the shared cathode. It can be seen that I_{p+} and $I_{p-substrat}$ are wavelength dependent – light with shorter wavelengths mainly generates a photocurrent in the shallow diode while light with longer wavelengths causes a current in the deep diode. The wavelength of the incident light can be determined by the ratio of the two anode currents.

6. MEASUREMENT SETUP

To characterize the color sensitivity of different photodiodes it is necessary to measure the responsivity curves of the diodes. Therefore an adequate measurement setup was developed. For each diode the wavelength of the incident light is stepped from 400 to 900nm and the light power and the corresponding generated photocurrent is measured for each wavelength. The responsivity curves can be calculated to compare the different diodes.

The measurement setup consists of several parts:

- Light source
- Monochromator
- Fiber optic beam splitter
- Optical power meter
- Electrometer
- Wafer prober

These components are connected together and the complete measurement is controlled by a LabVIEW program.

6.1. ASB-XE-175 XENON LIGHT SOURCE

As light source a 175W short-arc xenon (Xe) lamp which provides a broadband output from 250nm to 1200nm is used. Xe is generally used as light source for ultraviolet (UV), visible and near infrared (NIR) light. The spectrum curve in visible range is relatively flat compared to other light sources (Figure 6.1).

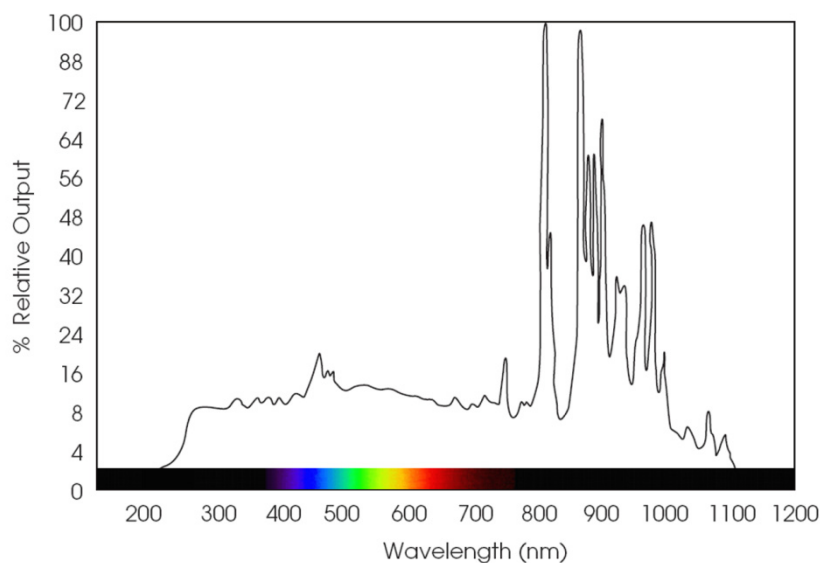


Figure 6.1 Output spectrum xenon lamp [21]

6. Measurement Setup

The CERMAX[®] LX175F xenon lamp is compact, rugged and its efficiency is enhanced by an integral parabolic reflector which provides precision system alignment and maximum transition of light energy. Figure 6.2 shows the xenon lamp placed inside heat sink and housing.



Figure 6.2 CERMAX[®] LX175F xenon lamp

Beam stability is reached instantly following lamp ignition without an imposed time delay [21]. The brightness of the light source can be controlled from 0 – 100%. Figure 6.3 shows the light source with the optical output on the left side, the brightness control in the middle and the main power switch on the right side.



Figure 6.3 ASB-XE-175 xenon light source

Figure 6.4 shows a view into the glowing xenon lamp. In the front the mounting bracket and the front cathode can be seen. The electric arc of the lamp burns between the front

cathode and the rear cathode which is mounted in the middle of the reflector. Thus the electric arc cannot be seen in this picture directly – only its reflection can be seen. There are two bright spots on the reflector – one brighter on the upper side and one below the center of the reflector. This is important when coupling the light of the source into the monochromator, because the entrance slit of the monochromator is many times smaller than the reflector area. Dependent on the position of the entrance slit relative to the xenon lamp more or less light is coupled into the monochromator. Therefore it seems useful to move the entrance slit to the brightest area of the lamp. Unfortunately is the brightest light spot in the lamp not very stable – there is jitter in the light power due to the thermal convection of the xenon gas inside the lamp. Thus it turned out that it is better to place the entrance slit of the monochromator to the bright area below the cathode attachment. Of course less optical power is coupled into the monochromator at this spot, but instead the light is a lot more stable which is important for the measurements.



Figure 6.4 View in the glowing xenon lamp

6.2. DIGIKRÖM CM110 MONOCHROMATOR

A monochromator acts as tunable bandpass filter for light. In combination with a broad-band light source it can be used to create a tunable light source. It can be used to isolate a narrow spectral radiation out of the spectral range of the source. This is needed for spectral measurements like the characterization of color-sensitive photodiodes.

The used monochromator is based on a Czerny-Turner with a dual grating turret. It has a focal length of 110mm and an f-number of 3.9. It is equipped with a standard RS232 interface and is controlled by easy-to-use software. It is also possible to write alternative software in Visual Basic[™], Visual C++[™] or LabVIEW. The monochromator is shown in Figure 6.5.



Figure 6.5 Digikröm CM110 [22]

The isolation of a narrow spectral radiation is accomplished by a dispersive element such as a grating together with a scanning mechanism. Figure 6.6 shows the functional principle of a grating monochromator.

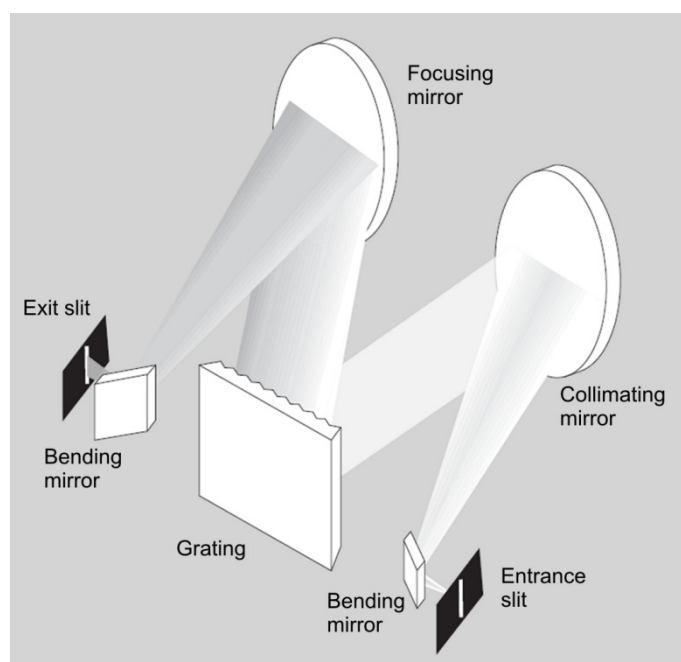


Figure 6.6 Functional principle of a monochromator [22]

6.2.1. GRATING FUNDAMENTALS

Gratings use a unique dispersion phenomenon to spread a spectrum of light in space by wavelength. A reflective diffraction grating has microscopic periodic corrugated

6. Measurement Setup

structure (grooves) embedded on a substrate material. The series of parallel grooves are spaced at about the wavelength of light. The grating surface is usually coated with metal for high reflectivity.

Interaction of light with a grating possessing grooves in the same size of the radiation wavelength exhibits diffraction. Light reflected from the grating surface is diffracted by the grooves. Monochromatic light incident on a reflective grating is diffracted first and then undergoes a destructive interference in most directions resulting in a cancellation at these angles. It is only along certain finite number of direction that rays from grooves survive as a result of constructive interference. These directions are termed as diffraction orders [22]. The light strikes the grating at an incident angle α and is then diffracted at an angle β (Figure 6.7).

If you want to see this phenomenon in a practical example, simply flip out the CD at the end of this work and put it with its plain side on top of a table. When you now look at the CD from different angles, the CD seems to change its color. This is due the diffraction of light on the CD surface.

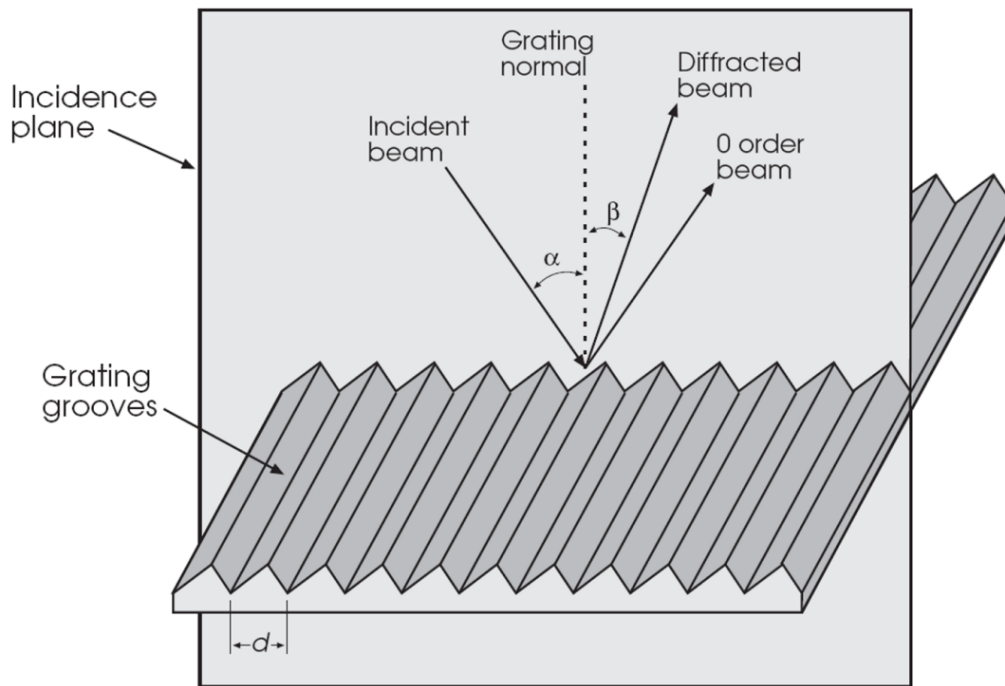


Figure 6.7 Diffraction grating [22]

When defining integer m as the diffraction order and d as groove spacing, maximum constructive interference occurs under the condition:

$$m\lambda = d(\sin \alpha + \sin \beta) \quad (6.20)$$

Several important characteristics are revealed by the above grating equation:

- For a given diffraction angle α , several values of λ may satisfy the equation for different orders m . First order radiation ($m=1$) of 900nm shares the same diffraction angle with second order 450nm or third order 300nm radiation.

- The diffraction order m may carry a sign of either positive or negative to reflect the fact that the incident light may be diffracted on either side of the grating normal.
- If parallel rays, carrying multiple wavelength components, fall on the grating, each wavelength within the same order will have a distinctive value of β determined by the grating equation. Consequently, a polychromatic light is spatially dispersed.

6.2.2. GRATING CHARACTERISTICS

Gratings are primarily characterized by their groove density and blaze wavelength. For example a 1200 x 300 grating would have a groove density of 1200 grooves per millimeter and a blaze wavelength at 300nm.

Groove Density

The groove density, groove frequency or pitch of a grating \bar{G} in gr/mm is defined as the reciprocal of groove spacing d .

Blaze Wavelength

Shaping individual grooves can alter the distribution of light into different orders. The optimization of groove profile to maximize grating efficiency in a certain spectral region is often referred to as blazing. The maximum grating efficiency occurs at the blaze wavelength.

Grating Efficiency

Grating efficiency is expressed as the ratio between monochromatic light diffracted into a given order and the incident monochromatic radiation. Figure 6.8 shows a typical grating efficiency curve.

Grating Type

Commercially available gratings are manufactured by processes including ruling, replication and holographic methods. Ruled gratings are mechanically ruled with a diamond-ruling engine on a surface coated with thin metal. Replicated gratings are produced by the replication of a master diffraction grating. Ruled and replicated gratings typically have grooves in a triangle format. The production of holographic gratings involves the photographic recording of laser generated interference patterns. Holographic gratings usually contain sinusoidal shaped grooves.

Reflective Coatings

Aluminum is primarily used as the reflective material for gratings throughout UV, visible and NIR regions. Protected aluminum coating is more resistant to oxidation, thus it is more suitable for UV use. For near infrared and infrared applications, gold coating demonstrates superior reflectance performance over aluminum.

Resolving Power

The resolving power of a grating R is the measure of its ability to separate two close wavelength lines. It can be expressed as the product of the diffraction order m and \bar{N} , the number of grooves being illuminated by the incident radiation:

$$R = m \cdot \bar{N} \quad (6.21)$$

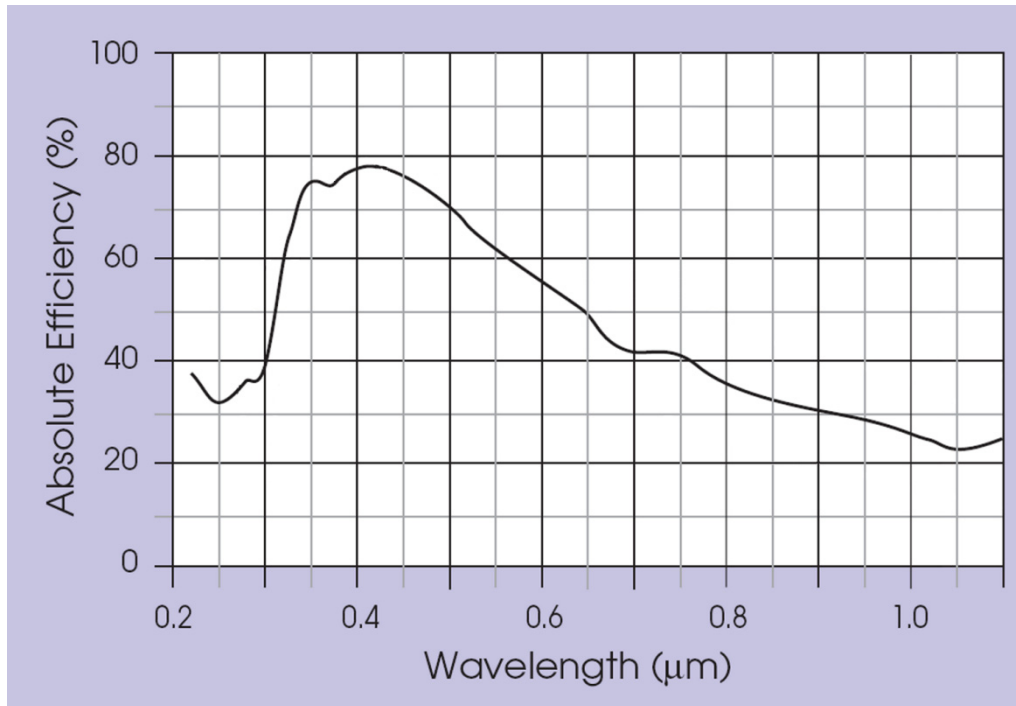


Figure 6.8 Grating efficiency curve [22]

6.2.3. MONOCHROMATOR CHARACTERISTICS

A grating (Czerny-Turner) monochromator consists of the following key components:

- Entrance slit
- Collimating/focusing optics
- Grating dispersing element
- Exit slit
- Driving mechanisms

A monochromator is a one-to-one imaging system in which the image of the entrance slit appears at the exit for each wavelength passed through the instrument. If the incident radiation is a continuous source, infinite series of overlapping monochromatic images of the entrance slit are found at the exit slit focal plane. Figure 6.9 shows the optical path of a Czerny-Turner monochromator.

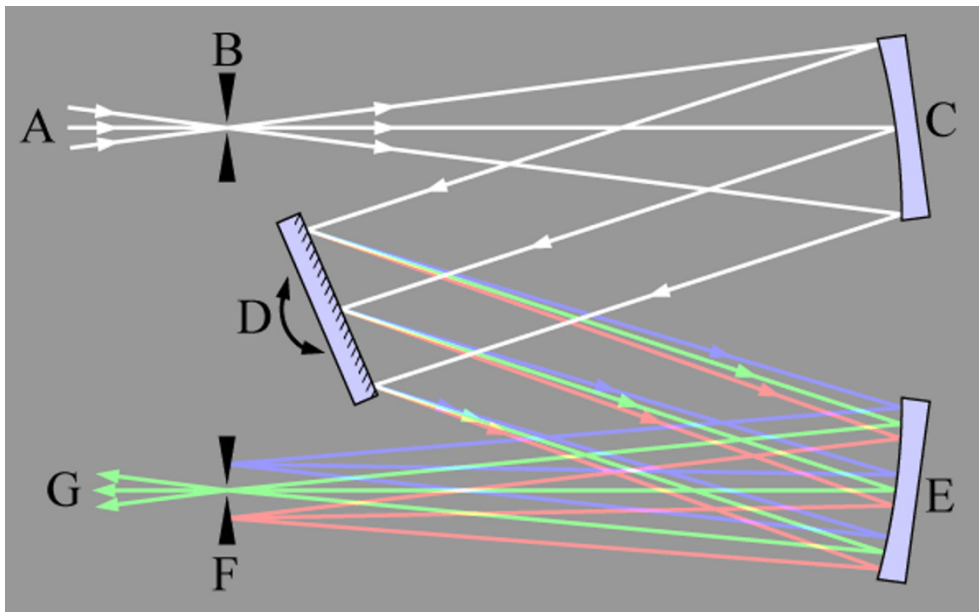


Figure 6.9 Optical path Czerny-Turner monochromator [23]

The incident radiation consisting of three wavelength components enters through an entrance slit, forms a narrow optical image, and is then directed to a collimating mirror. The collimating mirror produces a parallel beam and projects it onto the grating. The grating disperses the radiation into its component wavelengths at different angles in the plane of incidence. Then the focusing mirror reforms the image (of the slit) and focuses it on a focal plane. The exit slit isolates the desired spectral band by spatially discriminating against the unwanted bands as shown. Mechanical rotation of the grating about its vertical axis scans the images through the exit slit. In Figure 6.10 a Czerny-Turner with three different gratings can be seen.

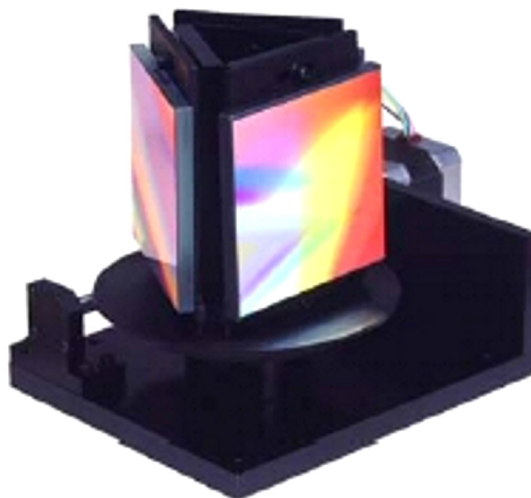


Figure 6.10 Triple grating turret of a Czerny-Turner [24]

Resolution

The Resolution of a monochromator is its ability to separate two close together spectral lines. For a fully illuminated grating, the resolution is given by the following equation:

$$\Delta\lambda = \frac{\lambda}{N} = \frac{\lambda}{W_g \cdot d} \quad (6.22)$$

where W_g is the grating width in mm.

Grating Equation

The grating equation describes the relationship between the angle of the grating and the output wavelength of a Czerny-Turner monochromator:

$$\lambda = \frac{(2 \cos \frac{\phi}{2}) \sin \theta}{m \cdot G} \quad (6.23)$$

where ϕ is the full Ebert angle. This is a fixed angle determined by the position of the grating, the collimating mirror and the focusing mirror. It is approximately 25.4° for the CM110.

θ is the angle that the grating rotates measured from the point at which white light is specular reflected through the instrument. The maximum angle is 70° for the CM110 [21].

Etendue and Transmission Efficiency

The percentage of light that can be sent from a light source through a monochromator would be a desirable measure of its throughput. Unfortunately, the properties of sources vary so much that this measure would not provide a useful standard. Instead, two separate specifications are useful:

- Etendue - a measure of the degree of coupling that can be achieved
- Transmission efficiency - a measure of how much of the input light exits the monochromator.

The etendue \bar{E} of an instrument is the product of the physical aperture in cm^2 and its angular aperture in steradians [22]:

$$\bar{E} = \frac{S_w \cdot S_h \cdot W_g^2}{F^2} \quad (6.24)$$

For a source of given brightness the maximum power in watts that can be coupled into the monochromator is the product of the brightness and the etendue.

The transmission efficiency \bar{T} describes the light loss within the spectrometer:

$$\bar{T} = R_m^N \cdot R_g \quad (6.25)$$

Where R_m is the reflectance of a single mirror, N the number of mirrors and R_g is the diffraction efficiency of the grating.

f-number

The f-number is defined as the ratio of diameter and focal length of an optic. It is a measure of the acceptance angle of an optical instrument. The f-number is a useful concept in judging optimum coupling between monochromators and sources. When the f-numbers are matched, the full aperture of the monochromator will be utilized.

Bandpass

Bandpass is the wavelength band exiting the monochromator at given wavelength and at given slit width. Figure 6.11 shows the measured relationship between the output light bandwidth and the slit width of the CM110 monochromator.

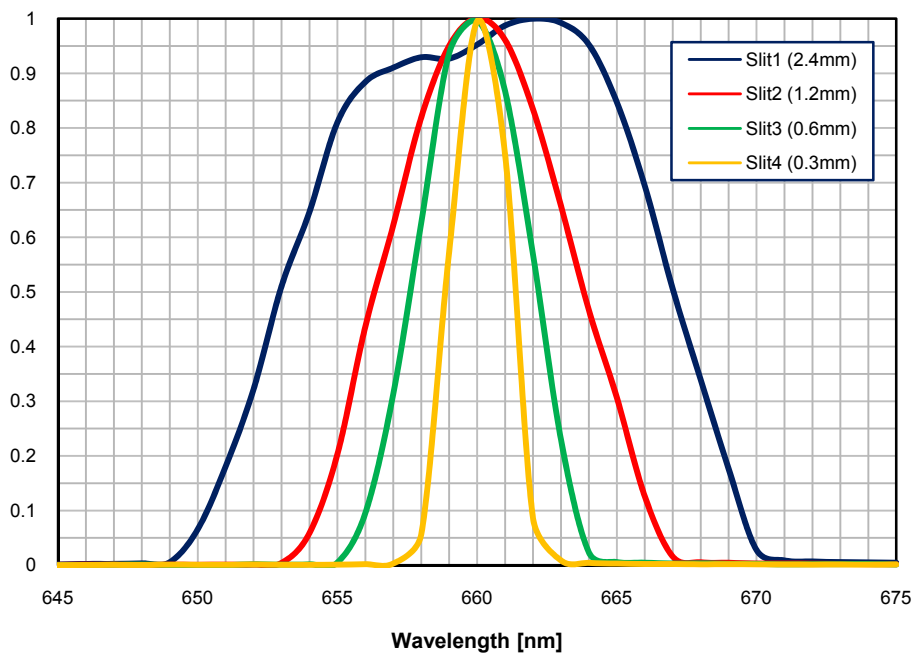


Figure 6.11 Bandwidth vs. slit width [25]

6.2.4. COLOR FILTER

For a given diffraction angle β , several values of λ may satisfy the grating equation (6.20) with the corresponding order m . Thus first order radiation ($m=1$) with a wavelength of λ shares the same diffraction angle as second order radiation ($m=2$) with a wavelength of $\lambda/2$ and third order radiation ($m=3$) with a wavelength of $\lambda/3$.

The wanted output is the first order radiation and therefore it is necessary to block radiation with $m>1$ by additional color filters. This is achieved by the use of two different filters placed at the exit of the monochromator and. Long pass order sorting

6. Measurement Setup

filters provide blocking of light radiation below the filter specific transition or cut-off wavelength. Figure 6.12 shows color filters with different transition wavelengths.



Figure 6.12 Color filters with different transition wavelengths [22]

The useable wavelength range of the xenon source and the monochromator reaches from 350nm to 1550nm. Therefore one color filter with a transition wavelength of 580nm and another filter with a transition wavelength of 850nm are used. Corresponding to Figure 6.13 the first filter has to be placed into the output beam for wavelengths greater than 650nm while the second filter is used for wavelengths greater than 1000nm.

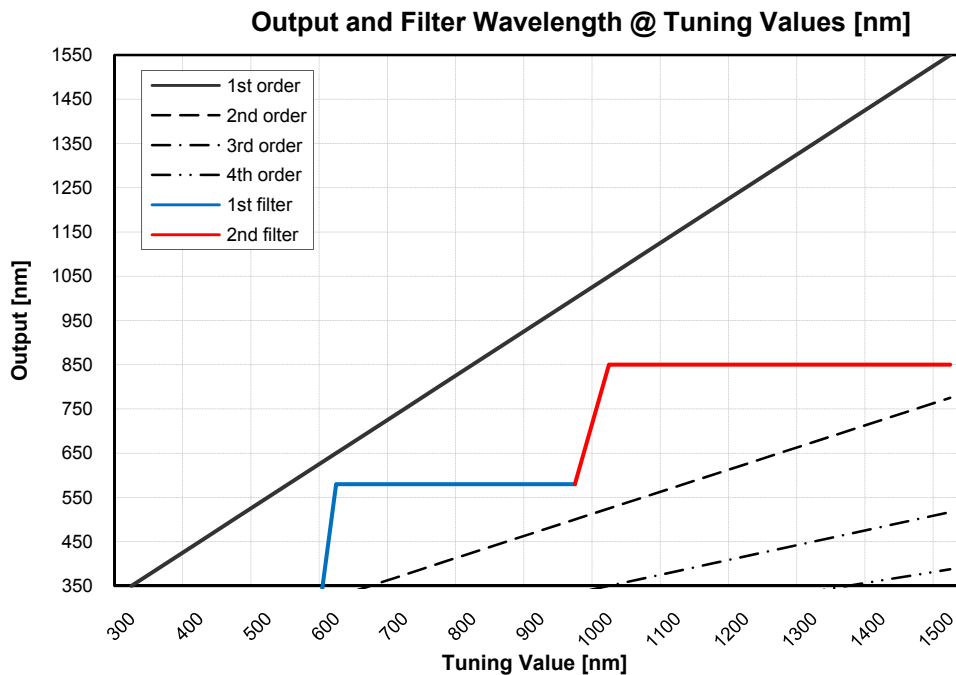


Figure 6.13 Output and filter wavelength vs. tuning values [24]

6.2.5. F-NUMBER FIBER OPTIC ADAPTER

The f-number adapter optically matches the numerical aperture of the fiber to the f-number of the monochromator, joins them mechanically and focuses the light from the exit slit onto the fiber. The demagnified slit image is concentrated onto the tip of the fiber to increase the efficiency of the coupling.

The adapter also allows three axes of precise fiber translation to place the tip of the fiber into the focus of the adapter. This is needed to achieve an optimal coupling ratio between the exit slit of the monochromator and the face of the fiber. Figure 6.14 shows a picture of the f-number adapter.



Figure 6.14 f-number fiber optical adapter [22]

6.2.6. MONOCHROMATOR SOFTWARE

The monochromator CM110 can be connected via a standard RS232 interface to any computer. The CM110 can be controlled with easy-to-use software which comes with the monochromator written in Visual Basic™.

It is also possible to write alternative software for the CM110 or to use the monochromator as a part of an automated measurement system. To simplify writing programs for the CM110 libraries with standard functions can be downloaded for different programming languages as Visual Basic 6.0, Visual C++ 6.0 or LabVIEW.

Figure 6.15 shows a screenshot of the CM110 Software.

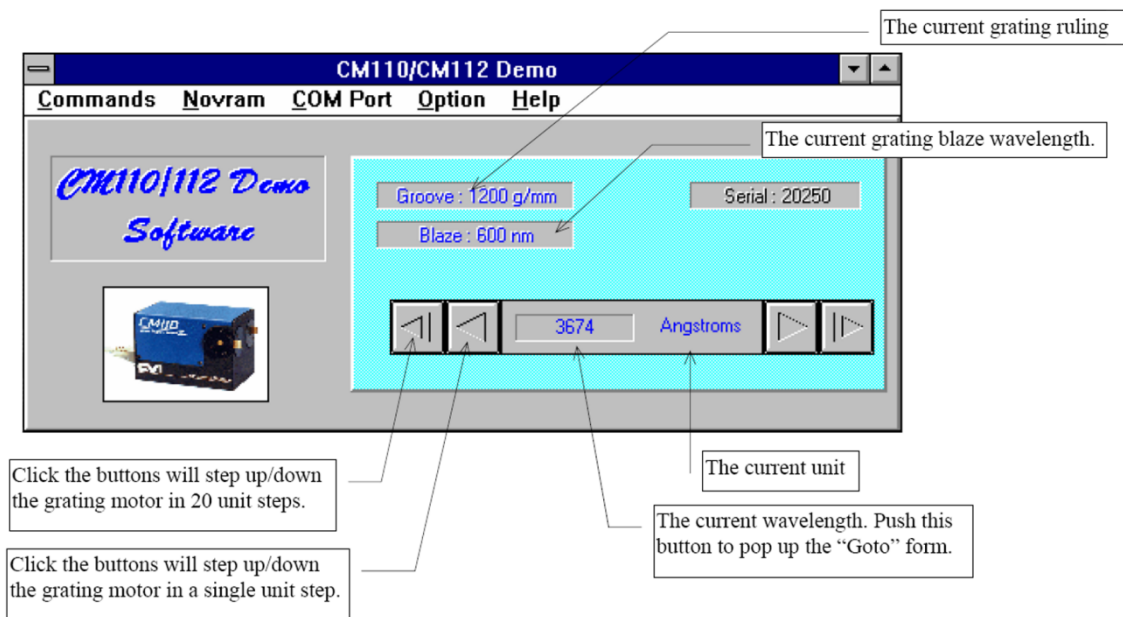


Figure 6.15 CM110 control software [25]

6.3. FIBER OPTIC BEAM SPLITTER

A fiber optic beam splitter is used to split light from one fiber into two or more fibers with minimum loss. Most splitters are designed bi-directional enabling the same product as splitter or coupler. They are available in single mode or multimode and different fibers. The coupling ratio can differ from 50:50 to 1:99. Also different package types are possible (Figure 6.16).

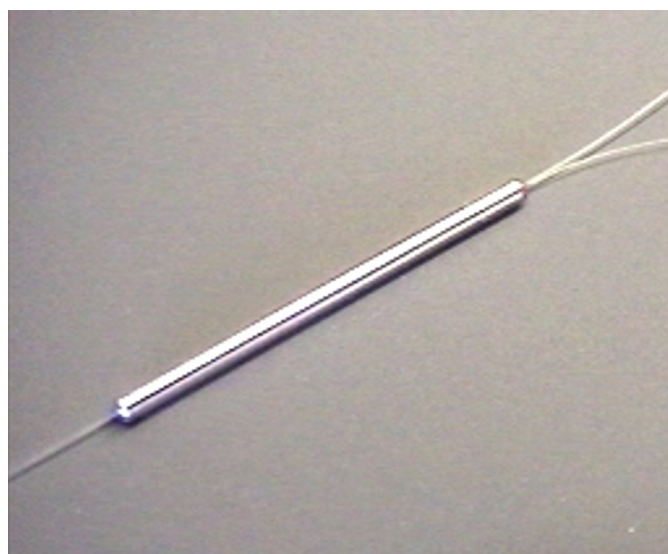


Figure 6.16 Optical beam splitter in tubular package [26]

6. Measurement Setup

For the measurement setup a 1x2 multimode splitter with a coupling ratio of 50:50 is used to split the light of the monochromator output into two parts. The used splitter has one entrance fiber and splits into a blue and a white exit fiber. One part of the light is used to illuminate the photodiode (DUT) (blue fiber) while the other part is measured by an optical power meter (white fiber). The power of the light that illuminates the photodiode P_{ph} is the product of the light power measured by the power meter P_m multiplied by the coupling ratio $\bar{\alpha}$.

$$P_{ph} = P_m \cdot \bar{\alpha} \quad (6.26)$$

Unfortunately the coupling ratio is not complete stable for the interesting wavelength range from 400 to 900nm. Its value alters about 5% over the whole wavelength range which is too much for exact power measurements. Therefore the coupling ratio was measured for a given input power (nominal monochromator output power) for all relevant wavelengths. Since the output power of the monochromator is in the sub μW regime it is useful to enhance the measurement resolution by averaging over a couple of measurements. Figure 6.17 shows the averaged measurements of the two 50% outputs over the full wavelength range.

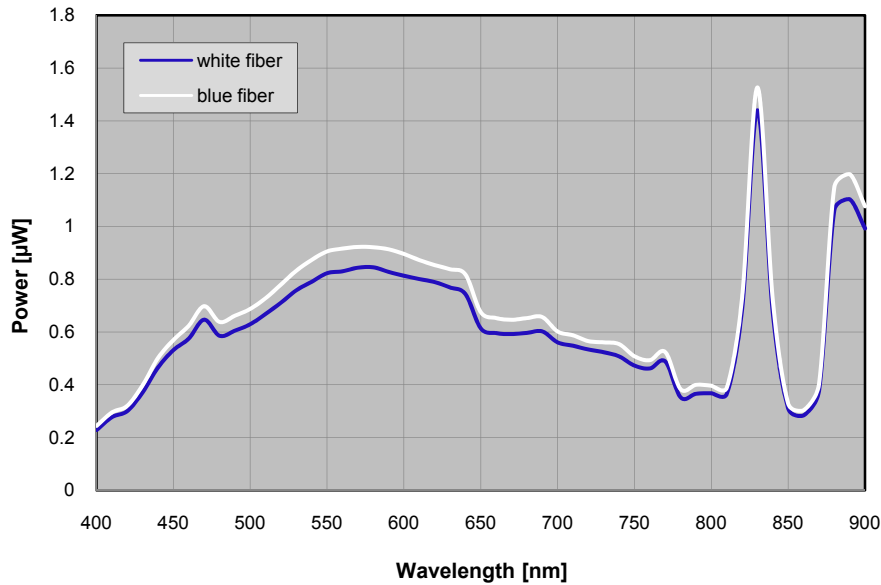
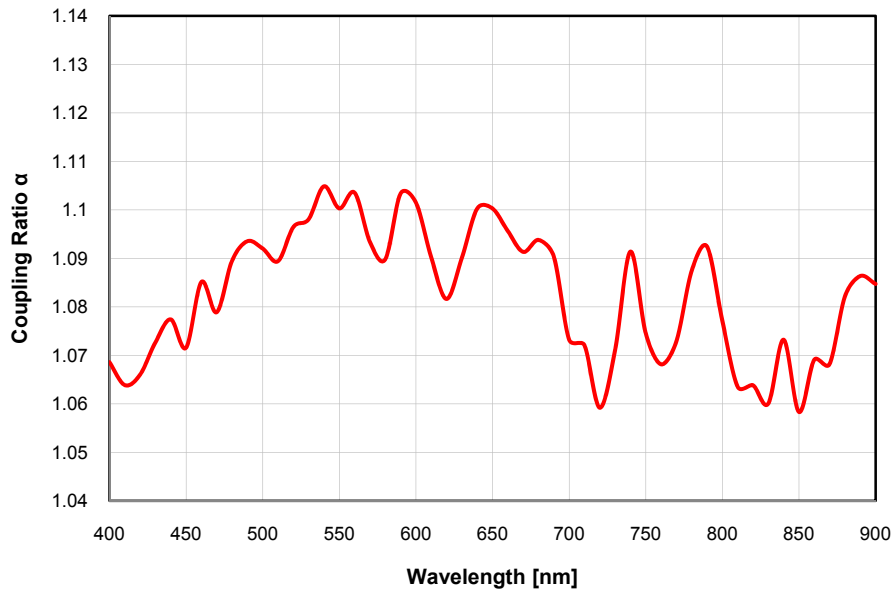


Figure 6.17 Splitter output power, white and blue fiber

The wavelength-dependent coupling ratio $\bar{\alpha}$ is calculated by:

$$\bar{\alpha}(\lambda) = \frac{P_{blue}(\lambda)}{P_{white}(\lambda)} \quad (6.27)$$

Figure 6.18 shows $\bar{\alpha}(\lambda)$ for the used optical beam splitter in the wavelength range from 400 to 900nm.

Figure 6.18 Coupling ratio $\bar{\alpha}$ vs. wavelength

It can be seen that the coupling ratio has a divergence of less than 5%. Nevertheless for exact measurements this measured coupling ratio was used to correct this systematic error. The light power that illuminates the photodiode (DUT) is the product of the light power measured with the optical power meter and the wavelength dependent coupling ratio $\bar{\alpha}(\lambda)$ (6.26).

6.4. OPHIR NOVA OPTICAL POWER METER

The Ophir Nova is a microprocessor-based laser power/energy meter providing a broad range of measurements and data handling options. Different measuring heads can be attached to the display for miscellaneous measuring tasks. It operates with thermopile, pyroelectric and photodiode heads, and uses smart connector technology. This means that all configuration and calibration information are stored in a small memory chip inside the smart head plug. The correct power and energy values are automatically shown when the head is plugged into the display. Figure 6.19 shows the Ophir Nova laser power/energy meter with the PD-300 photodiode head which was used to characterize the photodiodes.

6.4.1. PHOTODIODE HEAD PD-300

The photodiode sensor produces a current proportional to light intensity and has a high degree of linearity over a wide range of light power levels - from fractions of nW to about three mW. Above that light level the electron density in the photodiode becomes too large and its efficiency is reduced causing saturation and a lower reading. Thus the head has a built-in filter that reduces the light level on the detector to allow measurement up to 30mW without saturation. Additionally a removable extra filter is available which exceeds the measurement range up to 300mW [27].

6. Measurement Setup



Figure 6.19 Ophir Nova laser power/energy meter [27]

The PD-300 head has a dual detector head. The two detectors are identical and connected back to back. When background light falls on both detectors inside the head the both signals cancel each other. If on the other hand a distinct light beam is focused on one detector only, it produces the correct measurement output. Thus the head subtracts most of the background light while detecting the desired signal power. Figure 6.20 shows a schematic drawing of the head.

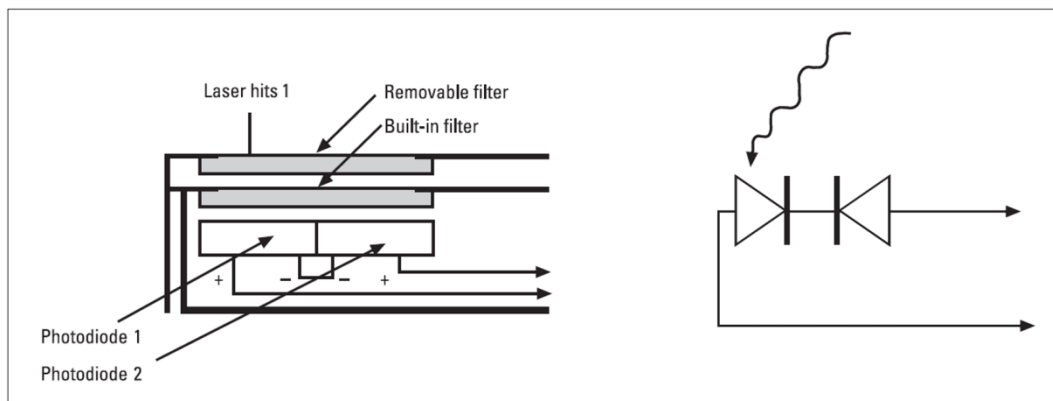


Figure 6.20 Schematic drawing of the PD-300 photodiode head [27]

The photodiode head has different sensitivity at different wavelengths. Also the filters used in the head have different transmission at different wavelengths. In order to compensate for this, each head has a built-in calibration curve with 1nm resolution over the whole measurement range (Figure 6.21).

To measure the light power at a certain wavelength the correct wavelength has to be chosen. Then the right correction factor is automatically extracted from the calibration curve inside the head and introduced into the measurement.

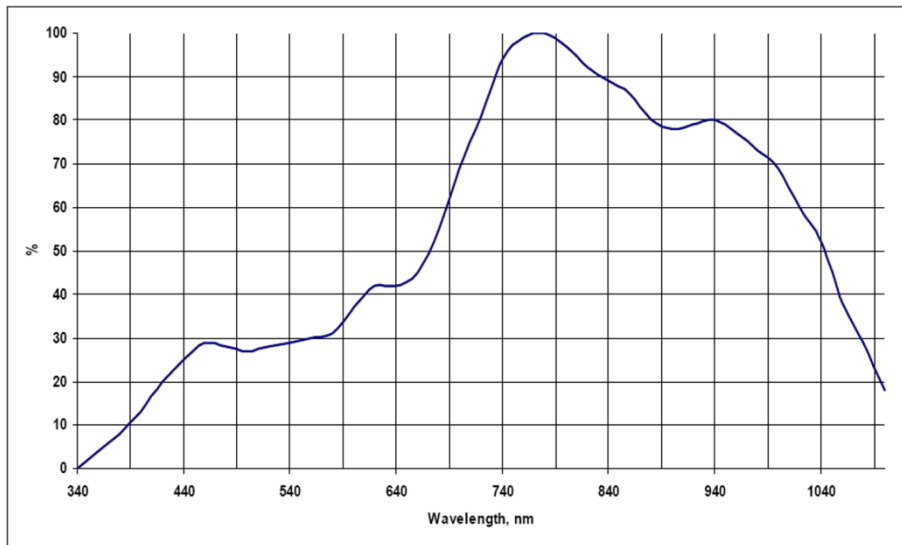


Figure 6.21 Calibration curve PD-300 [28]

6.4.2. SOFTWARE

The Ophir Nova energy/power meter can be connected to the PC via a standard RS232 interface. Data can be transferred from the head either real time or offline and it is also possible to control the Ophir Nova directly from the computer. This can be done either by the StarCom application (Figure 6.22) that comes with the power meter or via LabVIEW. To simplify the programming of LabVIEW applications LabVIEW subroutines (VIs) are also available.

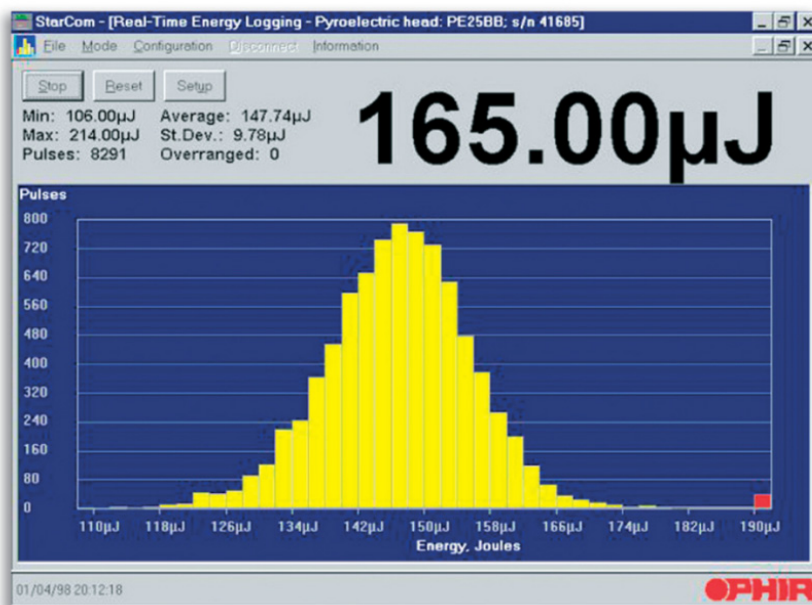


Figure 6.22 StarCom application screenshot [29]

6.5. KEITHLEY 6517A ELECTROMETER

The Keithley electrometer is used to measure the photocurrent I_{ph} generated by the color sensitive photodiodes. I_{ph} varies with the power and the wavelength of the incident light. The incident light power is only in the range of some μW and thus the generated photocurrent I_{ph} can be down to the nA-range. Therefore it is necessary to use a high sensitive electrometer like the Keithley 6517A (Figure 6.23).



Figure 6.23 Keithley 6517A electrometer [30]

The Keithley 6517A can measure currents down to the fA regime and has an internal voltage source for resistor measurements. This voltage source is used to reverse-bias the photodiode (DUT). The used voltage value is around 2V. To avoid electromagnetic disturbances during the measurement tri-axial cabling and shielding of the DUT is required. The test circuit is shown in Figure 6.24.

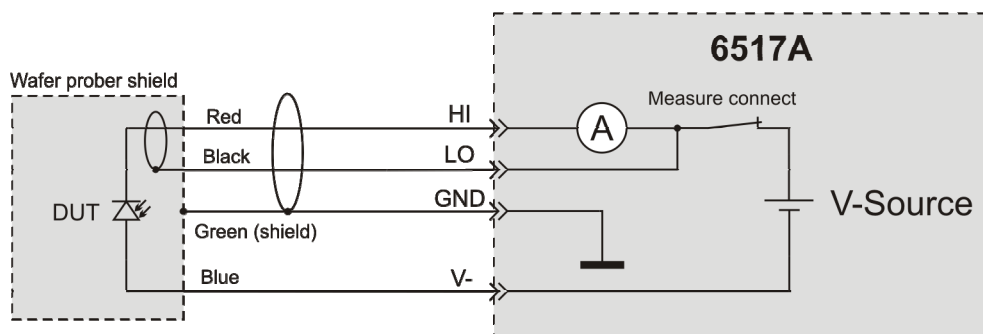


Figure 6.24 Test circuit

The electrometer can be connected to a PC via IEEE-488 bus or RS232 interface. The communication between the 6517A and the computer is carried out by SCPI orientated measurement commands. Drivers and libraries are available for different programming languages and LabVIEW.

For the measurement of the photodiodes the electrometer is controlled via a LabVIEW application which is discussed in chapter 7.

6.6. WAFER PROBER

For easy mass testing of the photodiodes a semiautomatic wafer prober was used. The whole wafer is mounted on the chuck inside the prober. The diodes are contacted with $100\mu\text{m}$ pitch prober needles directly connected to the measurement equipment. The light from the monochromator is conducted via an optical fiber with a diameter of $62.5\mu\text{m}$ to the photodiode surface. The diode has an active area of about $100\times 100\mu\text{m}^2$. Therefore it is easy to couple the complete light from the fiber into the semiconductor. The wafer can be moved with the chuck in x-, y- and z-direction via joystick or software. A high resolution camera is used to display the actual position of the DUT. The needles and the fiber can be moved independently into all three directions with micrometer probe heads.

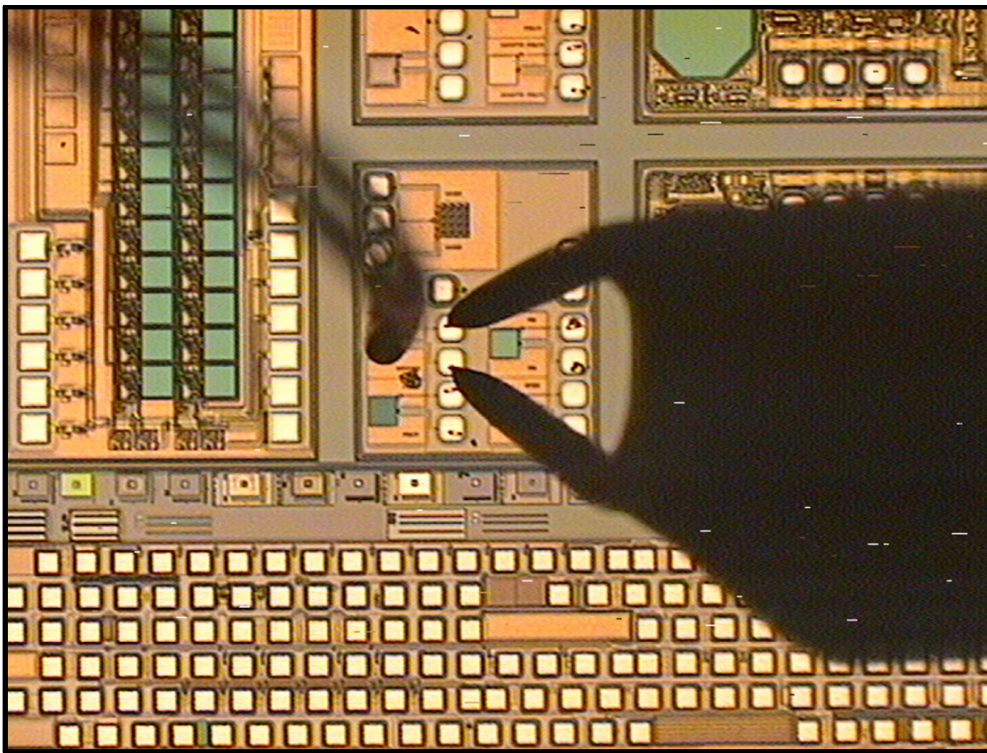


Figure 6.25 Photodiode measurement

Figure 6.25 shows a semiconductor wafer through the microscope. In the middle a chip with five different photodiodes can be seen. The green spots are the etched optical windows of the diodes while the white spots are the contact pads of the semiconductor chips. One photodiode is connected by the two needles on the right side. The fiber which conducts the light to the diode is seen on the left side. The fiber consists of the $62.5\mu\text{m}$ core (which carries the light) and the surrounding cladding. The surrounding cladding has an outer diameter of $125\mu\text{m}$. In the picture the sharp edge of the cladding can be seen on top of the $100\times 100\mu\text{m}$ photodiode. The fiber (cladding and core) covers the complete photodiode. Nevertheless the active area of the fiber is smaller than the diode. This way it is ensured that the complete optical power is induced into the active photodiode area. This is very important for sensitivity measurements.

6.7. COMPLETE SETUP

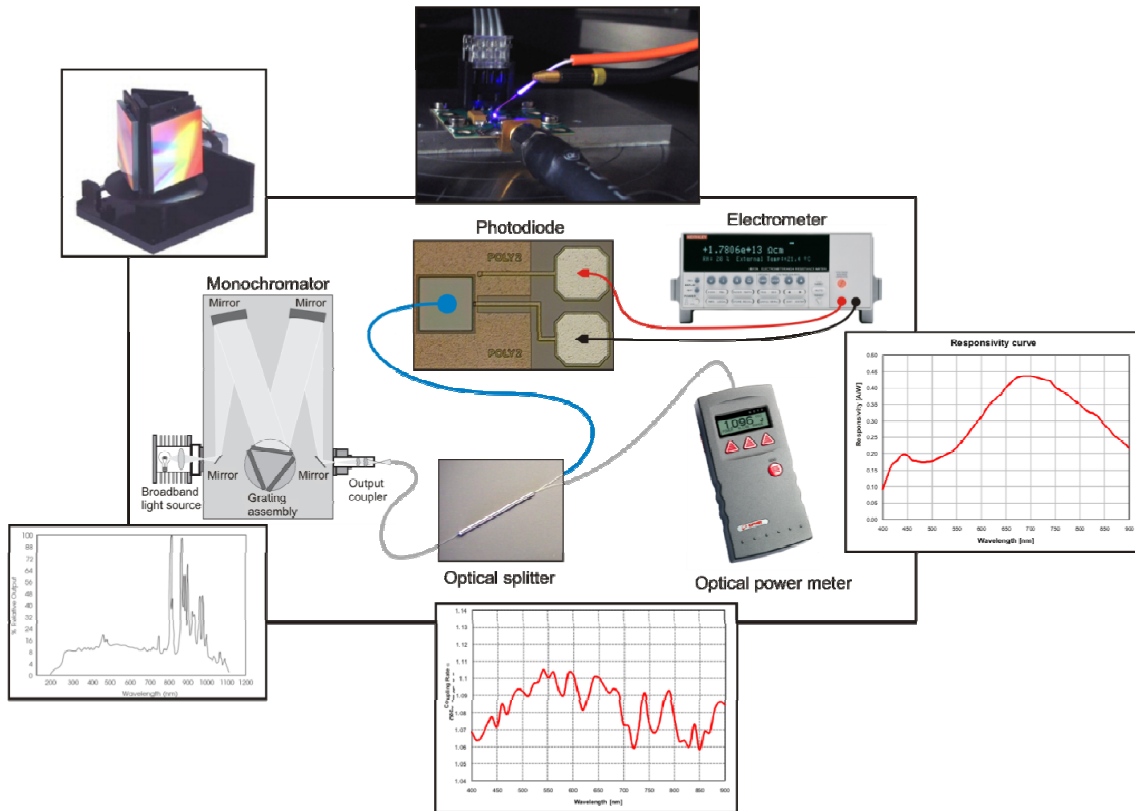


Figure 6.26 Complete measurement setup

Figure 6.26 shows the complete measurement setup. Broadband light produced by the xenon light source enters the monochromator through the entrance slit. In the monochromator the collimating mirror produces a parallel beam which is dispersed by a grating mounted on a turret (Figure 6.10). Dependent on the position of the turret the white radiation is diffracted into different angles. Then focusing mirror reforms the beam and focuses it on a focal plane. The exit slit isolates the desired spectral band (Figure 6.9).

The narrow band radiation is then split by the optical beam splitter at a ratio of 50:50. The power of one part is measured by the optical power meter while the other part illuminates the photodiode to be measured. The power of the light that falls on the diode is the product of the measured light power P_m and the coupling ratio α (6.26). The incident light generates a photocurrent which is measured by the electrometer.

The responsivity of the photodiode which is wavelength dependent is the quotient of the generated photocurrent I_{ph} and the incident light power P_{opt} (4.17). To record the responsivity curve of the diode, the responsivity is measured from 400 to 900nm wavelength in steps of 10nm and plotted versus the wavelength. To enhance the resolution of the measurement typical more than one measurement is conducted for each step. The result of the measurement is the average of all identical measurements. With these multiple measurements it is also possible to calculate a standard deviation for each

6. Measurement Setup

measurement to ensure high accuracy. The responsivity curve of a typical silicon PIN photodiode is shown in Figure 6.27.

This process is performed automatically by a LabVIEW application which controls the monochromator, the optical power meter and the electrometer. The LabVIEW program runs on a standard personal computer and is described in detail in chapter 7.

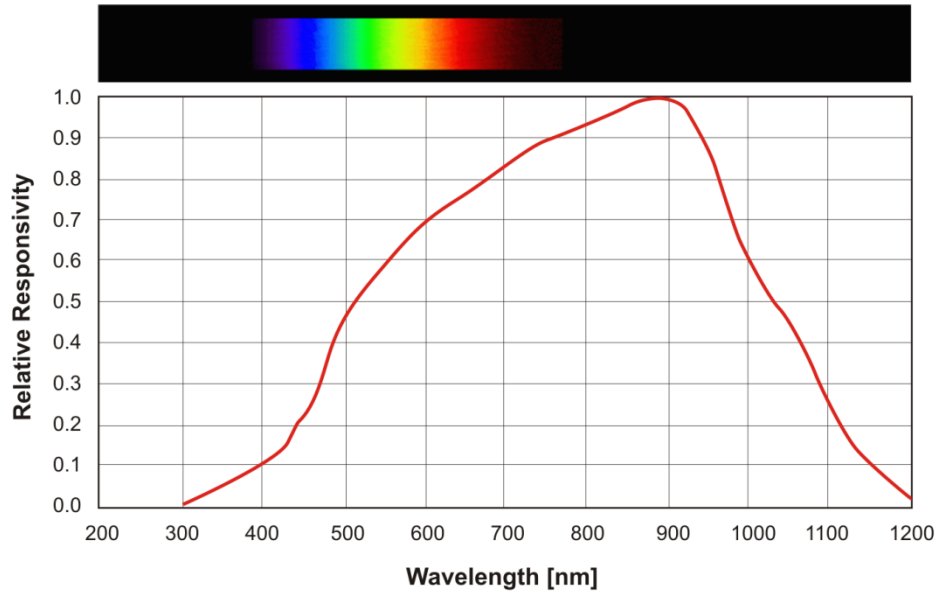


Figure 6.27 Typical responsivity curve of a silicon PIN photodiode [31]

7. LABVIEW APPLICATION

7.1. LABVIEW OVERVIEW

LabVIEW (Laboratory Virtual Instrumentation Engineering Workbench) is a platform and development environment for the visual programming language G from National Instruments. Originally released for the Apple Macintosh in 1986, LabVIEW is commonly used for data acquisition, instrument control and industrial automation on a variety of platforms including Microsoft Windows, various flavors of UNIX, Linux and Mac OS.

G is a dataflow programming language – program execution is determined by the structure of a graphical block diagram. Different function nodes are connected by drawing wires. Program variables are propagated via these wires and each node can execute as soon as all its input data become available. Therefore the programming language is capable of parallel execution.

LabVIEW allows the creation of user interfaces in the development cycle. Programs and subroutines are called virtual instruments (VIs). Each VI consists of three components:

- Block diagram
- Front panel
- Connector pane

The block diagram is used for “writing” the program. The front panel is the user interface which allows an operator to input data or extract data from a running program. It can also serve as a programmatic interface. The connector pane represents the VI as a subVI in block diagrams of calling VIs. Figure 7.1 shows an example of a LabVIEW front panel and the related block diagram.

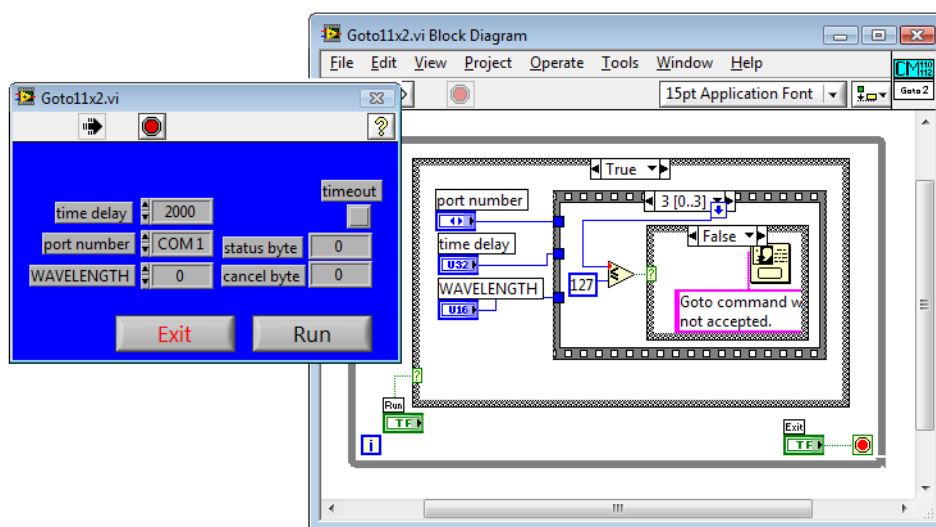


Figure 7.1 LabVIEW front panel and block diagram

Thus a virtual instrument can either be run as a program or as a sub node. If the VI is run as a program the front panel serves as a user interface. On the other hand, if the VI is run as a sub node, the front panel defines the inputs and outputs for the given node through the connector pane. This implies that each VI can be easily tested (stand alone) before being embedded as a subroutine into a larger program.

Another benefit of LabVIEW is the extensive support for accessing instrumentation hardware. Drivers and abstraction layers for many different types of instruments and buses are already included, or available for inclusion. All subroutines are based on a graphical interface. The abstraction layers offer standard software interfaces to communicate with hardware devices. Therefore even people with limited coding experience can write applications.

LabVIEW includes a compiler that produces native code for a CPU platform. The graphical code can be compiled into executable machine code. The LabVIEW syntax is strictly enforced during the graphical editing process. Compilation is started when the program is run or saved. In the latter case, the executable and the source code are merged into a single file. The executable runs with the help of the LabVIEW runtime engine. The runtime engine reduces compile time and also provides a consistent interface to various operating systems, graphic systems and hardware components. Thus the runtime environment makes the code portable across platforms [32].

7.2. PROGRAM FUNCTIONS

The LabVIEW program is used to perform automatic photodiode responsivity curve measurements. Thus the program controls the monochromator, the optical power meter and the electrometer in the measurement setup as seen in Figure 6.26.

The program splits into three functions:

- Set monochromator to straight-through operation for alignment
- Responsivity measurement at one distinct wavelength
- Responsivity curve measurement over a whole wavelength range

7.2.1. STRAIGHT-TROUGH OPERATION (FULL SPECTRUM)

With the straight-trough operation mode the grating of the monochromator is turned to an angle at which the full light spectrum is reflected by the grating (Ebert angle). Therefore the full spectrum can pass the monochromator without being bandwidth limited. In this state the maximum output power of the monochromator is achieved. This is done to achieve a bright, good visible spot at the end of the fiber. Thus this mode is used to adjust the end of the fiber onto the active area of the diode to achieve optimal coupling with minimum losses. This operation mode is not used for any measurement itself.

7.2.2. SINGLE WAVELENGTH MEASUREMENT (SINGLE STEP)


In this operation mode the wavelength value can be entered manually. The monochromator and the optical power meter are set at the selected wavelength and the

optical power and the generated photocurrent is measured. This operation mode is used to measure the responsivity at a certain wavelength.

7.2.3. RESPONSIVITY CURVE MEASUREMENT

In this operation mode the responsivity curve of a wavelength range that can be entered is measured automatically and the measurement data is written into an excel-file for further use. Additionally the graph of the responsivity curve is plotted on the screen. This mode is the most common mode for measurement tasks. Usually a complete responsivity curve is necessary to characterize a color sensitive photodetector.

7.3. PROGRAM MANUAL

The program needs for its execution either LabVIEW 8.0 or higher, or the according runtime version. The program files can be found on the attached CD in the directory \Responsivity curve. For faster program execution it is recommended to copy the whole directory to the hard disk. To execute the program the CM110 monochromator and the optical power meter Ophir Nova have to be connected to standard RS232 interfaces while the electrometer Keithley 6517A is connected to the GPIB IEEE-488 interface bus. Then the file `responsivity curve.vi` has to be started. The front panel opens and the application can be started by pressing .

The front panel (Figure 7.2) consists of six function blocks:

- Device Settings
- Full Spectrum
- Single Step
- Responsivity Curve
- Status
- Exit

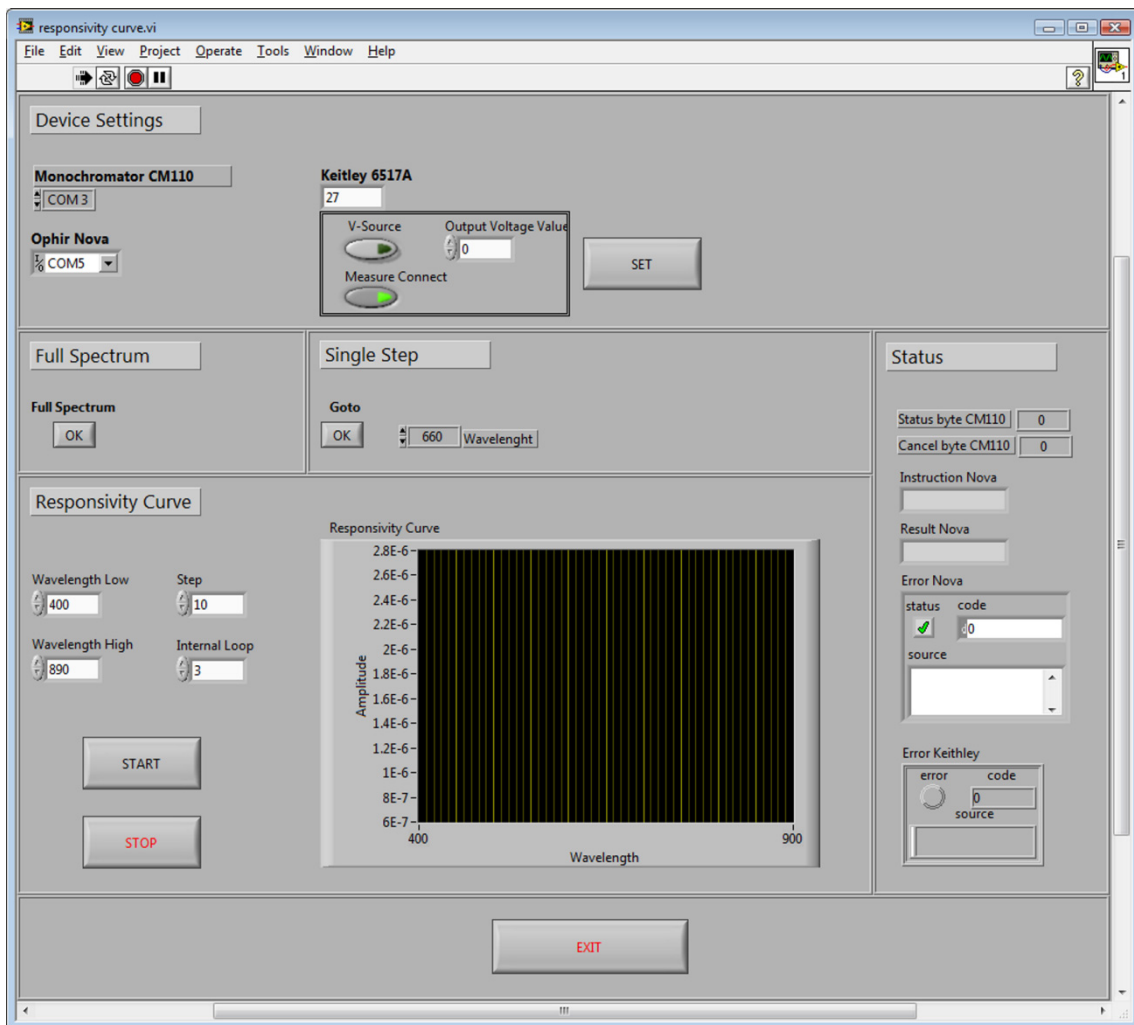



Figure 7.2 Front panel responsivity measurement

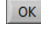
7.3.1. DEVICE SETTINGS

This function block holds the interface settings of the monochromator, the optical power meter and the electrometer. The monochromator and the Ophir Nova are connected to RS232 serial interfaces while the Keithley 6517A is connected via GPIB IEEE-488. The addresses of the RS232 interfaces can be changed by clicking the buttons beside the address window while the GPIB address of the Keithley 6517A has to be entered manually.


The device settings section also holds the settings for the internal voltage source of the electrometer. The voltage value can be changed by clicking the buttons beside the voltage window in the range from -20V to +20V. The voltage source can also be disabled when an external source is used to reverse-bias the photodiode. When the internal voltage source is not used it can be disconnected from the ampere meter by disabling the *Measure Connect* button (Figure 6.24). The default setting for the

Measure Connect is ON while *Voltage Source* is set to OFF for security reasons. The settings are transferred to the electrometer by pressing .



7.3.2. FULL SPECTRUM

In this function block the monochromator can be switched to straight-through mode. That means that the monochromator does not work as bandpass – the full light spectrum that enters the monochromator also leaves the monochromator. This mode is used for adjusting the fiber on the photodiode to be measured. The mode is entered when  is pressed and left when another wavelength is selected.

7.3.3. SINGLE STEP

In this mode a wavelength can be selected manually by using the up- and down-buttons. When  is pressed the monochromator and the optical power meter is set to the selected wavelength and the responsivity is measured.

7.3.4. RESPONSIVITY CURVE

This section is used to measure the responsivity curve of a photodiode for a wavelength range. The measurement starts at the wavelength value set at *Wavelength Low* and ends at the value entered at *Wavelength High*. With *Step* the wavelength step between two measurement points is set. The default values are 400nm for *Wavelength Low*, 900nm for *Wavelength High* and 10nm for *Step*. To enhance the accuracy of the measurement the measurement can be repeated automatically. *Internal Loop* sets the number of repetitive measurements. The responsivity curve shows the average value of the repetitive measurements. In the Excel file additionally the standard deviation for each responsivity value can be found to estimate the accuracy of the measurement. The responsivity curve measurement is started by pressing  and can be interrupted by pressing . When the measurement is started the user is prompted to remove possible filters from the filter holder and to enter the name of the output file which is written in Excel/CSV format. After this the measurement runs automatically and the responsivity curve is plotted in the *Responsivity Curve* window. At a wavelength of 650nm the user is prompted to put the first filter (580nm, orange) into the filter holder. At 1050nm the user is prompted to change the first filter (580nm, orange) with the second filter (890nm, red). When the measurement is finished the complete responsivity curve has been plotted on the screen and the output file is written to disk. If the same output file is used for multiply measurements the output data is appended at the end of the file. An example of the output file is shown in Table 7.1.

7. LabVIEW Application

Wavelength[nm]	Current mean meas.[A]	Curr.Sigma	Curr.Vari.	Light Power	Light Pow.Sigma	Light Pow.Vari	SplitterCorrectionValue	Light Power corr.	Wavelength[nm]	Responsivity[A/W]
4.00E+02	-1.67E-06	2.48E-08	6.14E-16	1.44E-07	1.76E-09	3.10E-18	1.03E+00	1.48E-07	4.00E+02	1.14E+01
4.50E+02	-7.63E-06	2.76E-07	7.62E-14	3.05E-07	1.00E-09	1.00E-18	1.04E+00	3.18E-07	4.50E+02	2.40E+01
5.00E+02	-1.12E-05	1.66E-07	2.76E-14	3.33E-07	3.46E-09	1.20E-17	1.05E+00	3.51E-07	5.00E+02	3.18E+01
5.50E+02	-1.41E-05	1.87E-07	3.51E-14	4.15E-07	3.79E-09	1.43E-17	1.06E+00	4.39E-07	5.50E+02	3.21E+01
6.00E+02	-1.54E-05	2.95E-07	8.70E-14	3.75E-07	5.86E-09	3.43E-17	1.05E+00	3.94E-07	6.00E+02	3.90E+01
6.50E+02	-1.02E-05	1.64E-07	2.70E-14	2.51E-07	4.76E-09	2.27E-17	1.07E+00	2.68E-07	6.50E+02	3.80E+01
7.00E+02	-1.09E-05	2.17E-07	4.70E-14	2.17E-07	3.27E-09	1.07E-17	1.05E+00	2.28E-07	7.00E+02	4.77E+01
7.50E+02	-7.69E-06	4.03E-08	1.63E-15	1.78E-07	1.30E-09	1.69E-18	1.05E+00	1.87E-07	7.50E+02	4.12E+01
8.00E+02	-5.41E-06	9.68E-08	9.36E-15	1.29E-07	2.95E-09	8.70E-18	1.05E+00	1.35E-07	8.00E+02	4.00E+01
8.50E+02	-3.47E-06	8.78E-08	7.71E-15	8.37E-08	3.22E-10	1.03E-19	1.03E+00	8.63E-08	8.50E+02	4.02E+01
9.00E+02	-9.52E-06	2.22E-07	4.93E-14	3.08E-07	2.08E-09	4.33E-18	1.08E+00	3.32E-07	9.00E+02	2.87E+01
Wavelength[nm]	Current mean meas.[A]	Curr.Sigma	Curr.Vari.	Light Power	Light Pow.Sigma	Light Pow.Vari	SplitterCorrectionValue	Light Power corr.	Wavelength[nm]	Responsivity[A/W]
4.00E+02	-1.67E-06	2.48E-08	6.14E-16	1.44E-07	1.76E-09	3.10E-18	1.03E+00	1.48E-07	4.00E+02	1.14E+01
4.50E+02	-7.63E-06	2.76E-07	7.62E-14	3.05E-07	1.00E-09	1.00E-18	1.04E+00	3.18E-07	4.50E+02	2.40E+01
5.00E+02	-1.12E-05	1.66E-07	2.76E-14	3.33E-07	3.46E-09	1.20E-17	1.05E+00	3.51E-07	5.00E+02	3.18E+01
5.50E+02	-1.41E-05	1.87E-07	3.51E-14	4.15E-07	3.79E-09	1.43E-17	1.06E+00	4.39E-07	5.50E+02	3.21E+01
6.00E+02	-1.54E-05	2.95E-07	8.70E-14	3.75E-07	5.86E-09	3.43E-17	1.05E+00	3.94E-07	6.00E+02	3.90E+01
6.50E+02	-1.02E-05	1.64E-07	2.70E-14	2.51E-07	4.76E-09	2.27E-17	1.07E+00	2.68E-07	6.50E+02	3.80E+01
7.00E+02	-1.09E-05	2.17E-07	4.70E-14	2.17E-07	3.27E-09	1.07E-17	1.05E+00	2.28E-07	7.00E+02	4.77E+01
7.50E+02	-7.69E-06	4.03E-08	1.63E-15	1.78E-07	1.30E-09	1.69E-18	1.05E+00	1.87E-07	7.50E+02	4.12E+01
8.00E+02	-5.41E-06	9.68E-08	9.36E-15	1.29E-07	2.95E-09	8.70E-18	1.05E+00	1.35E-07	8.00E+02	4.00E+01
8.50E+02	-3.47E-06	8.78E-08	7.71E-15	8.37E-08	3.22E-10	1.03E-19	1.03E+00	8.63E-08	8.50E+02	4.02E+01
9.00E+02	-9.52E-06	2.22E-07	4.93E-14	3.08E-07	2.08E-09	4.33E-18	1.08E+00	3.32E-07	9.00E+02	2.87E+01

Table 7.1 Output file example

7.3.5. STATUS

In the status block the status and the communication between the LabVIEW program and the monochromator, the optical power meter and the electrometer can be seen. It can be used to detect errors and for debugging.

7.3.6. EXIT

The  button stops the execution of the program.

7.4. BLOCK DIAGRAM

Figure 7.3 shows the complete block diagram of the program.

7. LabVIEW Application

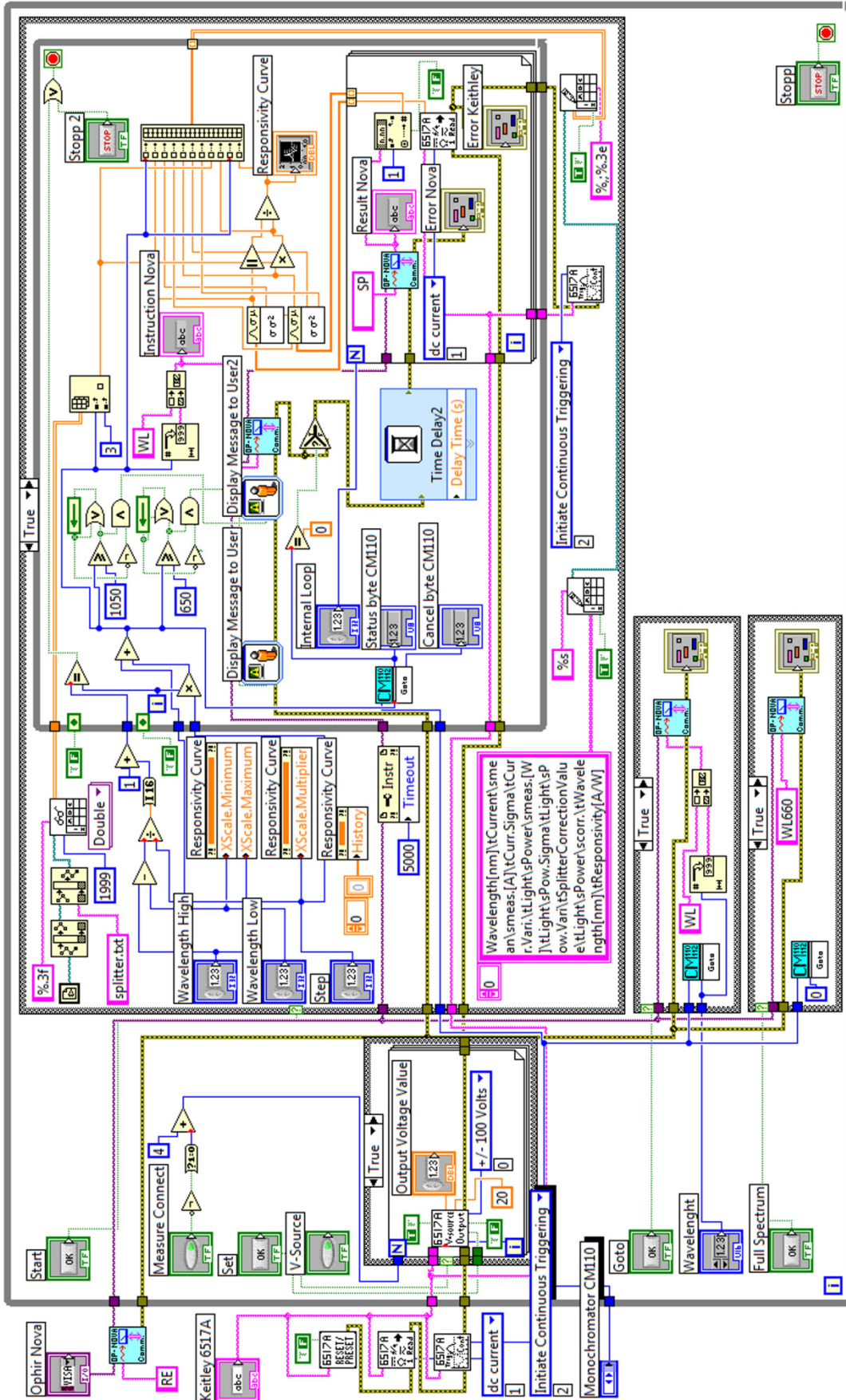


Figure 7.3 LabVIEW application block diagram

8. MEASUREMENT RESULTS

The photodiodes designed in chapter 5.2 and 5.3 are measured with the measurement setup described in chapter 6.7. To characterize the diodes their responsivity curve is measured in the wavelength range from 400 to 900nm. Thus the diodes were reverse-biased with 2V and the generated photocurrent is measured in dependence on the wavelength of the incident light. As reference a standard PIN photodiode of the same size ($100 \times 100 \mu\text{m}^2$) which was fabricated on the same semiconductor wafer was used. The current measurement circuit is shown in Figure 6.24. All diodes are measured directly on the semiconductor wafer (Figure 8.1).

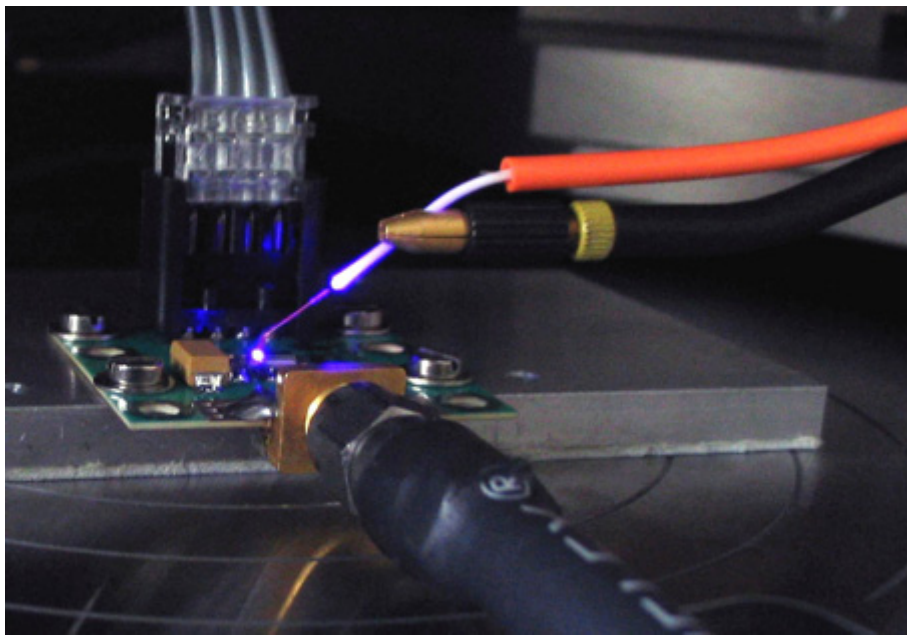


Figure 8.1 Photodiode measurement (bonded photodiode)

The wafer is fixed by vacuum on the chuck of the wafer prober. The light that illuminates the photodiode is brought to the diode optical window by an optical fiber. The electrical contact is established by prober needles (Figure 6.25). To see the fine structures of the photodiodes a microscope is used. Figure 8.2 shows a view through the microscope. On the chip seven different diodes can be seen. It is also possible to recognize the different colors of the different etched optical windows. The different colors are due to the different layers inside the optical windows acting as light filters. The dot structure of the polysilicon layer 1 that is needed to ensure the n^+ implant can also be seen on two diodes. In the upper row are also two diodes with three contacts – these are the stacked diodes with one shallow and one deep diode to filter the light due to the different penetration depths.

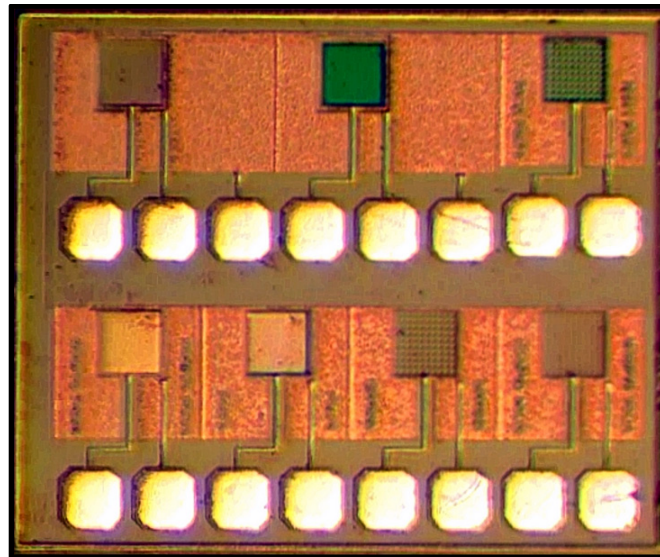


Figure 8.2 Different diode types

8.1. PIN PHOTODIODE

The standard PIN photodiode is only measured as a reference for the other diodes. The cross section of the PIN diode can be seen in Figure 5.1 and below a photo made through the microscope can be seen.

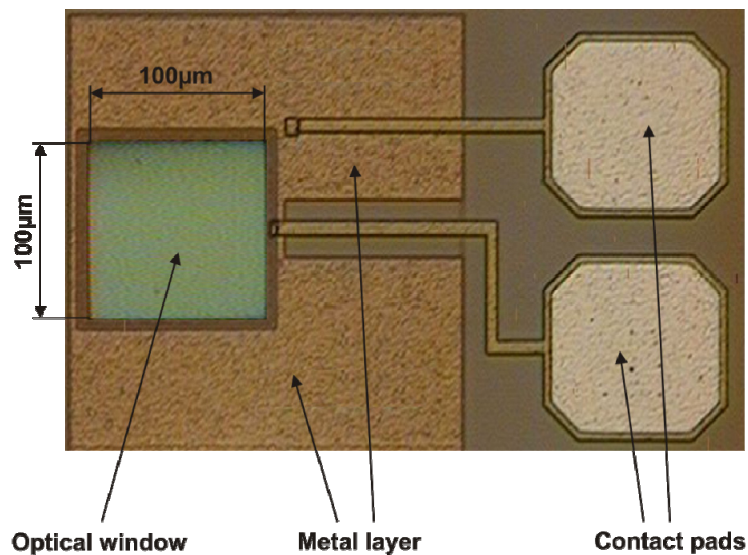


Figure 8.3 PIN photodiode

The green square on the left side is the optical window of the diode etched through the different oxide layers caused by the different process steps. The optical window is surrounded by a metal layer that avoids light penetration into the semiconductor beside

the active diode region. On the right side pads used for bonding or contacting the diode with probe needles are placed.

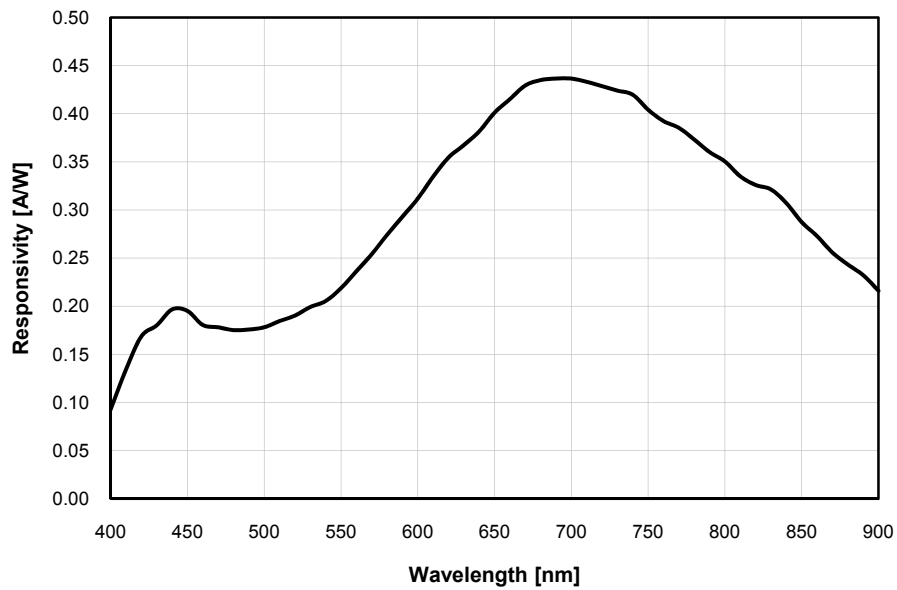


Figure 8.4 Responsivity curve PIN photodiode

The responsivity curve of a standard PIN photodiode is shown above. It can be seen that the responsivity changes relevant over the wavelength range even without additional filters. This graph is used as a reference for the designed color sensitive diodes.

8.2. PIN PHOTODIODE WITHOUT OPTICAL WINDOW

This diode type uses the oxide layers caused by the production process as optical filters.

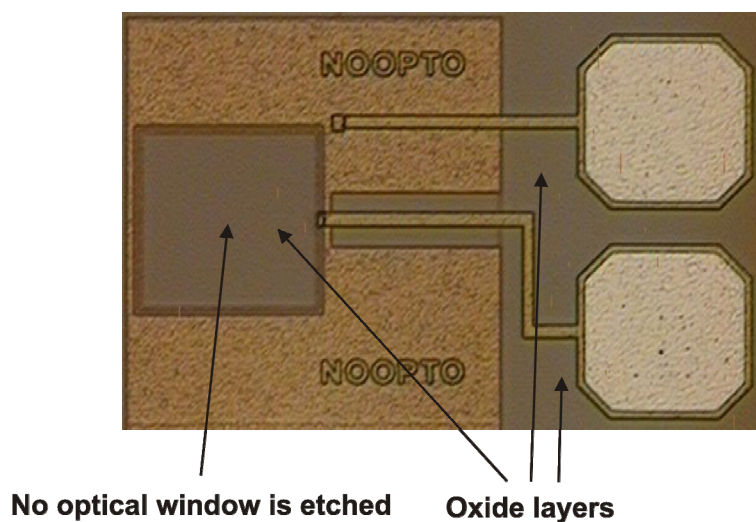


Figure 8.5 PIN Photodiode without optical window

8. Measurement Results

Figure 8.5 shows the photodiode without an optical window etched through the oxide layers. It can be seen that the active area of the diode has the same color as the region around the pads – the whole diode is covered with oxide layers. A cross section of this photodiode can be seen in Figure 5.7.

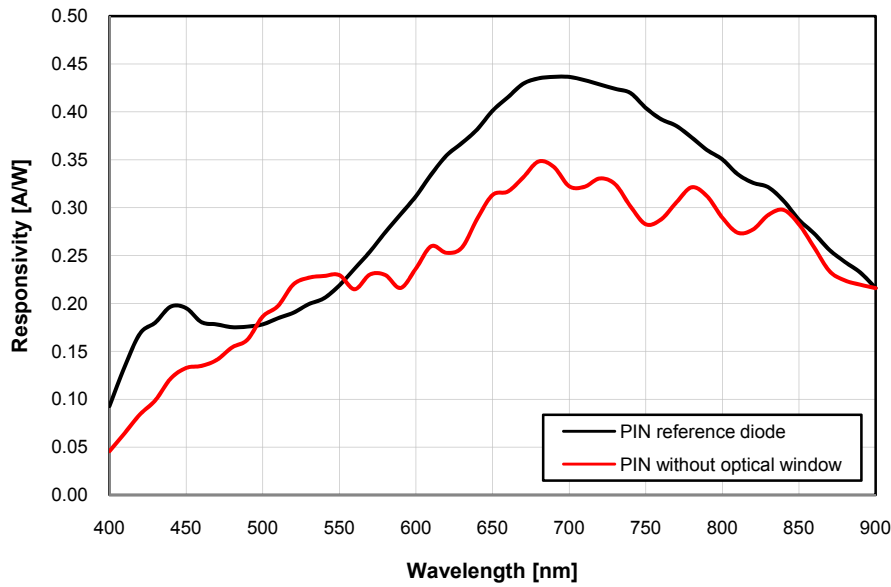


Figure 8.6 Responsivity curve without optical window

The responsivity curve of the diode is shown in Figure 8.6. Light with wavelength in the range from 400 to 480nm is absorbed by the oxide layers. For wavelengths greater than 500nm the responsivity of the photodiode without optical window shows oscillations.

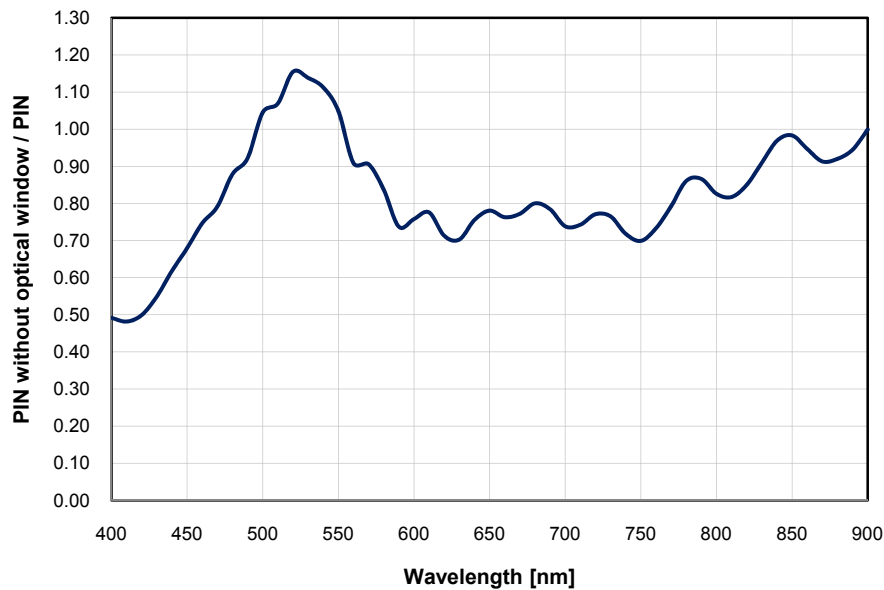
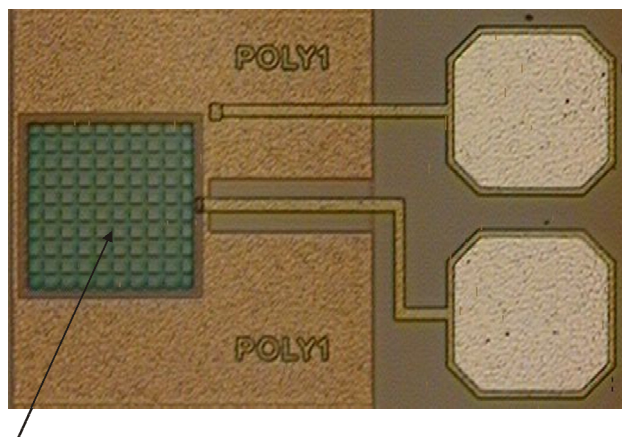


Figure 8.7 PIN without optical window / PIN

This oscillation is caused by a stack of different oxide layers. The thickness of each layer is in the regime of the wavelength. This multiple layers form a structure which can be compared with a Fabry-Pérot interferometer. Thus some wavelengths are reflected and other wavelengths are passed through resulting in the responsivity curve oscillation. The graph in Figure 8.7 shows the ratio of the PIN photodiode without optical window to a standard PIN photodiode. The comparison of the two responsivity curves shows even better responsivity for the diode without optical window at 525nm. Nevertheless is the performance of this diode extremely dependent on process variations (oxide thickness variations) and therefore it is questionable if a reliable application is possible. For color sensitive photodetectors this diode does not seem to be suitable. Nevertheless it helps to understand the influence of the oxide stack for other color sensitive diodes.

8.3. PHOTODIODE WITH POLYSILICON LAYER 1

This photodiode uses an additional polysilicon layer 1 dot structure as a color filter (Figure 8.8). The cross section of this diode is seen in Figure 5.8.



Polysilicon layer 1 dot structure

Figure 8.8 PIN photodiode with polysilicon layer 1

Figure 8.9 shows the responsivity curve of the PIN diode with additional polysilicon layer 1 in comparison with the standard PIN diode. A significant difference can only be seen for wavelengths below 500nm. Thus a combination of this diode and the standard PIN diode could be used to distinguish between light with wavelengths below and above 500nm.

8. Measurement Results

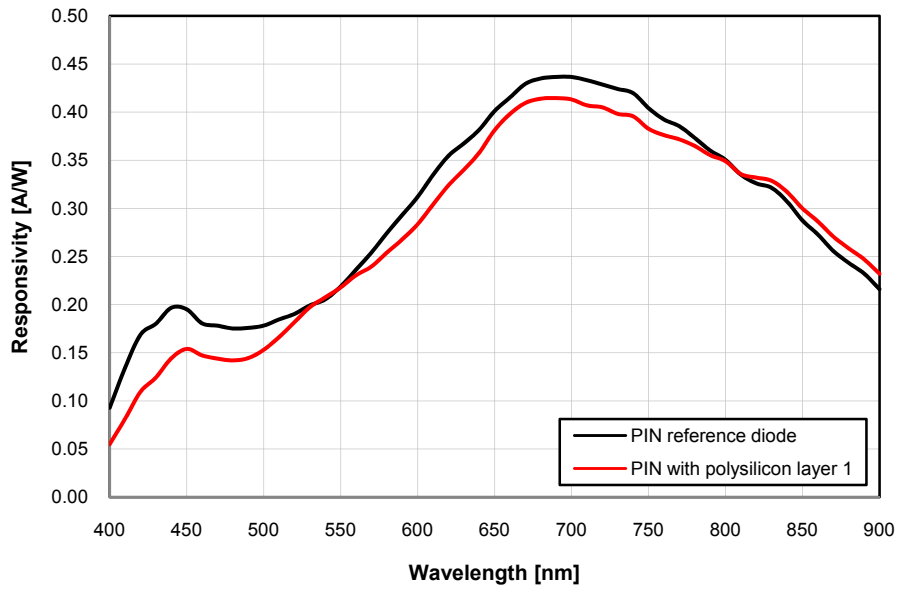


Figure 8.9 Responsivity curve polysilicon layer 1

The ratio between the two diode types is shown in Figure 8.10.

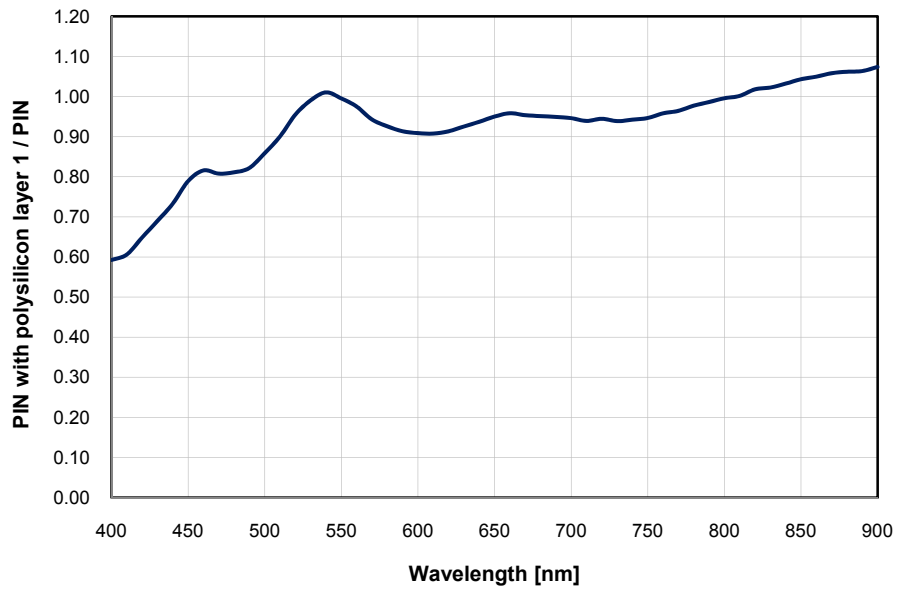


Figure 8.10 PIN with polysilicon layer 1 / PIN

8.4. PHOTODIODE WITH POLYSILICON LAYER 2

A photo of the diode with only additional polysilicon layer 2 is shown below and in Figure 5.10 the cross section can be found.

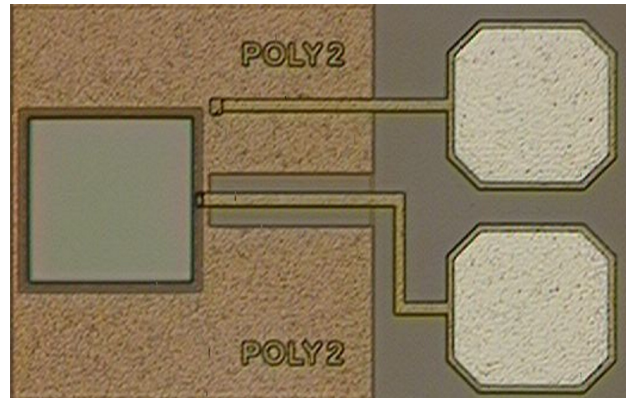


Figure 8.11 PIN photodiode with polysilicon layer 2

The comparison between the measured responsivity curve and the reference curve of the standard PIN photodiode can be found in Figure 8.12.

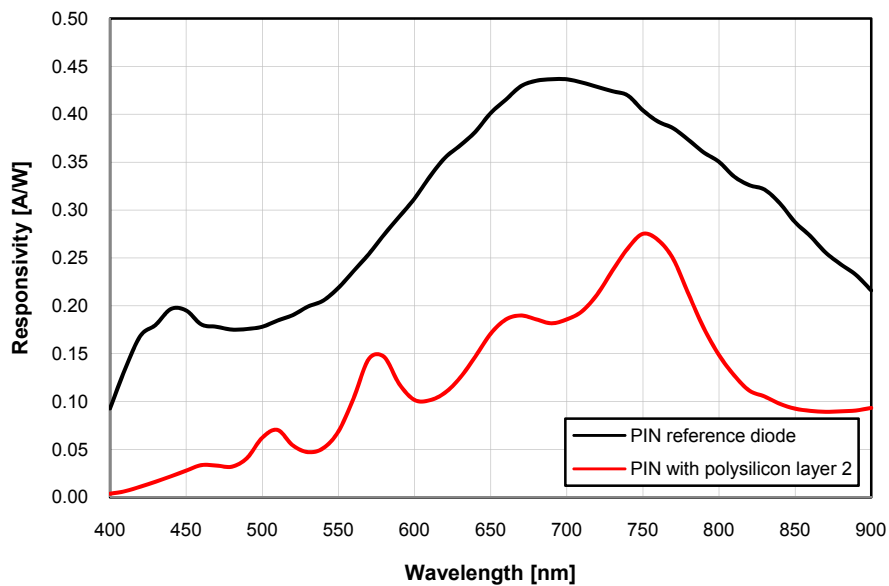


Figure 8.12 Responsivity curve polysilicon layer 2

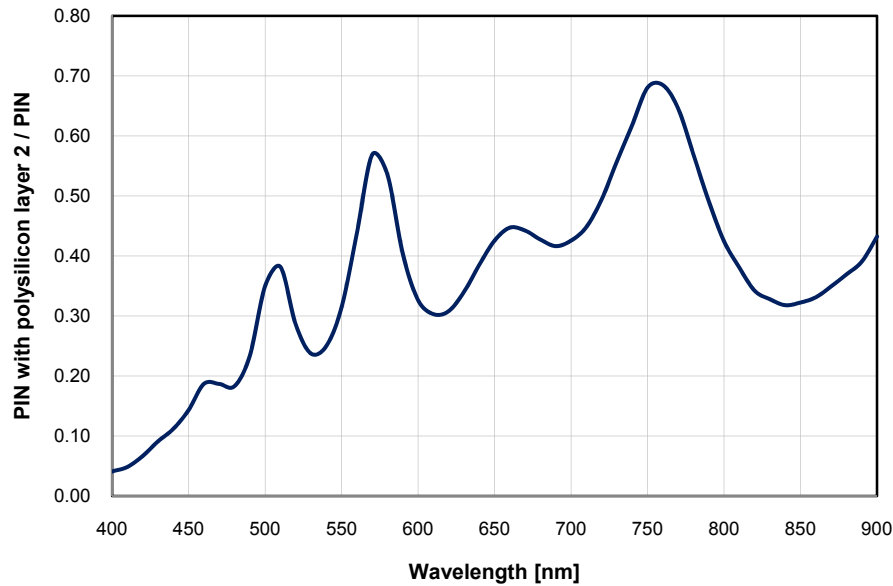


Figure 8.13 PIN with polysilicon layer 2 / PIN

The photodiode with the additional polysilicon layer 2 has a very poor responsivity compared with standard PIN diode. Additionally, the responsivity oscillates very strongly over the whole wavelength range. Thus, this diode type is not well suitable for color detection. It can be assumed that the oscillation is caused by the multi-layer stack and that the exact oscillations are very dependent on process parameters (variations).

8.5. PHOTODIODE WITH POLY 1 AND POLY 2 LAYER

In this photodiode, the color filtering effects of the two previous diodes are combined – a polysilicon layer 2 is placed over the polysilicon 1 dot structure as described in chapter 8.3. The view through the microscope on the diode looks similar to the diode with additional polysilicon layer 1 (Figure 8.8).

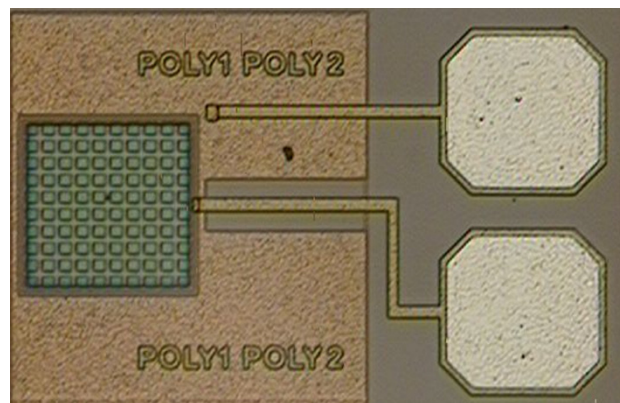


Figure 8.14 PIN photodiode with poly 1 and poly 2 layer

8. Measurement Results

The measurement result of this combined diode is shown below.

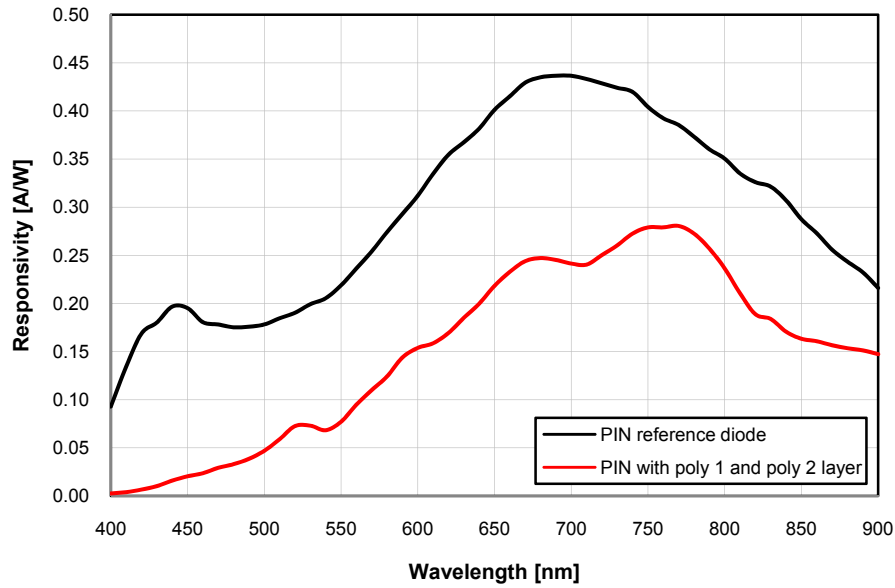


Figure 8.15 Responsivity curve poly 1 and poly 2 layer

The responsivity is very poor for light with wavelengths shorter than 500nm. Thus this diode can be used for detection of light in the green-blue regime. The ratio between this diode and the reference diode can be found in Figure 8.16.

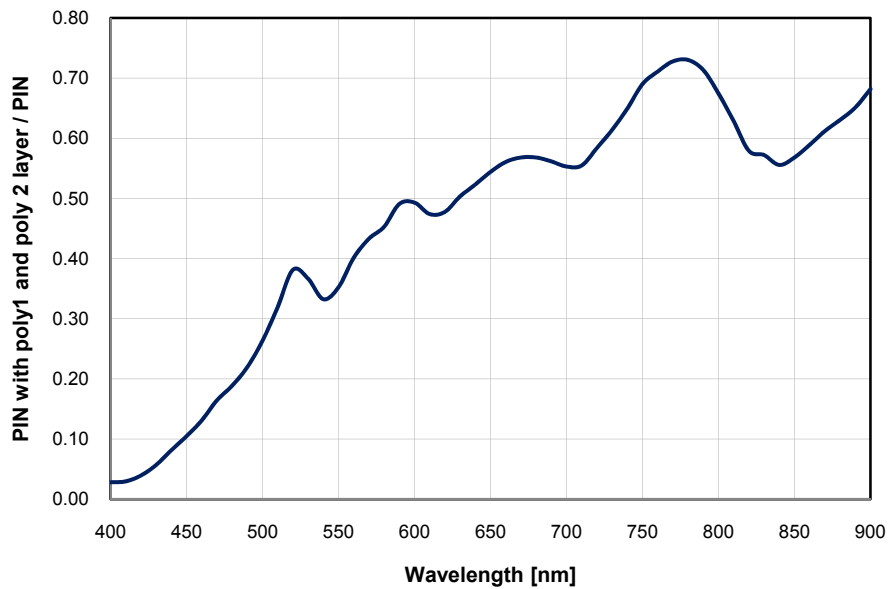


Figure 8.16 PIN with poly 1 and poly 2 layer / PIN

8.6. MIXED PHOTODIODE

The picture below shows the mixed photodiode which consists of many small photodiodes of two different types. On the same chip are also other diodes and reference structures realized. All cathodes of the same diode type are connected together. Both diode types share the same common anode. Thus three connection pads are required for the mixed type diode. The different cathode currents for different wavelengths of the incident light can be used to detect the light color.

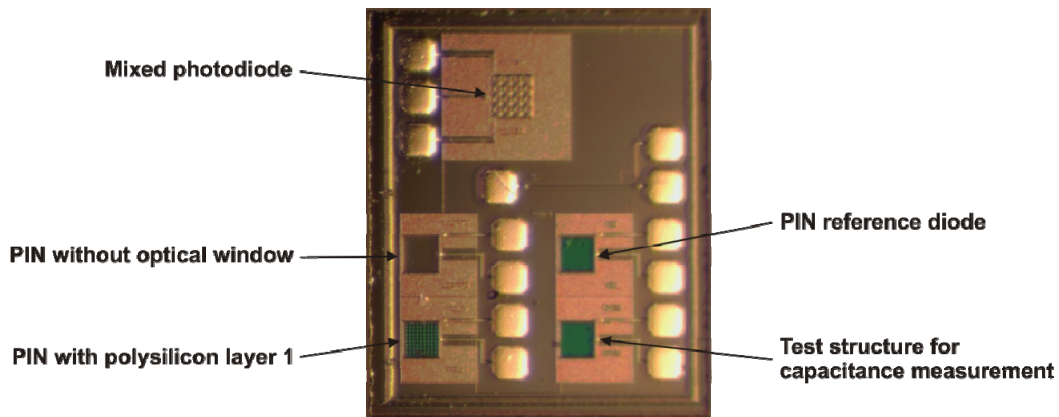


Figure 8.17 Comparison of different diode types

Figure 8.18 shows the responsivity curves of a mixed diode that consists of standard PIN diodes and PIN diodes with an additional polysilicon layer 2. Unfortunately the mixed diode does not work as expected. The two different diode types have nearly the same responsivity curve and additionally the responsivity of the two diodes is very poor compared with the reference diode.

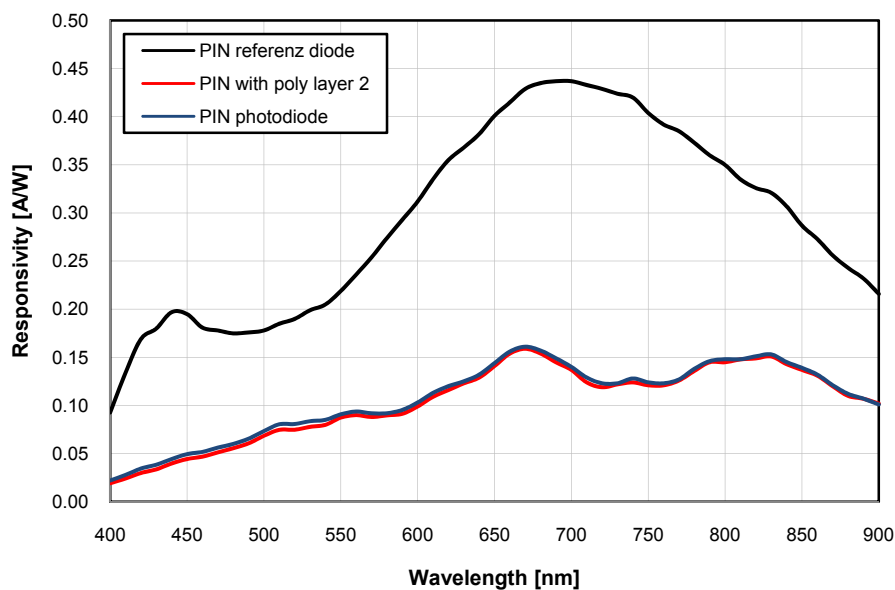


Figure 8.18 Responsivity curves mixed diodes

Due the small difference between the responsivity curves only the ratio of the responsivity of the two different diodes shows color sensitivity over the wavelength range (Figure 8.19).

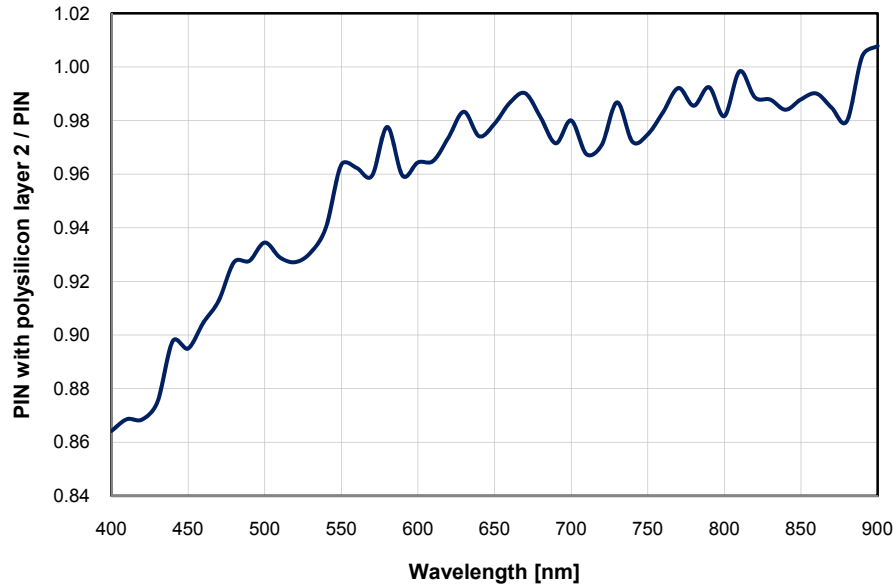


Figure 8.19 Ratio mixed diodes

8.7. PENETRATION DEPTH EFFECT DIODE

The penetration depth diode uses a completely different mechanism to detect the wavelength of the incident light than the other diodes mentioned above. Thus they have a completely different design as showed in Figure 5.14.

Two different anti serial diodes are manufactured in a vertical stack. Since the readout electrode for both diodes is the anode rather than the common cathode the voltage of the reverse-bias voltage source has to be reversed for measurements of these both diodes. The measurement results are shown in Figure 8.20.

It can be seen that the shallow diode has nearly the same responsivity curve as the reference diode below 500nm. From 500 to 650nm the responsivity is constant and decreases for longer wavelength.

The responsivity of the deep diode is nearly zero for wavelengths below 450nm and increases dramatically for larger wavelengths. For wavelengths longer than 750nm it has nearly the same responsivity as the reference diode.

Thus very good color sensitivity is achieved with this diode. The comparison of the measurements results with the Medici simulation (Figure 5.15) additionally shows very good correlation.

8. Measurement Results

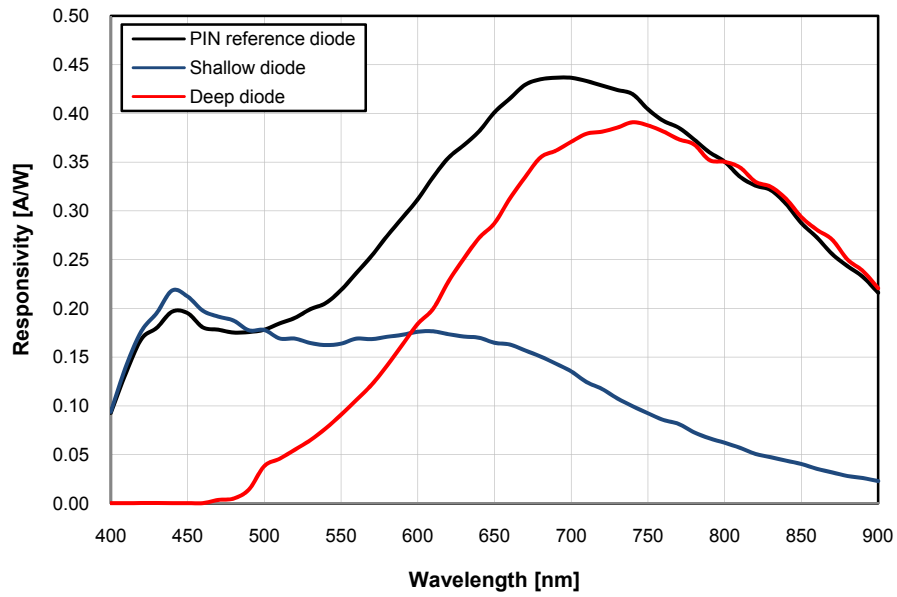


Figure 8.20 Responsivity curves deep and shallow diode

The difference between the shallow and the deep diode is plotted in Figure 8.21. The dependence of the wavelength of the incident light can be seen clearly.

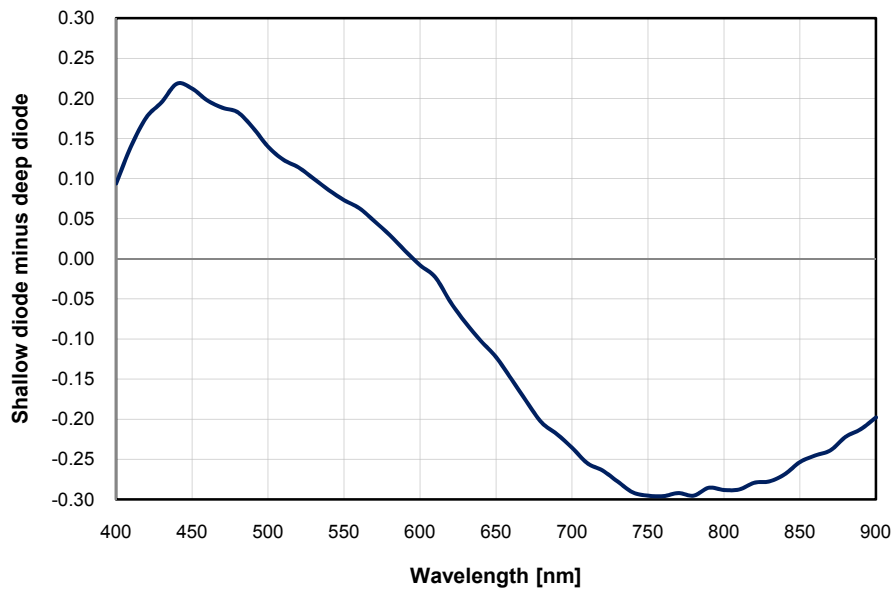


Figure 8.21 Shallow diode minus deep diode

9. CONCLUSION AND OUTLOOK

The presented integrated silicon photodiodes were designed with the aim to detect color without the use of additional production steps or auxiliary filters. The color sensitive photodiodes were produced in a standard X-FAB 0.6 μm BiCMOS process without modifications. The color sensitivity is achieved either by the use of additional layers of the X-FAB 0.6 μm BiCMOS process or by penetration depth properties of the semiconductor.

Two effects were used to realize the color sensitivity:

- The optical filtering properties of different layers (mainly polysilicon layers) of the X-FAB 0.6 μm process
- The different penetration depths of light for different wavelengths into the semiconductor

Multiple different diode types were taken into account to utilize the mentioned effects. Additionally semiconductor simulation was used to assist the design process. Afterwards the most prospecting diode type layouts were realized in the Cadence design framework.

The diodes were fabricated in the X-FAB 0.6 μm BiCMOS process. During the fabrication time a complete measurement setup for spectral measurements on semiconductor devices was developed. The measurement setup consists of a white light source, a monochromator and assisting high sensitivity current and optical power measurement devices. The complete measurement setup is controlled from a single PC application and allows fast and flexible characterization of semiconductor devices over the whole visible spectrum.

To evaluate the different fabricated photodiodes the responsivity curves in the wavelength range from 400 to 900nm were measured and compared to a standard PIN photodiode.

The results show that both effects can be used to design integrated photodiodes in a standard process with distinct color sensitivity. The use of external filters like e.g. Bayer filters is not necessary. Thus the performance of the different effects is remarkable.

The different layers of the BiCMOS process that might be used to filter light are effective only in the blue-green regime. Filtering in the red or NIR regime is not possible by using additional layers of the standard process. Additionally two other problems occur: The thickness of the used layers and the additionally produced unmaskable intermediate oxide layers lead to a major reduction of the photodiodes responsivity. Secondly the imprecise intermediate oxide layer thickness in the standard processes might lead to an unwanted performance variation even at minor process variations. For multiple layer stacks also heavy responsivity oscillations due to the thin layer structure can be observed.

Photodetectors using the penetration depth effect have a lot better performance. The shallow diode shows a very good responsivity for the blue-green regime and only very small responsivity for the red and NIR colors whereas the deep diode has nearly no responsivity for the blue-green regime and a very high responsivity for the red and NIR regime. Since the complete design resides inside the semiconductor, the standard optical window etch process can be implemented with these diodes. Therefore these diodes can reach the optimal responsivity in the same range of optimized standard PIN diodes.

Additionally positive is the effect that the color sensitivity is only related to the well defined penetration depth effect and is not disturbed by process variations. The realized photodiode using the penetration depth effect shows very good color sensitivity and should be considered the first choice when designing integrated color detectors without any additional filter layers.

Future developments might realize diodes using more than the two already realized vertical regions. In the standard BiCMOS process also a diode consisting of three vertical stacked pn junctions might be realized. Since correlation of the simulation results and the measurement results for the two layers diode was very good it can be expected that even a three layer diode can be designed with simulation assistance. Future work in multilayer diodes seems to be prosperous.

10. FIGURE INDEX

Figure 4.1 Lambert-Beer's law [2].....	7
Figure 4.2 Absorption coefficients of important semiconductor materials [3].....	8
Figure 4.3 Carrier mobility in silicon versus total doping concentration	10
Figure 4.4 Carrier mobility versus electric field for a low doping concentration.....	10
Figure 4.5 Carrier drift velocity versus electrical field for a low doping concentration	11
Figure 4.6 Drift and diffusion regions in a photodiode [8]	12
Figure 4.7 Transient behavior of the photocurrent for carrier drift and diffusion	12
Figure 4.8 Semiconductor with antireflection coating	14
Figure 4.9 Spectral responsivity of real photodetectors and theoretical limit [9].....	15
Figure 4.10 PIN photodiode	15
Figure 4.11 Drift region and distribution of the electric field in a PIN photodiode [8]	16
Figure 4.12 Bayer filter pattern [12]	17
Figure 4.13 Profile/cross section of a Bayer mosaic sensor [12]	18
Figure 4.14 Different patterns that can be used [13]	18
Figure 4.15 CYGM filter pattern [14].....	19
Figure 4.16 RGBE filter pattern [16]	19
Figure 4.17 Spectral light absorption in silicon [17]	21
Figure 4.18 Color absorption in silicon and the vertical color sensor.....	21
Figure 4.19 Bayer filter pattern vs. vertical image sensor [19]	22
Figure 4.20 Edge detection – Bayer filter pattern vs. vertical image sensor	22
Figure 5.1 Optical PIN diode [20].....	24
Figure 5.2 Cross section of diode window edge with ARC [17]	25
Figure 5.3 Optical PIN diode in the Virtuoso editor	25
Figure 5.4 N-I-P Diode profiles, depletion width and light penetration	26
Figure 5.5 Additional layers of the BiCMOS process as color filters	27
Figure 5.6 Light absorption in silicon nitride [17].....	28
Figure 5.7 PIN photodiode without optical window	28
Figure 5.8 Photodiode with polysilicon layer 1	29
Figure 5.9 Polysilicon layer 1 grid structure.....	29
Figure 5.10 Photodiode with polysilicon layer 2.....	30
Figure 5.11 Photodiode with polysilicon 1 and polysilicon layer 2.....	31
Figure 5.12 Mixed photodiode.....	32
Figure 5.13 Detail of a mixed photodiode	32
Figure 5.14 Penetration depth effect diode	33
Figure 5.15 Medici simulation depth effect diode.....	34
Figure 6.1 Output spectrum xenon lamp [21].....	35
Figure 6.2 CERMAX [®] LX175F xenon lamp	36
Figure 6.3 ASB-XE-175 xenon light source.....	36
Figure 6.4 View in the glowing xenon lamp	37
Figure 6.5 Digikröm CM110 [22].....	38
Figure 6.6 Functional principle of a monochromator [22].....	38
Figure 6.7 Diffraction grating [22].....	39
Figure 6.8 Grating efficiency curve [22]	41
Figure 6.9 Optical path Czerny-Turner monochromator [23].....	42
Figure 6.10 Triple grating turret of a Czerny-Turner [24]	42

10. Figure Index

Figure 6.11 Bandwidth vs. slit width [25]	44
Figure 6.12 Color filters with different transition wavelengths [22]	45
Figure 6.13 Output and filter wavelength vs. tuning values [24].....	45
Figure 6.14 f-number fiber optical adapter [22]	46
Figure 6.15 CM110 control software [25]	47
Figure 6.16 Optical beam splitter in tubular package [26].....	47
Figure 6.17 Splitter output power, white and blue fiber.....	48
Figure 6.18 Coupling ratio $\bar{\alpha}$ vs. wavelength.....	49
Figure 6.19 Ophir Nova laser power/energy meter [27]	50
Figure 6.20 Schematic drawing of the PD-300 photodiode head [27].....	50
Figure 6.21 Calibration curve PD-300 [28]	51
Figure 6.22 StarCom application screenshot [29]	51
Figure 6.23 Keithley 6517A electrometer [30].....	52
Figure 6.24 Test circuit.....	52
Figure 6.25 Photodiode measurement.....	53
Figure 6.26 Complete measurement setup.....	54
Figure 6.27 Typical responsivity curve of a silicon PIN photodiode [31].....	55
Figure 7.1 LabVIEW front panel and block diagram.....	56
Figure 7.2 Front panel responsivity measurement.....	59
Figure 7.3 LabVIEW application block diagram	62
Figure 8.1 Photodiode measurement (bonded photodiode).....	63
Figure 8.2 Different diode types.....	64
Figure 8.3 PIN photodiode	64
Figure 8.4 Responsivity curve PIN photodiode.....	65
Figure 8.5 PIN Photodiode without optical window	65
Figure 8.6 Responsivity curve without optical window	66
Figure 8.7 PIN without optical window / PIN	66
Figure 8.8 PIN photodiode with polysilicon layer 1.....	67
Figure 8.9 Responsivity curve polysilicon layer 1	68
Figure 8.10 PIN with polysilicon layer 1 / PIN	68
Figure 8.11 PIN photodiode with polysilicon layer 2	69
Figure 8.12 Responsivity curve polysilicon layer 2	69
Figure 8.13 PIN with polysilicon layer 2 / PIN	70
Figure 8.14 PIN photodiode with poly 1 and poly 2 layer	70
Figure 8.15 Responsivity curve poly 1 and poly 2 layer	71
Figure 8.16 PIN with poly 1 and poly 2 layer / PIN.....	71
Figure 8.17 Comparison of different diode types.....	72
Figure 8.18 Responsivity curves mixed diodes	72
Figure 8.19 Ratio mixed diodes	73
Figure 8.20 Responsivity curves deep and shallow diode.....	74
Figure 8.21 Shallow diode minus deep diode.....	74

11. TABLE INDEX

Table 4.1 Absorption coefficients α and intensity factors I_0 of silicon [4] [5]	8
Table 4.2 Electron and hole mobility and further parameters of silicon [3]	9
Table 7.1 Output file example	61

12. REFERENCES

1. **Carl Hepburn**. Britney Spears' Guide to Semiconductor Physics. [Online] [Cited: 05 07, 2008.] <http://britneyspears.ac/lasers.htm>.
2. **Beer-Lambert law**. Wikipedia. [Online] 2 11, 2008. [Cited: 2 13, 2008.] http://en.wikipedia.org/wiki/Beer-Lambert_law.
3. **Zimmermann, H.** *Silicon Optoelectronic Integrated Circuits*. Vienna : Springer-Verlag Berlin Heidelberg, 2004. ISBN 3-540-40518-6.
4. **Palik, E. D.** *Handbook of optical constants of solids*. Orlando : Academic Press, Inc, 1985.
5. **Studna, D. E. Aspnes and A. A.** *Phys. Rev. B* 27(2). 1983.
6. **Caughey, D. M. and Thomas, R. E.** *Carrier mobilities in silicon empirically related to doping an field*. s.l. : Proc. IEEE 55, 1967.
7. **Selberherr, S.** *Process and device modeling for VLSI*. s.l. : Microelectron, 1984.
8. **Zimmermann, H.** *Integrated Silicon Optoelectronics*. Vienna : Springer-Verlag Heidelberg New York, 2000. 3-540-66662-1.
9. **Ghazi, A.** *Entwurf und Realisierung von integrierten Photodetektoren und CMOS-Schaltkreisen für optische Speichersysteme*. Aachen : Wissenschaftsverlag Mainz, 2000.
10. **Zimmermann, H.** Improved CMOS-integrated photodiodes and their application in OEICs. *IEEE Int. Workshop on High Performance Electron Devices for Microwave & Optoelectronic Applications*. 1997.
11. **Alexander, Stephen B.** *Optical Communication Receiver Design*. s.l. : SPIE Press, 1997. ISBN 0819420239.
12. **Bayer Filter**. Wikipedia. [Online] 29 3, 2008. [Cited: 04 12, 2008.] http://en.wikipedia.org/wiki/Bayer_filter.
13. **Hamilton, John Compton and John.** Color Filter Array 2.0. *A Thousand Nerds*. [Online] Kodak Blog, 06 14, 2007. [Cited: 04 12, 2008.] <http://johncompton.1000nerds.kodak.com/default.asp?item=624876>.
14. **CYGM filter**. Wikipedia. [Online] 02 9, 2008. [Cited: 04 12, 2008.] http://en.wikipedia.org/wiki/CYGM_filter.
15. **Askey, Phil.** Sony announce new RGBE CCD. *DPRReview.com*. [Online] 07 15, 2003. [Cited: 04 12, 2008.] <http://www.dpreview.com/news/0307/03071601sonyrgbeccd.asp>.
16. **RGBE filter**. Wikipedia. [Online] 11 08, 2007. [Cited: 04 12, 2008.] http://en.wikipedia.org/wiki/RGBE_filter.
17. **X-FAB Semiconductor Foundries.** *Photo Diode Manual*. Erfurt : X-FAB Semiconductor Foundries, 2002.
18. **Merrill, R. B.** *Color Separation in an Active Pixel Cell Imaging Array Using a Triple-Well-Structure*. *US patent 5,965,875,1999* 1999.
19. **Foveon.** X3 Technologie Direct Image Sensor. *Foveon*. [Online] Foveon Inc., 2007. [Cited: 04 13, 2008.] <http://www.foveon.com/article.php?a=67>.
20. **X-FAB Semiconductor Foundries.** *Process Specification XB06 - 0.6µm BiCMOS*. Erfurt : X-FAB Semiconductor Foundries, 2005.
21. **Spectral Products.** *ASB-XE-175EX and ASB-XE-175 Xenon Fiber Optic Lightsource*. s.l. : Spectral LLC, 2003.
22. —. *Spectral Products Catalog*. Putnam, USA : Spectral LLC, 2003.
23. **Monochromator**. Wikipedia. [Online] 11 17, 2007. [Cited: 04 23, 2008.] <http://en.wikipedia.org/wiki/Monochromator>.

12. References

24. **Spectral Products.** Spectral Products. [Online] Spectral Products, 2003. [Cited: 04 24, 2008.] <http://www.spectralproducts.com/catalog/index.php>.
25. —. *Digikröm CM110/CM112 Monochromator/Spectrograph User Manual.* s.l. : Spectral Products, 2000.
26. **FONT.** Fiber Optic Network Technology. [Online] 05 2007. [Cited: 04 24, 2008.] <http://www.fiberwdm.ca/>.
27. **Ophir - Spiricon Inc.** Power/Energy Meter Catalog. Logan, USA : Ophir - Spiricon Inc., 2007.
28. **Ophir Optronics.** *Nova Laser Power/Energy Monitor User Manual.* s.l. : Ophir Optronics. P/N 1J06013 Rev 3.27-1.
29. —. *StarCom32 User Manual and Programmer's Guide.* s.l. : OphirOptronics. P/N 1J06025 Rev 3.11-1.
30. **Keithley.** *Datasheet 6517A Electrometer/High Resistance Meter.* USA : Keithley.
31. Sam's Laser FAQ. [Online] Samuel M. Goldwasser, 2007. [Cited: 05 01, 2008.] <http://members.misty.com/don/sipdresp.gif>.
32. **LabView.** Wikipedia. [Online] 04 29, 2008. [Cited: 05 01, 2008.] <http://en.wikipedia.org/wiki/LabVIEW>.

13. APPENDIX A: DATASHEET LIGHT SOURCE

SP ————— SPECTRAL PRODUCTS

ASB-XE-175EX and ASB-XE-175 Xenon Fiber Optic Lightsource

- Provides optimum illumination to fiber optics for remote applications.
- High intensity (5600° K) Xenon output.
- Contains CERMAX® high intensity xenon lamp.



FEATURES:

- High Color Temperature (5600°K)
- CERMAX® Collimated Xenon Lamp
- Brightness Control (0 - 100%)
- Portable and Light Weight
- Cool White Light with the UV/IR Suppressed ASB-XE-175

APPLICATIONS:

- Endoscopy
- Spectroscopy
- Microscopy
- Visual Inspection
- Boroscopes
- Machine Vision
- Optical Scanning
- Data and Video Projection

Optimum Remote or Direct Illumination

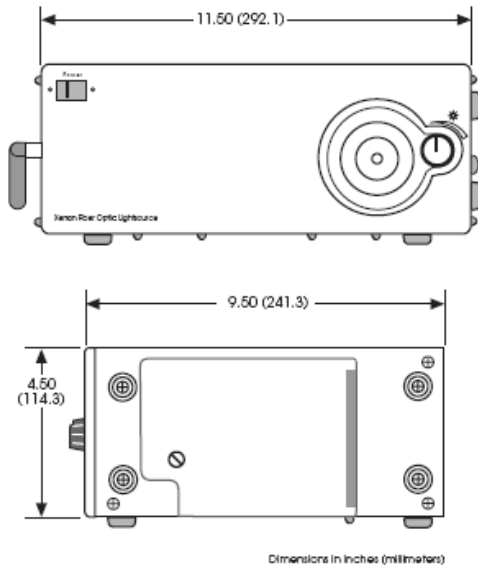
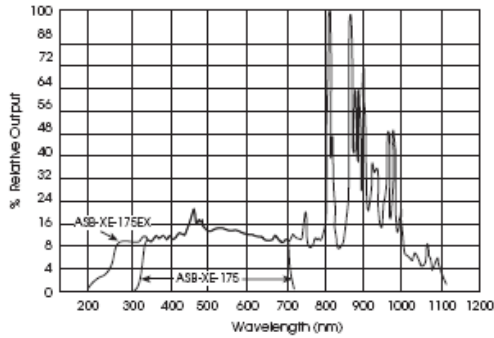
The ASB-XE-175EX is a compact and light weight high intensity fiber optic light source. It is especially suitable as a light source for spectroscopy, microscopy, optical scanning, medical and industrial uses, as well as for use with CVI's popular Digikröm monochromators and spectrographs.

The ASB-XE-175EX uses a CERMAX® compact high intensity xenon lamp, state of the art optics and a high efficiency lightweight switching power supply in one compact package.

The 175W short-arc xenon lamp provides broadband output from 250 to 1100nm. This lamp is compact, rugged, and easily focused to a liquid light guide (sold separately). The lamp efficiency is enhanced by the integral parabolic reflector which provides precision system alignment and maximum transition of light energy. Beam stability is achieved instantly following lamp ignition and the ASB-XE-175EX provides instant re-ignition without an imposed time delay.

revised 6/05

SP SPECTRAL PRODUCTS



Specifications:

- Lamp:**
- Type:** CERMAX® LX175F
- Power:** 200 Watts (maximum)
- Power Range:** 150-200 W
- Color Temperature:** 5600°K
- Current:** 14 amps DC (nominal)
- Average Life:** Typically 1000 hours (500 hours minimum)
- Voltage:** 12-17V (14V nominal)
- Trigger Voltage:** 25 Kilovolts
- Boost Voltage:** 140-200 Volts
- Current Leakage:** < 300mA

- Weight:** 7.5 lbs. (3.4 kg)
- Input Line:** 95-136 VAC, 50/60 Hz (only)
- Input Current:** 3.5 amp.

- Environment:**
- Operating:** +6 to +45 °C
- Storage:** -40 to +70 °C

- Front Panel:** Brightness Control (0-100%)
Output Aperture

- Side Panel:** Main Power (On/Off)
Line Cord Jack (IEC 320)
(US to IEC Line Cord included)
Fuse Holder - MDL-5

- Caution:** Damage to glass or fused silica fiber optic lightguides can occur due to high temperatures associated with Xenon lamps. Use our liquid light guides (order separately).

Ordering Information: Please indicate product number plus description when ordering.

- ASB-XE-175EX** Extended Xenon Source (200-1100nm)
- ASB-XE-175** Ozone Blocking Xenon Source (320-700nm)
- ASB-XE-175EX-BUV** Replacement Extended bulb
- ASB-XE-175-BF** Replacement Ozone Blocking bulb
- AF5000-50001111-S10S** Liquid Light Guide (270-720nm) S Type
- AF5000-50001111-V10S** Liquid Light Guide (340-750nm) V Type

Please see the AF series section in this catalog for more details about Liquid Light Guides and other Fiber Assemblies.

revised 6/03

14. APPENDIX B: DATASHEET MONOCHROMATOR CM110

SP ————— SPECTRAL PRODUCTS

Digikröm CM110

Compact 1/8 Meter Computer-Controlled Monochromator/Spectrograph

- *Compact size - Only 5¼" x 3¼" x 3¼"*
- *Connects to any computer via standard RS232 interface.*
- *Double grating turret allows for a broad spectral range coverage.*
- *May be factory configured as a monochromator or a spectrograph.*
- *Yields average efficiency TRIPLE that of a concave holographic grating monochromator/spectrograph.*
- *Scans in both directions and in nanometers, Ångstroms, microns, wave-numbers, or eV.*
- *Change slits on the fly.*
- *Monochromator may be factory configured for right angle or straight through beam path.*
- *Suitable for fluorescence, radiometry, process control, colorimetry, tunable filtering, Raman spectroscopy, among others.*

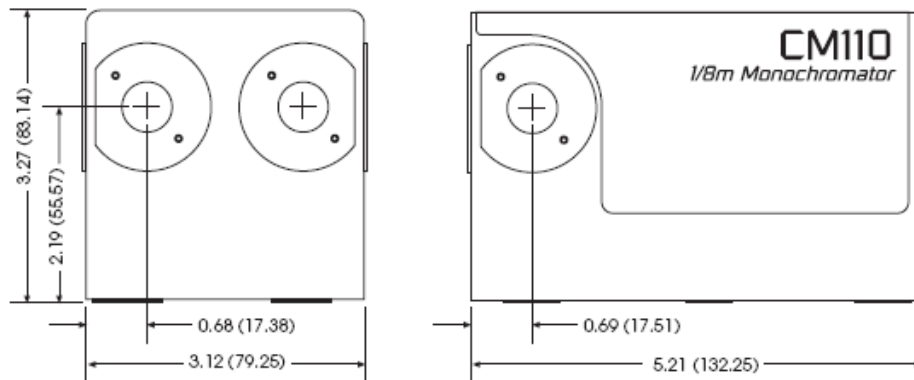


The Leader: Price, Performance, Versatility

Single piece base construction, direct grating drive, and anti-backlash gearing ensure this unit is rugged and stable enough for demanding applications. Loaded with SP Optics and able to hold two high quality gratings, the CM110 is ideal for spectrometry in the UV to IR spectrums. Each instrument is calibrated and certified prior to delivery and comes with easy-to-use software.

rev. 6/03

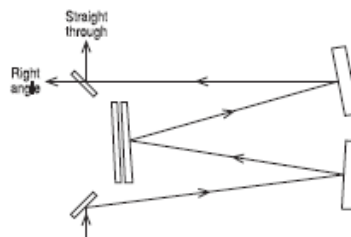
SP SPECTRAL PRODUCTS



Dimensions - inches (millimeters)

Front View

Side View



Optical Path

Specifications:

Design: Czerny-Turner, dual-grating turrets
Focal Length: 110mm
f/#: 3.9
Beam Path: Straight Through standard, Right Angle provided on request.
Wavelength Drive: Worm and wheel with microprocessor control and anti-backlash gearing. Bi-directional. Usable in positive or negative grating orders.
Wavelength Precision: 0.2nm
Wavelength Accuracy: ± 0.2nm
Slewing Speed: > 100nm/second
Stray Light: < 10⁻⁵
Slits: Standard Set includes; 0.125mm, 0.15mm, 0.30mm, 0.6mm, 1.2mm and 2.4mm x 4.0mm. For other sizes, consult SP.
Max Resolution: < 1nmw/1200G/mm grating and standard slits
Gratings: One to two gratings (30 x 30mm) must be purchased. See Appendix A for options.

Software: Demonstration control program and LabView driver included.
Power: UL listed 110/220V power pack
Interface: RS232 standard
Warranty: One year

- Options:**
- Hand-held control module with function keys and display for local control
 - IEEE-488 interface
 - Interface cables
 - Gold optics
- See options and accessories

Ordering Information: Please indicate product number plus description when ordering.

CM110	Dual Grating Turret, 1/8 meter Monochromator
CMSP110	Dual Grating Turret, 1/8 meter Spectrograph

rev 6/03

15. APPENDIX C: DATASHEET ORDER

SORTING FILTERS



AB Series

Order Sorting Filters

- Provides blocking of light radiation below filter specific transition or cut-on wavelength.
- Made from semi-conductor material.
- Allows for various mounting options.
- Offers several filter choices.



Select Light Radiation Easily

The AB30XX Series of Long Pass Order Sorting Filters provide blocking of light radiation below the filter specific transition or cut-on wavelength.

They can be mounted in the AB202 Filter Carrier or in the AB300 Automated Six Position Filter Wheel. The AB202 Filter Carrier is inserted into the AB200 Filter Mount Assembly. The AB3032, AB3058, AB3066, AB3072, and AB3085 are long-wave pass, color glass filters and are available in 25.4 mm diameter.

The average high transmittance (TH) of the color glass filters is greater than 90%. The average high transmittance value is the average transmittance of the filter between the first peak after the cut-on wavelength to the peak before the cut-off wavelength. The transition interval of the AB30XX Series Filters is listed in the following table. The transition interval is the distance (nm) from the cut-on wavelength to the cut-on peak.

The AB3100, AB3190, AB3300, AB3370, AB3720, AB3400, and the AB3840 Order Sorting Filters are made of semiconductor materials. These long-wave pass filters are anti-reflection coated for operation from the long-pass wavelength to at least twice that wavelength.

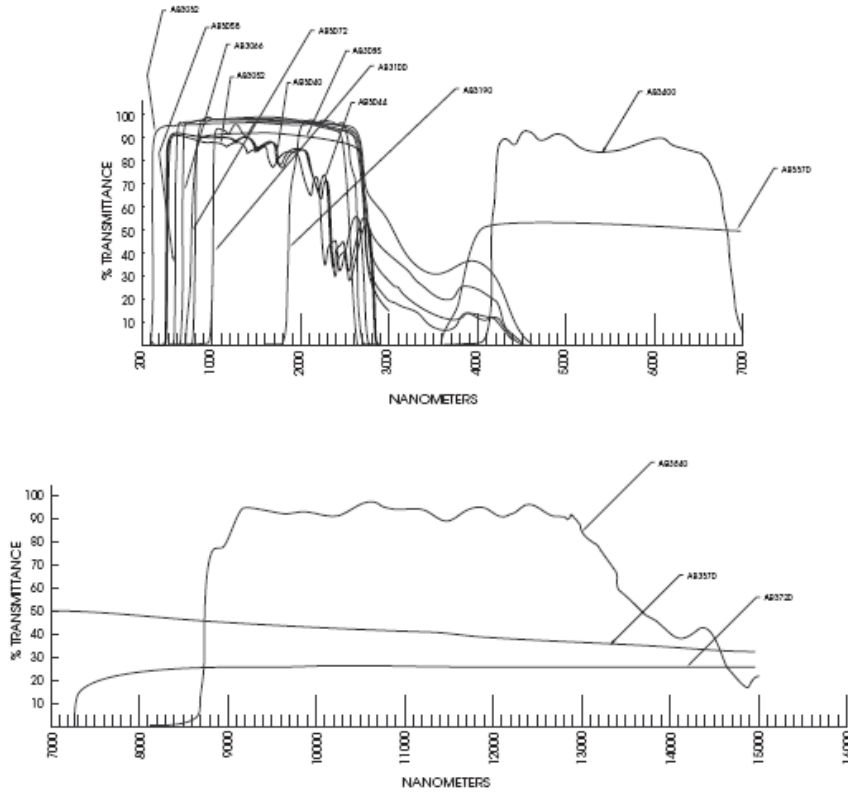
The average high transmittance for the AB3100, AB3190, AB3400, and AB3840 filters is greater than 75%.

These long-pass semiconductor filters are 1 inch (25.4mm) diameter with a thickness of 0.083" or less (2.1mm). These filters can also be mounted in the AB201 Filter Carrier or in the AB300 Automated Six Position Filter Wheel.

The blocking average for all of the filters is 0.1% below the passband through the UV wavelengths.

revised 6/03

SP SPECTRAL PRODUCTS



Transmittance curves of Order Sorting Filters

Specifications:

- Size:** 25.4mm Ø
- Thickness:** 2.1 mm typical
- Material:** Schott optical glass or equivalent
- Surface Quality:** Commercial polish
- Mounting Options:** AB201 Filter Carrier
AB300 Series Automated Filter Wheels

Check Out our Filter catalog for Many More Filter options.

Ordering Information: Please indicate product number plus description when ordering.

Part Number	Transition λ_{τ} (nm)	Transition Tolerance (\pm nm) $\Delta\lambda_{\tau}$
AB3032	320	7
AB3040	400	7
AB3044	440	7
AB3052	520	10
AB3058	580	5
AB3066	660	5
AB3072	720	10
AB3085	850	10
AB3100	1000	25
AB3190	1900	35
AB3300	3000	50
AB3370	3700	80
AB3400	4000	150
AB3580	5800	100
AB3720	7200	185
AB3840	8400	300

revised 6/05

16. APPENDIX D: DATASHEET F-NUMBER FIBER OPTIC ADAPTER

SP ————— SPECTRAL PRODUCTS

AF-L Series

f/# Matching Fiber Optic Adapters

- *High efficiency.*
- *Enables precise alignment.*
- *Provides a broad spectral range with UV grade lenses.*
- *Allows quick connect/disconnect while maintaining alignment.*
- *Use on input or output ports.*
- *Connects SMA, FC/PC, ST, or 10mm diameter Fiber Connectors.*



The AF-L Series of Fiber Optic Adapters will optically match the Numerical Aperture of a SP fiber (NA=0.22) to the f/# of a SP Monochromator or spectrograph while mechanically joining the two.

As an input adapter, the AF-L Series focuses the light from the fiber onto the entrance slit. The magnified fiber image fills more of the slit. All of the light entering the slit strikes the grating. The efficiency of this coupling is 4 to 20 times better than a direct non-matched coupling.

As an output adapter, the AF-L Series focuses the light from the exit slit onto the fiber. The demagnified slit image concentrates light onto the fiber's face and takes advantage of the fiber's "faster" collection angle. The efficiency of this coupling is 2 to 4 times better than direct non-matched coupling.

These dramatic increases in efficiency support applications where low light levels make direct fiber coupling impractical.

Fluorescence analysis, spectral analysis of LEDs and laser diodes, and detector characterization all benefit from this efficiency. Fibers used as detection probes with the AF-L Series can take full advantage of their inherent wide acceptance angle for increased light collection. Fibers used as illumination probes with the AF-L Series can deliver up to 4 times more intensity than with direct coupling. In addition, the fiber will illuminate over its full Numerical Aperture.

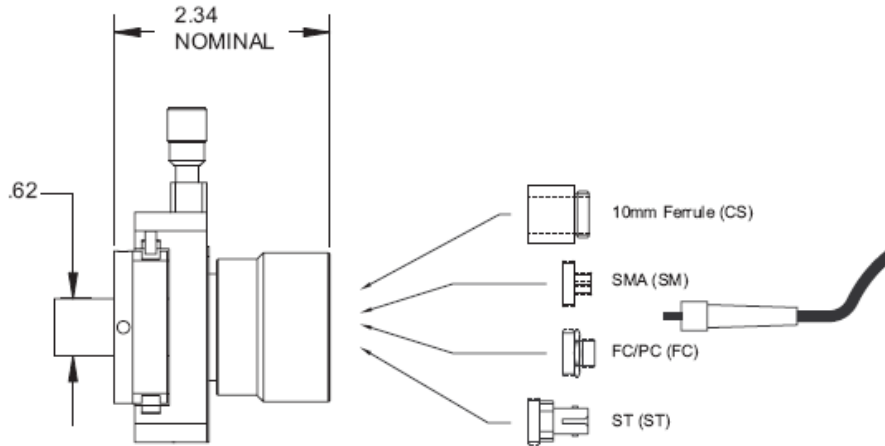
The AF-L Series **allow three axes of precise fiber translation**. Precision of better than 0.001" in linear movement is typical.

Because UV lenses are standard, the AF-L Series provides better than 90% transmission from 200nm to 1900nm.

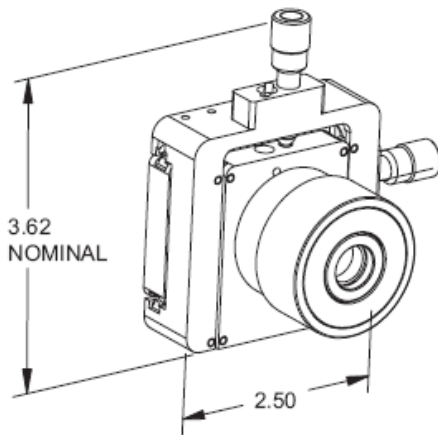
revised 6/03



SPECTRAL PRODUCTS



Dimensions in inches



Specifications:

Adjustment:

X and Y Axes 80-pitch adjustment screws, 0.0002" linear movement for 5° of adjustment screw rotation; 10mm range

Z-Axis 0.0005" linear movement for 5° of collar rotation; 5mm range

Wavelength Range:

200-1900nm @ > 90% transmission

Warranty: One year

Ordering Information: Please indicate product number plus description when ordering.

f/# matching Fiber Optic Adapter for CMSeries monochromators/spectrographs

- AFCM-L-SM** with SMA end plate
- AFCM-L-FC** with FC/PC end plate
- AFCM-L-ST** with ST end plate
- AFCM-L-CS** with 10mm ferrule end plate

f/# matching Fiber Optic Adapter for DK240/DK242 monochromators/spectrographs

- AFDK240-L-SM** with SMA end plate
- AFDK240-L-FC** with FC/PC end plate
- AFDK240-L-ST** with ST end plate
- AFDK240-L-CS** with 10mm ferrule end plate

f/# matching Fiber Optic Adapter for DK480 monochromators/spectrographs

- AFDK480-L-SM** with SMA end plate
- AFDK480-L-FC** with FC/PC end plate
- AFDK480-L-ST** with ST end plate
- AFDK480-L-CS** with 10mm ferrule end plate

revised 6/03

17. APPENDIX E: DATASHEET OPHIR NOVA

POWER/ENERGY METER

Ophir smart displays are true plug-and-play instruments. With all head information and calibration stored in the head plug, just plug in any one of over 150 Ophir smart heads and the instrument is calibrated and configured to measure laser power and energy with that head.

NOVA

- Leading and most popular Ophir display
- Compatible with all Ophir heads: thermal, pyroelectric and photodiode
- Single shot energy measurement with thermal heads
- Optional RS232 computer interface with Windows software
- Power and energy logging with graphical display and statistics
- Power averaging
- Easy to use soft keys, menu-driven
- Screen graphics
- Backlight and rechargeable battery
- Analog output
- EMI rejection



Compatible with the complete range of Ophir thermal (power and energy), pyroelectric and photodiode heads, Nova is truly versatile: measuring from pW to KW, μ J to 200J. With the optional scope adapter, you can connect your pyro head to an oscilloscope and see every pulse up to the maximum frequency permitted by the head.

Smart connector heads automatically configure and calibrate Nova when plugged in. Soft keys guide you through the screen graphics. Finished working? Your configuration can be saved for future use.

Nova's exclusive autoranging tune screen displays laser power graphically and displays maximum power. Zoom and time scale can be adjusted by user.

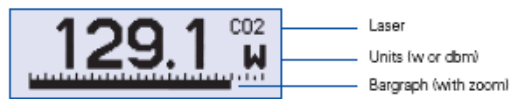
Selected Screens

Digital Power Screen

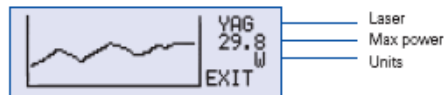
- CW industrial, medical and scientific lasers
- picoWatt to 20KW with appropriate heads

Laser Tuning Screen or Power Log Screen (not shown)

- Maximizing laser power
- User selected time period and zoom



Press Menu button or soft keys to make legends visible (not shown).



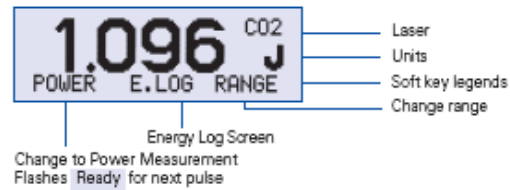
Press Menu button or soft keys to make legends visible.



17. Appendix E: Datasheet Ophir Nova Power/Energy Meter

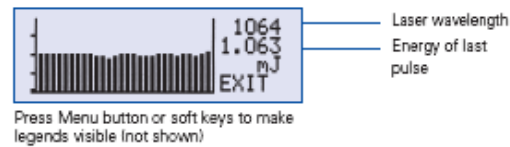
Energy Measurement Screen

- Pyroelectric and thermopile heads-single pulse
- Pyroelectric frequency measurement (not shown)



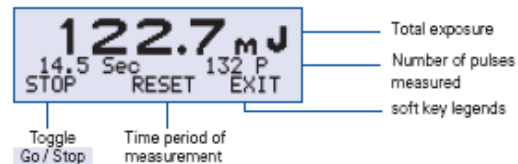
Energy Log Screen

- Pyroelectric heads
- Thermopile heads-successive single pulses
- Continuous scroll
- Energy statistics



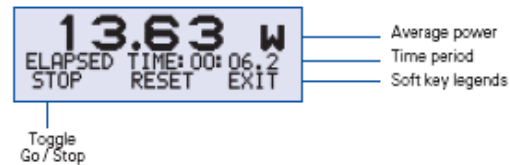
Pyroelectric Exposure Screen

- Sum or average energies over user selected time period / number of pulses
- Medicine, photolithography



Average Screen

- Thermopile, photodiode and pyroelectric heads
- Periodic (1/3 sec to 30 sec) or continuous (10 sec to 1 hour) average for fast-changing or slow-changing laser



Specifications

Display:	High legibility 32 x 122 pixel graphics supertwist LCD with switchable electroluminescent backlight. Large 12mm digits.
Features:	Many screen features: including power with bar graph, energy, average, exposure, frequency, graphs, and more. Analog output 1V f.s.
Refresh:	15 times / sec.
Case:	Molded high-impact plastic with kickstand and EMI conductive shielding, to allow use even in proximity to pulsed lasers.
Size:	Very compact: 203 x 95 x 38mm.
Battery:	Rechargeable 12 volts. 18 hours use between charges. Charger (included) also functions as AC adapter.
Head features:	Works with thermopile, pyroelectric, and photodiode heads. Automatic, continuous, background cancellation with PD300 heads. Submicrojoule and multikilohertz capability with model PE10 head. All heads use smart connector containing configuration information.
Program features:	Preferred startup configuration can be set by user. User can recalibrate power or energy. Response time. Zero offset.

Ordering Information		
Item	Description	Ophir P/N
Nova	Nova universal smart head display for thermal, pyroelectric and photodiode heads	7201500
Carrying Case	Carrying case 33x29x10 cm. For display and up to three heads	1J02079
Nova RS232 assemblies - allow Nova display to communicate with PC and be controlled by PC		
Nova RS232 Assembly	RS232 adapter with standard 2 meter cable (including software)	78105
Nova RS232 Assembly	RS232 adapter with 5 meter cable (including software)	781062
Nova RS232 Assembly	RS232 adapter with 8 meter cable (including software)	781061
Battery Pack	Replacement battery pack for Nova	7211200



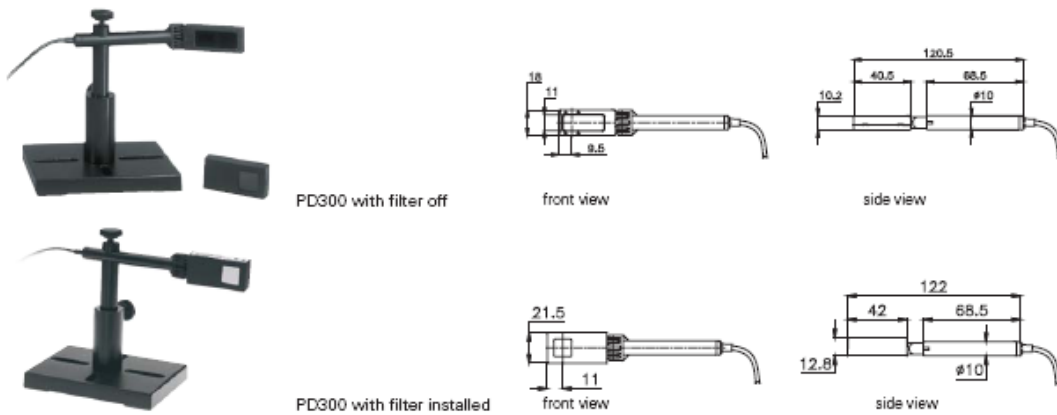
18. APPENDIX F: DATASHEET PHOTO-DIODE HEAD PD-300

PD300 / PD300-1W / PD300-3W

CW power 1nW-30mW (300mW / 1W or 3W with supplied filter)

Recommended Use: Low power CW lasers (HeNe, diode, etc.), out of fiber measurement

Special Features: Automatic background subtraction, F.O. adapters available



PD300 / PD300-1W				PD300-3W		
	PD300 / PD300-1W Filter out	PD300 Filter in	PD300-1W Filter in	Spectral Response:	Filter out	Filter in
Spectral Response:	350 – 1100nm	430 – 1100nm	430 – 1100nm		350 – 1100nm	430 – 1100nm
Power Scales:	30.00mW/3.000mW/ 300.0µW/30.00µW/ 3.000µW/300.0nW/ 30.00nW/dBm	300.00mW / 30.0mW / dBm	1.000W/300.00mW/ 30.0mW/dBm		100.0mW/30.00mW / 3.000mW/300.0µW / 30.00µW /3.000µW / 300.0nW /dBm	3.000W/300.00mW/ 30.0mW/dBm
Maximum Power vs. Wavelength:						
<488nm	30mW	300mW	1W	<488nm	100mW	3W
633nm	20mW	300mW	1W	633nm	100mW	3W
670nm	13mW	200mW	1W	670nm	100mW	2.5W
790nm	10mW	100mW	0.6W	790nm	100mW	2W
904nm	10mW	150mW	0.7W	904nm	100mW	2W
1064nm	25mW	250mW	1W	1064nm	100mW	3W
Damage Threshold:	10W/cm ²	50W/cm ²	50W/cm ²	Damage Threshold:	10W/cm ²	150W/cm ²
Max Pulse Energy:	2µJ	20µJ	100µJ	Max Pulse Energy:	20µJ	500µJ
Accuracy:				Accuracy:		
(including errors due to temp. variations)	±10% 360 – 400nm ±3% 400 – 950nm ±5% 950 - 1100nm	±5% 430-950nm ±7% 950-1100nm	±5% 430-950nm ±7% 950 - 1100nm	(including errors due to temp. variations)	±10% 360-400nm ±3% 400-950nm ±5% 950 - 1100nm	±5% 430-950nm ±7% 950 – 1100nm
Aperture:	10mm x 10mm					
Response Time:	0.2s					
Beam Position Dependence:	±2%			±2% ±3% over 70% of area		
Noise:	0.02nW at mid spectrum with filter out			0.2nW at mid spectrum with filter out		
Background Subtraction:	95 – 98% of background is cancelled automatically under normal room conditions, even when changing continuously			N.A.		

Ordering Information		
Item	Description	Ophir P/N
PD300	350-1100nm, up to 300mW	7202410
PD300-1W	350-1100nm, up to 1W	7202411A
PD300-3W-V1	350-1100nm, up to 3W and for high power densities	7202426
Fiber adapters	See page 54 for fiber adapter ordering information	



19. APPENDIX G: DATASHEET KEITHLEY

6517A ELECTROMETER

6517A

Electrometer/High Resistance Meter



Keithley's 5½-digit Model 6517A Electrometer/High Resistance Meter offers accuracy and sensitivity specifications unmatched by any other meter of this type. It also offers a variety of features that simplify measuring high resistances and the resistivity of insulating materials. With reading rates of up to 125 readings/second, the Model 6517A is also significantly faster than competitive electrometers, so it offers a quick, easy way to measure low-level currents.

Exceptional Performance Specifications

The half-rack-sized Model 6517A has a special low current input amplifier with an input bias current of <math><3\text{fA}</math> with just 0.75fA p-p (peak-to-peak) noise and <math><20\mu\text{V}</math> burden voltage on the lowest range. The input impedance for voltage and resistance measurements is 200TΩ for near-

ideal circuit loading. These specifications ensure the accuracy and sensitivity needed for accurate low current and high impedance voltage, resistance, and charge measurements in areas of research such as physics, optics, nanotechnology, and materials science. A built-in $\pm 1\text{kV}$ voltage source with sweep capability simplifies performing leakage, breakdown, and resistance testing, as well as volume ($\Omega\text{-cm}$) and surface resistivity (Ω/square) measurements on insulating materials.

Wide Measurement Ranges

The Model 6517A offers full autoranging over the full span of ranges on current, resistance, voltage, and charge measurements:

- Current measurements from 1fA to 20mA
- Voltage measurements from 10μV to 200V
- Resistance measurements from 50Ω to 10¹⁶Ω
- Charge measurements from 10fC to 2μC

- Measures resistances up to 10¹⁶Ω
- 1fA–20mA current measurement range
- <math><20\mu\text{V}</math> burden voltage on lowest current ranges
- 200TΩ input impedance
- <math><3\text{fA}</math> bias current
- Up to 125 rdgs/s
- 0.75fA p-p noise
- Built-in $\pm 1\text{kV}$ voltage source
- Unique voltage reversal method for high resistance measurements
- Optional plug-in scanner cards

Ordering Information

6517A Electrometer/High Resistance Meter

Accessories Supplied

237-ALG-2 Low Noise Triax Cable, 3-slot Triax to Alligator Clips, 2m (6.6 ft)

8607 Safety High Voltage Dual Test Leads

6517-TP Thermocouple Bead Probe

CS-1305 Interlock Connector

ACCESSORIES AVAILABLE

CABLES		ADAPTERS	
6517A-ILC-3	Interlock Cable	237-BNC-TRX	Male BNC to 3-Lug Female Triax Adapter
7007-1	Shielded IEEE-488 Cable, 1m (3.2 ft)	237-TRX-NG	Triax Male-Female Adapter with Guard Disconnected
7007-2	Shielded IEEE-488 Cable, 2m (6.5 ft)	237-TRX-T	3-Slot Male Triax to Dual 3-Lug Female Triax Tee Adapter
7009-5	RS-232 Cable	237-TRX-TBC	3-Lug Female Triax Bulkhead Connector (1.1kV rated)
7078-TRX-3	Low Noise Triax Cable, 3-slot Triax Connectors, 0.9m (3 ft)	7078-TRX-BNC	3-Slot Male Triax to BNC Adapter
7078-TRX-10	Low Noise Triax Cable, 3-slot Triax Connectors, 3m (10 ft)	7078-TRX-GND	3-Slot Male Triax to BNC Adapter with guard removed
7078-TRX-20	Low Noise Triax Cable, 3-slot Triax Connectors, 6m (20 ft)	7078-TRX-TBC	3-Lug Female Triax Bulkhead Connector with Cap
8501-1	Trigger Link Cable, 1m (3.3 ft)	SOFTWARE	
8501-2	Trigger Link Cable, 2m (6.6 ft)	6524	High Resistance Measurement Software
8503	Trigger Link Cable to 2 male BNCs, 1m (3.3 ft)	RACK MOUNT KITS	
8607	1kV Source Banana Cables	4288-1	Single Fixed Rack Mounting Kit
PROBES		4288-2	Dual Fixed Rack Mounting Kit
6103C	Voltage Divider Probe	SCANNER CARDS	
6517-RH	Humidity Probe with Extension Cable	6521	Low Current Scanner Card
6517-TP	Temperature Bead Probe (included with 6517A)	6522	Voltage/Low Current Scanner Card
TEST FIXTURE		 GPIB INTERFACES	
8009	Resistivity Test Fixture	KPCI-488LP	IEEE-488 Interface/Controller for the PCI Bus
		KPXI-488	IEEE-488 Interface Board for the PXI Bus
		KUSB-488A	IEEE-488 USB-to-GPIB Interface Adapter

1.888.KEITHLEY (U.S. only)

www.keithley.com

KEITHLEY

6517A

Electrometer/High Resistance Meter

VOLTS			
Range	5½-Digit Resolution	Accuracy (1 Year) ¹ 18°-28°C ±(%rdg+counts)	Temperature Coefficient 0°-18°C & 28°-50°C ±(%rdg+counts)/°C
2 V	10 µV	0.025 + 4	0.003 + 2
20 V	100 µV	0.025 + 3	0.002 + 1
200 V	1 mV	0.06 + 3	0.002 + 1

¹ When properly zeroed, 5½-digit, 1 PLC (power line cycle), median filter on, digital filter = 10 readings.

NMRR: 60dB on 2V, 20V, >55dB on 200V, at 50Hz or 60Hz ±0.1%.

CMRR: >120dB at DC, 50Hz or 60Hz.

INPUT IMPEDANCE: >200TΩ in parallel with 20pF, <2pF guarded (1MΩ with zero check on).

SMALL SIGNAL BANDWIDTH AT PREAMP OUTPUT: Typically 100kHz (-3dB).

AMPS			
Range	5½-Digit Resolution	Accuracy (1 Year) ¹ 18°-28°C ±(%rdg+counts)	Temperature Coefficient 0°-18°C & 28°-50°C ±(%rdg+counts)/°C
20 pA	100 aA ²	1 + 30	0.1 + 5
200 pA	1 fA ²	1 + 5	0.1 + 1
2 nA	10 fA	0.2 + 30	0.1 + 2
20 nA	100 fA	0.2 + 5	0.03 + 1
200 nA	1 pA	0.2 + 5	0.03 + 1
2 µA	10 pA	0.1 + 10	0.005 + 2
20 µA	100 pA	0.1 + 5	0.005 + 1
200 µA	1 nA	0.1 + 5	0.005 + 1
2 mA	10 nA	0.1 + 10	0.008 + 2
20 mA	100 nA	0.1 + 5	0.008 + 1

¹ When properly zeroed, 5½-digit, 1PLC (power line cycle), median filter on, digital filter = 10 readings.

² aA = 10⁻¹⁸A, fA = 10⁻¹⁵A.

INPUT BIAS CURRENT: <3fA at T_{cal}. Temperature coefficient = 0.5fA/°C.

INPUT BIAS CURRENT NOISE: <750aA p-p (capped input), 0.1Hz to 10Hz bandwidth, damping on. Digital filter = 40 readings.

INPUT VOLTAGE BURDEN at T_{cal} ±1°C: <20µV on 20pA, 2nA, 20nA, 2µA, 20µA ranges. <100µV on 200pA, 200nA, 200µA ranges. <2mV on 2mA range. <4mV on 20mA range.

TEMPERATURE COEFFICIENT OF INPUT VOLTAGE BURDEN: <10µV/°C on pA, nA, µA ranges.

PREAMP SETTling TIME (to 10% of final value): 2.5µs typical on pA ranges, damping off, 4s typical on pA ranges damping on, 15ms on nA ranges, 2ms on µA and mA ranges.

NMRR: >95dB on pA, 60dB on nA, µA, and mA ranges at 50Hz or 60Hz ±0.1%.

COULOMBS			
Range	5½-Digit Resolution	Accuracy (1 Year) ^{1,2} 18°-28°C ±(%rdg+counts)	Temperature Coefficient 0°-18°C & 28°-50°C ±(%rdg+counts)/°C
2 nC	10 fC	0.4 + 5	0.04 + 3
20 nC	100 fC	0.4 + 5	0.04 + 1
200 nC	1 pC	0.4 + 5	0.04 + 1
2 µC	10 pC	0.4 + 5	0.04 + 1

¹ Specifications apply immediately after charge acquisition. Add

$$(iA + \frac{|Q_{av}|}{RC}) T_A$$

where T_A = period of time in seconds between the coulombs zero and measurement

Q_{av} = average charge measured over T_A and RC = 360,000 typical.

² When properly zeroed, 5½-digit, 1PLC (power line cycle), median filter on, digital filter = 10 readings.

INPUT BIAS CURRENT: <4fA at T_{cal}. Temperature coefficient = 0.5fA/°C.

OHMS (Normal Method)					
Range	5½-Digit Resolution	Accuracy ¹		Auto V Source	Amps Range
		(10-100% Range) 18°-28°C (1 Yr.) ±(% rdg+counts)	(10-100% Range) 0°-18°C & 28°-50°C ±(% rdg+counts)		
2 MΩ	10 Ω	0.125 + 1	0.01 + 1	40 V	200 µA
20 MΩ	100 Ω	0.125 + 1	0.01 + 1	40 V	20 µA
200 MΩ	1 kΩ	0.15 + 1	0.015 + 1	40 V	2 µA
2 GΩ	10 kΩ	0.225 + 1	0.035 + 1	40 V	200 nA
20 GΩ	100 kΩ	0.225 + 1	0.035 + 1	40 V	20 nA
200 GΩ	1 MΩ	0.35 + 1	0.110 + 1	40 V	2 nA
2 TΩ	10 MΩ	0.35 + 1	0.110 + 1	400 V	2 nA
20 TΩ	100 MΩ	1.025 + 1	0.105 + 1	400 V	200 pA
200 TΩ	1 GΩ	1.15 + 1	0.125 + 1	400 V	20 pA

¹ Specifications are for auto V-source ohms, when properly zeroed, 5½-digit, 1PLC, median filter on, digital filter = 10 readings. If user selectable voltage is required, use manual mode. Manual mode displays resistance (up to 10¹⁶Ω) calculated from measured current. Accuracy is equal to accuracy of V-source plus accuracy of selected Amps range.

PREAMP SETTling TIME: Add voltage source settling time to preamp settling time in Amps specification.

OHMS (ALTERNATING POLARITY METHOD)
The alternating polarity sequence compensates for the background (offset) currents of the material or device under test. Maximum tolerable offset up to full scale of the current range used.

Using Keithley 8009 fixture

REPEATABILITY: ΔI_{bg} × R/V_{ALT} + 0.1% (1σ) (instrument temperature constant ±1°C).

ACCURACY: (V_{src}Err + I_{amm}Err) × R/V_{ALT}

where: ΔI_{bg} is a measured, typical background current noise from the sample and fixture.

V_{ALT} is the alternating polarity voltage used.

V_{src}Err is the accuracy (in volts) of the voltage source using V_{ALT} as the setting.

I_{amm}Err is the accuracy (in amps) of the ammeter using V_{ALT}/R as the rdg.

VOLTAGE SOURCE			
Range	5½-Digit Resolution	Accuracy (1 Year) 18°-28°C ±(% setting + offset)	Temperature Coefficient 0°-18°C & 28°-50°C ±(% setting+offset)/°C
100 V	5 mV	0.15 + 10 mV	0.005 + 1 nV
1000 V	50 mV	0.15 + 100 mV	0.005 + 10 nV

MAXIMUM OUTPUT CURRENT:

±10mA; active current limit at <11.5mA for 100V range.

±1mA; active current limit at <1.15mA for 1000V range.

SETTLing TIME: <8ms to rated accuracy for 100V range.

<50ms to rated accuracy for 1000V range.

NOISE: <150µV p-p from 0.1Hz to 10Hz for 100V range.

<1.5mV p-p from 0.1Hz to 10Hz for 1000V range.

1.888.KEITHLEY (U.S. only)

www.keithley.com

KEITHLEY

6517A

Electrometer/High Resistance Meter

TEMPERATURE (Thermocouple)

Thermocouple Type	Range	Accuracy (1 Year) ¹ 18°–28°C ±(% rdg + °C)
K	–25°C to 150°C	±(0.3% + 1.5°C)

¹ Excluding probe errors, T_{out} ± 5°C, 1 PLC integration time.

HUMIDITY

Range	Accuracy (1 Year) ¹ 18°–28°C, ±(% rdg + % RH)
0–100%	±(0.3% + 0.5)

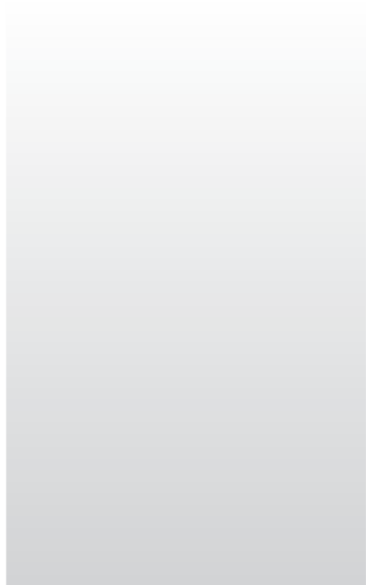
¹ Humidity probe accuracy must be added. This is ±3% RH for Model 6517-8H, up to 65°C probe environment, not to exceed 85°C.

IEEE-488 BUS IMPLEMENTATION

IMPLEMENTATION: SCPI (IEEE-488.2, SCPH-1993).
 TRIGGER TO READING DONE: 150ms typical, with external trigger.
 RS-232 IMPLEMENTATION: Supports SCPI 1991.0.
 Baud Rates: 300, 600, 1200, 2400, 4800, 9600, 19.2k.
 PROTOCOLS: Xon/Xoff, 7- or 8-bit ASCII, parity-odd/even/none.
 CONNECTOR: DB-9 TXD/RXD/GND.

GENERAL

DISPLAY: 6½-digit vacuum fluorescent multiline.
 RANGING: Automatic or manual.
 CONVERSION TIME: Selectable 0.01PLC to 10PLC.
 MAXIMUM INPUT: 250V peak, DC to 60Hz sine wave; 10s per minute maximum on mA ranges.
 MAXIMUM COMMON MODE VOLTAGE (DC to 60Hz sine wave): Electrometer, 500V peak; V Source, 750V peak.
 ISOLATION (Meter COMMON to chassis): Typically 10⁶Ω in parallel with 500pF.
 INPUT CONNECTOR: Three big triaxial on rear panel.
 2V ANALOG OUTPUT: 2V for full range input. Non-inverting in Volts mode, inverting when measuring Amps, Ohms, or Coulombs. Output impedance 10kΩ.
 PREAMP OUTPUT: Provides a guard output for Volts measurements. Can be used as an inverting output or with external feedback in Amps and Coulombs modes.
 EXTERNAL TRIGGER: TTL compatible External Trigger and Electrometer Complete.
 GUARD: Switchable voltage guard available.
 DIGITAL I/O AND TRIGGER LINE: Available, see manual for usage.
 EMU/RFI: Meets VDE-0871 and FCC Class B limits.
 EMC: Conforms to European Union Directive 89/336/EEC.
 SAFETY: Conforms to European Union Directive 73/23/EEC (meets EN61010-1/IEC 1010).
 READING STORAGE: 50,000 max. readings (SCM mode).
 READING RATE:
 To internal buffer 125 readings/second¹
 To IEEE-488 bus 115 readings/second^{1,2}
 Bus transfer 2500 readings/second²
¹ 0.01PLC, digital filters off, front panel off, temperature + RH off
² Binary transfer mode.
 DIGITAL FILTER: Median and averaging.
 ENVIRONMENT: Operating: 0°–50°C; relative humidity 70% non-condensing, up to 35°C. Storage: –25° to +65°C.
 WARM-UP: 1 hour to rated accuracy (see manual for recommended procedure).
 POWER: 105–125V or 210–250V (external switch selected), 90–110V (internal switch selected), 50–60Hz, 50VA.
 PHYSICAL: Case Dimensions: 90mm high × 214mm wide × 369mm deep (3½ in. × 8½ in. × 14½ in.).
 Working Dimensions: From front of case to rear including power cord and IEEE-488 connector: 15.5 inches.
 Net Weight: <4.6kg (<10.1 lbs.).
 Shipping Weight: <9.5kg (<21 lbs.).



1.888.KEITHLEY (U.S. only)
www.keithley.com

